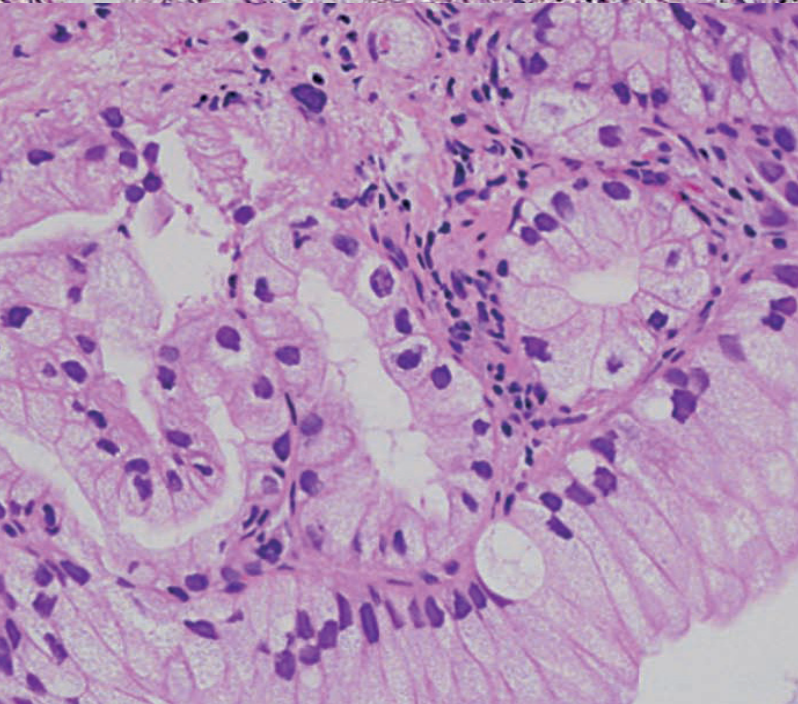


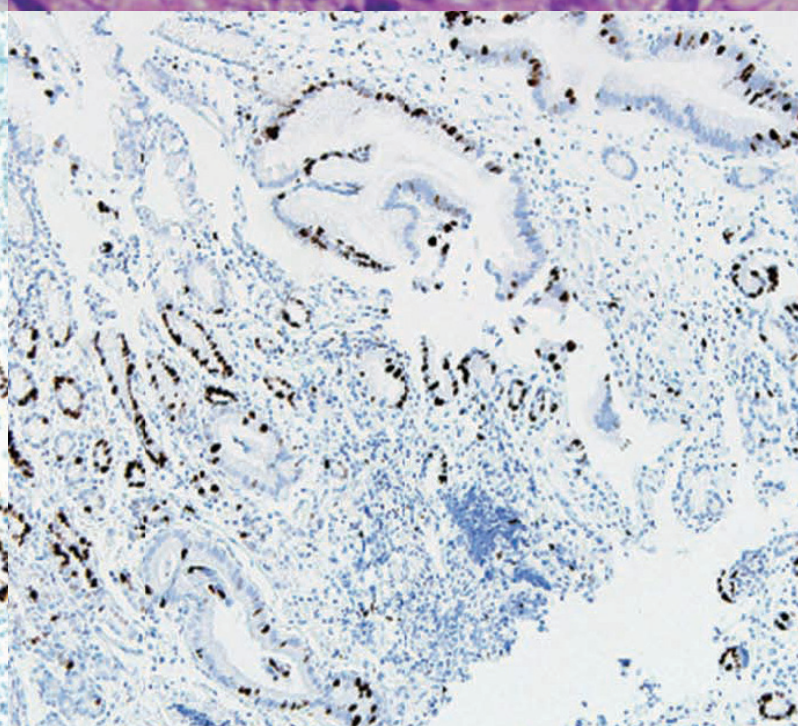
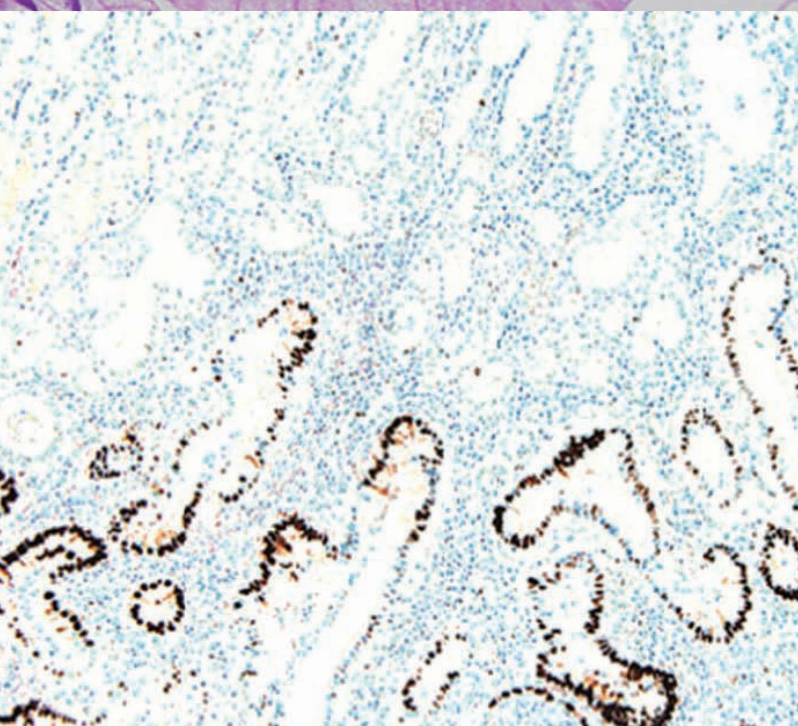
# JPTM

Journal of Pathology  
and Translational Medicine

March 2022  
Vol. 56 / No.2  
jpatholm.org  
pISSN: 2383-7837  
eISSN: 2383-7845



*Extremely Well-  
Differentiated  
Adenocarcinoma  
of the Stomach*



## Aims & Scope

The *Journal of Pathology and Translational Medicine* is an open venue for the rapid publication of major achievements in various fields of pathology, cytopathology, and biomedical and translational research. The Journal aims to share new insights into the molecular and cellular mechanisms of human diseases and to report major advances in both experimental and clinical medicine, with a particular emphasis on translational research. The investigations of human cells and tissues using high-dimensional biology techniques such as genomics and proteomics will be given a high priority. Articles on stem cell biology are also welcome. The categories of manuscript include original articles, review and perspective articles, case studies, brief case reports, and letters to the editor.

## Subscription Information

To subscribe to this journal, please contact the Korean Society of Pathologists/the Korean Society for Cytopathology. Full text PDF files are also available at the official website (<https://jpatholm.org>). *Journal of Pathology and Translational Medicine* is indexed by Emerging Sources Citation Index (ESCI), PubMed, PubMed Central, Scopus, KoreaMed, KoMCI, WPRIM, Directory of Open Access Journals (DOAJ), and CrossRef. Circulation number per issue is 50.

## Editors-in-Chief

Jung, Chan Kwon, MD (*The Catholic University of Korea, Korea*) <https://orcid.org/0000-0001-6843-3708>

Park, So Yeon, MD (*Seoul National University, Korea*) <https://orcid.org/0000-0002-0299-7268>

## Associate Editors

Shin, Eunah, MD (*Yongin Severance Hospital, Yonsei University, Korea*) <https://orcid.org/0000-0001-5961-3563>

Kim, Haeryoung, MD (*Seoul National University, Korea*) <https://orcid.org/0000-0002-4205-9081>

Bychkov, Andrey, MD (*Kameda Medical Center, Japan; Nagasaki University Hospital, Japan*) <https://orcid.org/0000-0002-4203-5696>

## Editorial Board

Avila-Casado, Maria del Carmen, MD (*University of Toronto, Toronto General Hospital UHN, Canada*)

Bae, Young Kyung, MD (*Yeungnam University, Korea*)

Bongiovanni, Massimo, MD (*Lausanne University Hospital, Switzerland*)

Bova, G. Steven, MD (*University of Tampere, Finland*)

Choi, Joon Hyuk (*Yeungnam University, Korea*)

Chong, Yo Sep, MD (*The Catholic University of Korea, Korea*)

Chung, Jin-Haeng, MD (*Seoul National University, Korea*)

Fadda, Guido, MD (*Catholic University of Rome-Foundation Agostino Gemelli University Hospital, Italy*)

Fukushima, Noriyoshi, MD (*Ijichi Medical University, Japan*)

Go, Heounjeong (*University of Ulsan, Korea*)

Hong, Soon Won, MD (*Yonsei University, Korea*)

Jain, Deepali, MD (*All India Institute of Medical Sciences, India*)

Kakudo, Kennichi, MD (*Izumi City General Hospital, Japan*)

Kim, Jang-Hee, MD (*Ajou University, Korea*)

Kim, Jung Ho, MD (*Seoul National University, Korea*)

Kim, Se Hoon, MD (*Yonsei University, Korea*)

Komuta, Mina, MD (*Keio University, Tokyo, Japan*)

Kwon, Ji Eun (*Ajou University, Korea*)

Lai, Chiung-Ru, MD (*Taipei Veterans General Hospital, Taiwan*)

Lee, C. Soon, MD (*University of Western Sydney, Australia*)

Lee, Hye Seung, MD (*Seoul National University, Korea*)

Lee, Sung Hak (*The Catholic University, Korea*)

Liu, Zhiyan, MD (*Shanghai Jiao Tong University, China*)

Lkhagvadorj, Sayamaa, MD (*Mongolian National University of Medical Sciences, Mongolia*)

Moran, Cesar, MD (*MD Anderson Cancer Center, U.S.A.*)

Paik, Jin Ho, MD (*Seoul National University, Korea*)

Park, Jeong Hwan (*Seoul National University, Korea*)

Ro, Jae Y., MD (*Cornell University, The Methodist Hospital, U.S.A.*)

Sakhujia, Puja, MD (*Govind Ballabh Pant Hospital, India*)

Shahid, Pervez, MD (*Aga Khan University, Pakistan*)

Song, Joon Seon, MD (*University of Ulsan, Korea*)

Tan, Puay Hoon, MD (*National University of Singapore, Singapore*)

Than, Nandor Gabor, MD (*Semmelweis University, Hungary*)

Tse, Gary M., MD (*The Chinese University of Hong Kong, Hong Kong*)

Yatabe, Yasushi, MD (*Aichi Cancer Center, Japan*)

Zhu, Yun, MD (*Jiangsu Institution of Nuclear Medicine, China*)

## Ethic Editor

Choi, In-Hong, MD (*Yonsei University, Korea*)

Huh, Sun, MD (*Halym University, Korea*)

## Statistics Editors

Kim, Dong Wook (*National Health Insurance Service Ilsan Hospital, Korea*)

Lee, Hye Sun (*Yonsei University, Korea*)

## Manuscript Editor

Chang, Soo-Hee (*InfoLumi Co., Korea*)

## Layout Editor

Kim, Haeja (*iMiS Company Co., Ltd., Korea*)

## Website and JATS XML File Producers

Cho, Yoonsang (*M2Community Co., Korea*)

Im, Jeonghee (*M2Community Co., Korea*)

## Administrative Assistants

Kim, Da Jeong (*The Korean Society of Pathologists*)

Jeon, Annmie (*The Korean Society for Cytopathology*)

## Contact the Korean Society of Pathologists/the Korean Society for Cytopathology

**Publishers:** Nam, Jong Hee, MD, Gong, Gyungyub, MD

**Editors-in-Chief:** Jung, Chan Kwon, MD, Park, So Yeon, MD

**Published by the** Korean Society of Pathologists/the Korean Society for Cytopathology

### Editorial Office

Room 1209 Gwanghwamun Officia, 92 Saemunan-ro, Jongno-gu, Seoul 03186, Korea

Tel: +82-2-795-3094 Fax: +82-2-790-6635 E-mail: [office@jpatholm.org](mailto:office@jpatholm.org)

#1508 Renaissancetower, 14 Mallijae-ro, Mapo-gu, Seoul 04195, Korea

Tel: +82-2-593-6943 Fax: +82-2-593-6944 E-mail: [office@jpatholm.org](mailto:office@jpatholm.org)

**Printed by** iMiS Company Co., Ltd. (JMC)

Jungang Bldg. 18-8 Wonhyo-ro 89-gil, Yongsan-gu, Seoul 04314, Korea

Tel: +82-2-717-5511 Fax: +82-2-717-5515 E-mail: [ml@smileml.com](mailto:ml@smileml.com)

**Manuscript Editing by** InfoLumi Co.

210-202, 421 Pangyo-ro, Bundang-gu, Seongnam 13522, Korea

Tel: +82-70-8839-8800 E-mail: [infolumi.chang@gmail.com](mailto:infolumi.chang@gmail.com)

Front cover image: Comparison between extremely well-differentiated adenocarcinoma of the stomach and its mimickers (p69).

© Copyright 2022 by the Korean Society of Pathologists/the Korean Society for Cytopathology

© Journal of Pathology and Translational Medicine is an Open Access journal under the terms of the Creative Commons Attribution Non-Commercial License (<https://creativecommons.org/licenses/by-nc/4.0>).

© This paper meets the requirements of KS X ISO 9706, ISO 9706-1994 and ANSI/NISO Z.39.48-1992 (Permanence of Paper).

## CONTENTS

---

### ORIGINAL ARTICLES

- 63 **Extremely well-differentiated adenocarcinoma of the stomach: diagnostic pitfalls in endoscopic biopsy**  
Jongwon Lee, In-Seob Lee, Ji Yong Ahn, Young Soo Park, Jihun Kim
- 73 **Fatty acid synthetase expression in triple-negative breast cancer**  
Jin Hee Park, Hye Seung Han, So Dug Lim, Wook Youn Kim, Kyoung Sik Park, Young Bum Yoo, Seung Eun Lee, Wan-Seop Kim
- 81 **Blocking Toll-like receptor 9 attenuates bleomycin-induced pulmonary injury**  
Badr Alzahrani, Mohamed M. S. Gaballa, Ahmed A. Tantawy, Maha A. Moussa, Salma A. Shoulah, Said M. Elshafae

### CASE REPORTS

- 92 **An unusual case of microsatellite instability-high/deficient mismatch repair (MSI-H/dMMR) diffuse large B-cell lymphoma revealed by targeted gene sequencing**  
Bogyeong Han, Sehui Kim, Jiwon Koh, Jeong Mo Bae, Hongseok Yun, Yoon Kyung Jeon
- 97 **Colorectal adenocarcinoma with enteroblastic differentiation: diagnostic challenges of a rare case encountered in clinical practice**  
Evi Abada, Ifeoma C. Anaya, Othuke Abada, Anthony Lebbos, Rafic Beydoun
- 103 **Recurrent malignant solitary fibrous tumor of the scalp: a case report and literature review**  
Ahmed Rabie, Abdulkarim Hasan, Yasein Mohammed, Ayman Abdelmaksoud, Ali A. Rabaan

### LETTERS TO THE EDITOR

- 109 **And the story goes on: non-conventional dysplasia of the colorectum**  
Lavisha S. Punjabi, Yi Neng Lai, Anjula Thomas
- 111 **Renal cell carcinoma concomitant with multiple myeloma**  
Anubhav Narwal, Prashant Ramteke, Lalit Kumar, Saumyaranjan Mallick

---

## NEWSLETTER

- 113    What's new in molecular genetic pathology 2022: immune checkpoint inhibitor biomarkers and select solid tumors  
Patricia C. Tsang, Guoli Chen

**Instructions for Authors** for *Journal of Pathology and Translational Medicine* are available at <http://jpatholm.org/authors/authors.php>

# Extremely well-differentiated adenocarcinoma of the stomach: diagnostic pitfalls in endoscopic biopsy

Jongwon Lee<sup>1</sup>, In-Seob Lee<sup>2</sup>, Ji Yong Ahn<sup>3</sup>, Young Soo Park<sup>1</sup>, Jihun Kim<sup>1</sup>

Departments of <sup>1</sup>Pathology, <sup>2</sup>Surgery, and <sup>3</sup>Gastroenterology, Asan Medical Center, University of Ulsan College of Medicine, Seoul, Korea

**Background:** Extremely well-differentiated adenocarcinoma (EWDA) is a deceptively bland-looking adenocarcinoma of the stomach. It often causes diagnostic problems, especially in endoscopic biopsy samples. To better recognize this deceptively bland lesion, we carefully reviewed a series of EWDA treated at our institution. **Methods:** A total of 55 specimens from 19 patients were obtained. Endoscopic, gross and microscopic features defining EWDA were described and documented. For comparison, hyperplastic polyp specimens were randomly selected and analyzed. **Results:** Most cases (18 of 19, 94.7%) were advanced gastric cancer (AGC) and primarily located in the body of the stomach (15 of 19, 79.0%). The majority of AGCs were non-ulcerated (11 of 18, 61.1%) with an undermining growth pattern and a relatively small mucosal involvement. Specific histologic features included an irregular glandular shape, an undulating apical cytoplasmic border, disproportionately large glands, a variably distended mucinous cytoplasm. Classical features, such as small infiltrating glands or desmoplastic reactions, were barely observed. Identification of irregularly spaced nuclei and disruption of the foveolar epithelial structure, along with atypical features described above were helpful in making a diagnosis especially in gastric forceps biopsies. **Conclusions:** Awareness of the histomorphologic characteristics described in this report would lead to timely diagnosis and prevent repeated endoscopic procedures.

**Key Words:** Stomach neoplasms; Adenocarcinoma; Missed diagnosis

**Received:** August 26, 2021 **Revised:** October 8, 2021 **Accepted:** October 12, 2021

**Corresponding Author:** Jihun Kim, MD, Department of Pathology, Asan Medical Center, University of Ulsan College of Medicine, 88 Olympic-ro 43-gil, Songpa-gu, Seoul 05505, Korea

Tel: +82-2-3010-4556, Fax: +82-2-472-7898, E-mail: jihunkim@amc.seoul.kr

Extremely well-differentiated adenocarcinoma (EWDA) of the stomach is a rare and an understudied neoplasm the diagnosis of which is especially challenging due to bland nuclear features and subtle architectural atypia. Intestinal- and gastric-type EWDA are its subgroups, mimicking intestinal metaplasia and normal foveolar epithelium, respectively. Intestinal-type EWDA consist of intestinal-type glands with various amounts of goblet and Paneth cells [1]. Gastric-type EWDA are described as mucin-rich columnar cells with basally located, bland-looking nuclei mimicking hyperplastic foveolar epithelium or dilated pyloric glands [2].

Due to its deceptively bland morphology, misinterpretations of EWDA in gastric forceps biopsy are fairly common [2]. However, not many reports discuss its diagnostic histomorphology comprehensively. Therefore, we tried to extract applicable gross, histomorphologic features recurring in 19 EWDA from our in-

stitution assuming that EWDA exhibit several indicative histological and growth patterns applicable in diagnostic approaches.

## MATERIALS AND METHODS

### Case selection

EWDA was defined as neoplastic glands comprised of highly differentiated cells mimicking intestinal metaplasia or normal gastric foveolar epithelium with mild nuclear atypia, according to the definition by Yao et al. [1], applied with slight modification. EWDA cases were identified and collected through routine clinical practice. In the screening process, the intestinal-type EWDA presented as early gastric cancers (EGCs) with the well-known crawling-type or shaking-hand-type morphologies were excluded. We focused more on the identification of advanced EWDA that were relatively diagnostically urgent. The malig-

nant nature was confirmed either by surgically resected specimens or by unequivocal clinical presentations as metastatic disease. The confirming procedure was warranted because the histologic appearances of EWDA were not easily recognizable due to deceptively bland morphologies. After the confirmation of malignant nature, we collected all related pre-operative biopsy samples. Fourteen cases from the authors' institutional archive from 2018 to 2021 were collected by two pathologists (JL and JK).

To estimate the prevalence of EWDA, we reviewed 608 consecutive surgically resected advanced gastric cancers (AGCs) treated at our institution in 2010. AGCs were selected because most of the archived cases were AGCs. Five of them (5 of 608, 0.08%) fulfilled the criteria for EWDA, thus total of 19 cases was available for our study design. Patient characteristics, surgical and endoscopic findings with follow-up data were obtained from the medical records of Asan Medical Hospital.

### Endoscopic assessment

Endoscopic data from available cases was collected and reviewed by expert gastroenterology specialist (JYA). The tumors were then classified as subepithelial-tumor-like lesions, slightly elevated or depressed lesions, or AGC Borrmann types according to the widely accepted endoscopic definition.

### Histologic assessment and statistical analysis

Hematoxylin and eosin-stained sections for pretreatment biopsies and surgical specimens were available for all, and two pathologists (JL and JK) independently evaluated their gross findings, histomorphology, pathologic TN stage, and lymphovascular invasion statuses. Any discrepancy was resolved in consensus sessions under a multiheaded microscope. The ulcer proportion, defined as area of gross ulceration divided by the area of the entire tumor, were calculated in surgically resected ulcerated EWDA and control group AGCs from the year 2010. We used a non-parametric test (Mann-Whitney) to determine the p-value for differences between the groups. Statistical analysis was performed using SPSS software ver. 18.0 (SPSS Inc., Chicago, IL, USA), with  $p \leq .05$  considered statistically significant.

All cases were evaluated and documented for the following histologic features observed in EWDA (Fig.1, Supplementary Fig. S1): inharmonious disproportionate glands, irregularly shaped glands, undulating apical mucin border, and markedly distended mucinous cytoplasm. Inharmonious disproportionate glands referred to glands disproportionately larger than surrounding non-neoplastic glands. Irregular glandular shapes indicated irregular glandular structures that were cut off or distorted. Un-

dulating mucin border described irregular, wobbly border of apical mucin caps. Markedly distended mucinous cytoplasm of EWDA cells indicated very large tumor cells sometimes exceeding 40 times the size of mature lymphocytes.

Background mucosa was also microscopically studied in terms of the presence of atrophic gastritis or intestinal metaplasia in adjacent mucosa. The time intervals between the initial biopsy and treatment, type of treatment, and the number of procedures performed were recorded. The original diagnoses of pretreatment biopsies were collected and compared with the final diagnoses.

### Immunohistochemical analysis

Formalin-fixed paraffin-embedded tissue blocks were available for all. To determine the tumor immunophenotype, immunohistochemical staining was performed using antibodies against MUC-5AC (1:100, mouse monoclonal, clone MRQ-19, catalog No.292M-96, Cell Marque, Rocklin, CA, USA), MUC-2 (1:50, mouse monoclonal, clone Ccp58, catalog No. NCL-MUC-2, Novocastra, Newcastle upon Tyne, UK), MUC-6 (1:200, mouse monoclonal, clone CHL5, catalog No. NCL-MUC-6, Novocastra), CDX-2 (1:500, mouse monoclonal, clone EPR2764Y, catalog No. 235R-16, Cell Marque), c-erbB2 (1:8, mouse monoclonal, clone 4B5, catalog No. 790-4493, Ventana, Tusan, AZ, USA), p53 (1:1,000, clone DO-7, Dako, Glostrup, Denmark), Ki-67 (1:200, mouse monoclonal, clone MIB1, catalog No. M7240, Dako) and PTEN (1:100, rabbit monoclonal, clone 138G6, catalog No. 9559, Cell Signaling, Danvers, MA, USA). Expression of mucin core proteins and CDX-2 were investigated to help classification of tumors into gastric- or intestinal- subtypes. C-erbB2 immunohistochemistry was done to find out the potential therapeutic targets. We did p53 and Ki-67 immunohistochemistry to determine their helpfulness in identifying the EWDA. Finally, PTEN immunohistochemistry was performed to confirm the PTEN protein expression loss in the case (case No. 3) with a certain *PTEN* mutation. All staining procedures were performed using a Ventana autostainer according to the manufacturer's instructions.

Cytoplasmic staining for mucin core proteins (MUC5AC, MUC2, and MUC6) and nuclear staining for CDX-2 were considered positive. C-erbB2 staining was evaluated based on traditional human epidermal growth factor receptor 2 (HER2) immunohistochemistry scoring guidelines [3]. Cases scored equivocal for C-erbB2 were tested for HER2 gene copy-number by silver-enhanced in situ hybridization. For scoring, we followed general guidelines for HER2 copy-number evaluation as described by Jeong et al. [4]. Two pathologists (JL and JK) independently scored

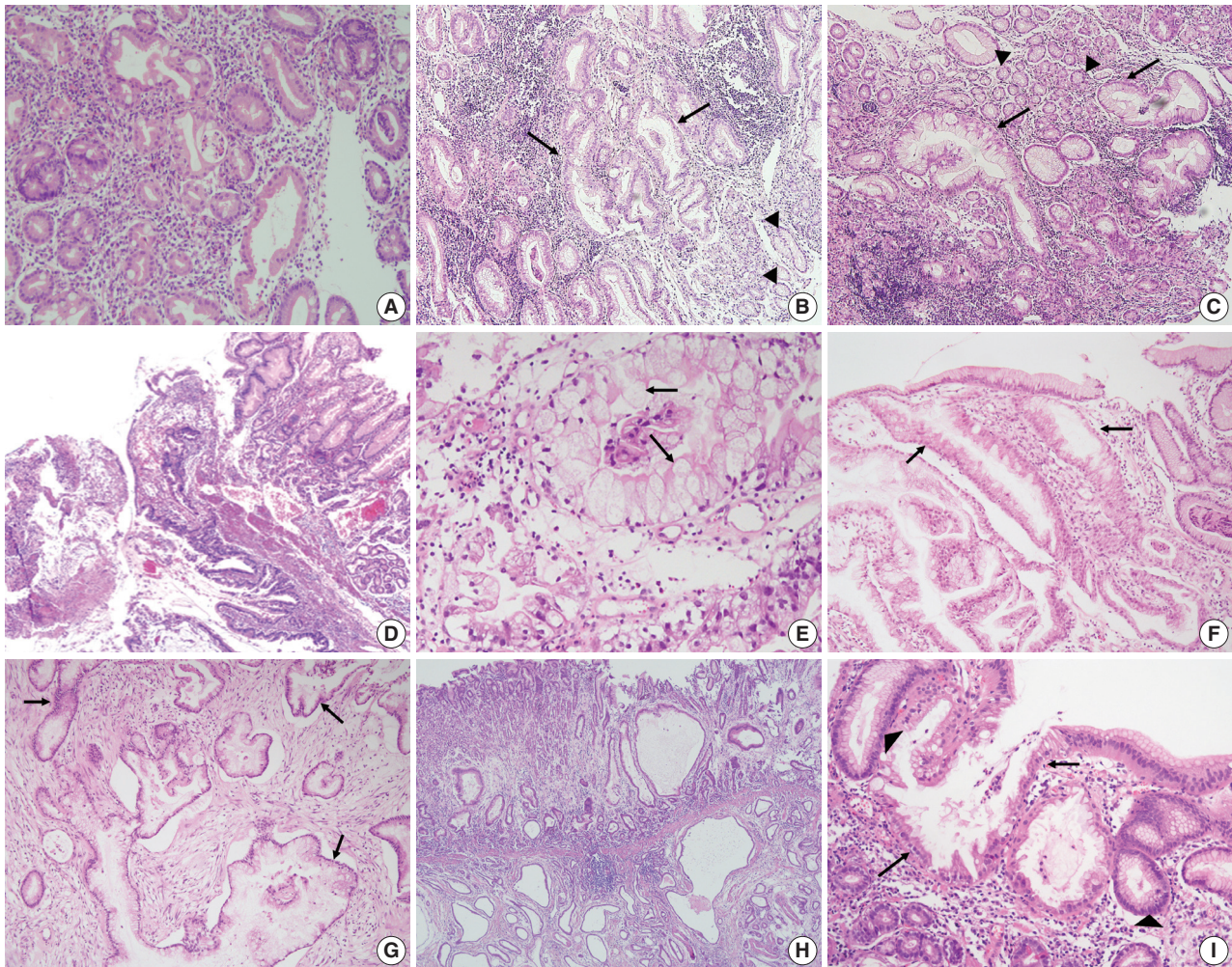


**Fig. 1.** Representative photomicrographs of extremely well-differentiated adenocarcinoma (EWDA). (A) Intestinal-type EWDA featuring goblet cells is observed in case No. 12. (B) Irregularly shaped glands (arrows) opposed to normal foveolar glands (arrowheads) are observed in case No. 4. (C) Inharmoniously large glands (arrows) are noticeable against benign foveolar glands (arrowheads) in case No. 4. (D) A focal mucosal opening giving way to larger, deeply seated glands is noted, resembling lobular endocervical glandular hyperplasia of the uterine cervix (case No. 17). (E) Extremely large neoplastic glands, at least 20 times the size of normal lymphocytes, are noted in case No. 2. An undulating apical mucinous border is also observed (arrows). (F, G) Case No. 3 shows bland-looking gastric-type EWDA glands (arrows) both in gastric (F) and omental biopsy specimens (G). (H) Case No. 11 shows cystically dilated thin neoplastic glands invading the muscularis propria with gastritis cystica profunda-like portions in the submucosa. (I) Glandular cancerization (arrows) in the background of normal foveolar glands (arrowheads) is more commonly found in EWDA than in conventional gastric carcinomas.

the immunostaining, and any discrepancy was resolved by consensus. Selective next-generation sequencing (NGS) data were available for three cases (case Nos. 2, 3, and 9). NGS was performed according to our routine clinical targeted cancer panel as described previously [5].

## RESULTS

### Clinicopathologic features

The clinical information of the 19 cases were listed in Table 1.

The median age of the patients was 63 years (range, 31 to 81 years) and the male to female ratio was 5.3:1 (16:3). The majority of the tumors (15 of 19, 79.0%) were located in the body of stomach in contrast to the usual type gastric carcinomas in which antral location is more common. The median tumor size in the resected cases was 4.0 cm in the greatest dimension (range, 2.2 to 10.0 cm). Most of the cases were clinically or pathologically proven AGCs (18 of 19, 94.7%).

Most patients were treated with surgery and adjuvant chemotherapy (11 of 19, 57.9%). Surgery alone was performed in two

**Table 1.** Clinical information of 19 cases of EWDA

Case No.	Age (yr)	Sex	Treatment	Follow-up (mo)	Status
1	77	F	ESD	17	NED
2	66	F	Chemotherapy	19	AWD
3	31	M	Chemotherapy	0.5	DOD
4	56	F	Surgery <sup>a</sup>	35	AWD
5	60	M	Surgery <sup>a</sup>	28	NED
6	62	M	Surgery <sup>a</sup>	23	NED
7	39	M	Surgery <sup>a</sup>	26	NED
8	67	M	Chemotherapy	14	DOD
9	72	M	Surgery <sup>a</sup>	26	AWD
10	69	M	Surgery <sup>a</sup>	16	NED
11	58	M	Surgery <sup>a</sup>	8	NED
12	61	M	Surgery <sup>a</sup>	15	NED
13	48	M	Chemotherapy <sup>b</sup>	13	NA
14	63	M	Surgery <sup>a</sup>	80	NA
15	79	M	Surgery <sup>c</sup>	121	NA
16	65	M	Surgery <sup>a</sup>	70	NA
17	81	M	Surgery <sup>a</sup>	79	DOD
18	55	M	Surgery <sup>c</sup>	15	NA
19	66	M	Surgery <sup>c</sup>	15	NED

EWDA, extremely well-differentiated adenocarcinoma; F, female; ESD, endoscopic submucosal dissection; NED, no evidence of disease; AWD, alive with disease; M, male; mo, months after diagnosis; DOD, died of disease; NA, not available (cannot be assessed).

<sup>a</sup>Surgery and adjuvant chemotherapy; <sup>b</sup>Chemotherapy and metastatectomy (right hemicolectomy); <sup>c</sup>Surgery alone.

patients (2 of 19, 10.5%). Four of the five initially metastatic cases received chemotherapy without gastric resection (4 of 19, 21.1%). Endoscopic submucosal dissection was performed on the EGC (case 1, 1 of 19, 5.3%). The majority of the surgically resected AGC cases infiltrated to the subserosa (pT3, 7 of 14, 50.0%). The other cases penetrated to the serosa (pT4a, 4 of 14, 28.6%) or invaded muscularis propria (pT2, 3 of 14, 21.4%). The EGC case invaded the submucosa (pT1b). Lymphovascular invasion was present in some resected specimens including the EGC case (5 of 15, 33.3%). Nodal metastasis was histologically identified in some of the surgically resected cases (5 of 15, 33.3%). Only one (case No. 14) of such cases showed a very minor (< 1%) component of moderately differentiated adenocarcinoma. Even in the metastatic lymph nodes, the tumors retained their extremely well-differentiated morphology.

Patients were followed up for variable time intervals, ranging from 0.5 to 121 (median, 19 months) (Table 1). Some patients were alive without evidence of disease at last contact (8 of 19, 42.1%), while others were lost to follow-up (5 of 19, 26.3%). Of the five patients with distant metastasis at the time of diagnosis, the majority died of the disease at 5 months, 12 months, and 15 months after initial chemotherapy (3 of 19, 15.7%). The others were alive with disease at last contact (3 of 19, 15.7%).

**Table 2.** Pathologic and endoscopic information of 19 cases of EWDA

Case No.	Tumor size, greatest dimension (mm)	Location	Endoscopic impression	Mucosal ulceration	Macroscopic finding <sup>a</sup>	T/N	Distant metastasis <sup>b</sup>	Lymphovascular invasion
1	33	Body	SET	Absent	EGC IIa	T1b/Nx	Absent	Present
2	NA	Body	SET	Absent	Borrmann 1	T2/N+ <sup>b</sup>	Present	NA
3	NA	Body	SET	Absent	Borrmann 1	T3/N+	Present	NA
4	50	Body	Slight elevation	Absent	Borrmann 3	T3/N1	Absent	Absent
5	25	Body	Slight elevation	Absent	Borrmann 1	T4a/N0	Absent	Present
6	40	Cardia	Typical Borrmann 3	Present	Borrmann 3	T3/N3a	Absent	Absent
7	22	Body	Slight elevation	Absent	AGC mimicking EGC type IIa	T3/N0	Absent	Absent
8	NA	Body	Borrmann 4	Absent	Borrmann 4	T3/N+	Present	NA
9	100	Body	Slight elevation	Absent	Borrmann 4	T3/N0	Present	Absent
10	40	Body	Slight elevation	Absent	Borrmann 3	T3/N0	Absent	Present
11	33	Body	Slight elevation	Absent	AGC mimicking EGC type IIa	T4a/N0	Absent	Present
12	52	Body	Slight depression	Absent	AGC mimicking EGC type IIc	T4a/N0	Absent	Absent
13	NA	Body	Borrmann 4	Absent	Borrmann 4	T2N+	Present	NA
14	57	Antrum	Typical Borrmann 2	Present	Borrmann 2	T3N2	Absent	Absent
15	33	Body	Typical Borrmann 3	Present	Borrmann 3	T2N0	Absent	Absent
16	65	Body	NA	Present	Borrmann 3	T4aN3	Absent	Present
17	25	Cardia	SET	Present	Borrmann 1	T3N1	Absent	Present
18	33	Cardia	Typical Borrmann 3	Present	Borrmann 3	T2N0	Absent	Absent
19	30	Body	Slight elevation	Absent	Borrmann 4	T2N0	Absent	Absent

EWDA, extremely well-differentiated adenocarcinoma; SET, subepithelial tumor; EGC, early gastric cancer; NA, cannot be assessed; AGC, advanced gastric cancer.

<sup>a</sup>Macroscopic finding was classified according to World Health Organization criteria; <sup>b</sup>N+, clinically assessed nodal metastasis.

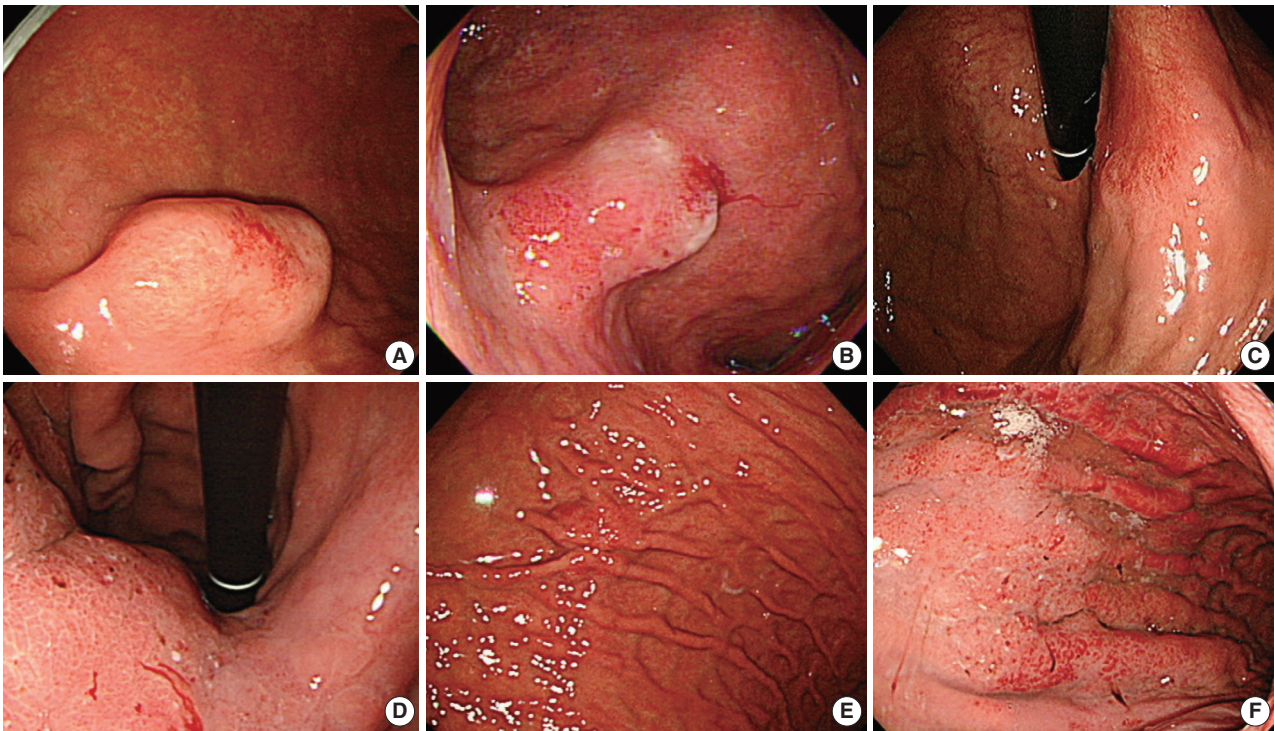


**Fig. 2.** Endoscopic appearances of diagnostically difficult extremely well-differentiated adenocarcinoma cases. (A) A mucosal elevation with mostly intact mucosa simulating a subepithelial tumor is noted (case No. 1). (B) A slightly elevated lesion with vascular engorgement is noted at angle (case No. 6). (C) A slightly depressed lesion is observed in case No. 12. (D) Diffusely thickened gastric wall in the gastric body is observed (case No. 9). (E) A slightly elevated mass is identified in case No. 7. (F) Thickened gastric folds with vascular engorgement (endoscopically Borrmann type 4) are seen in case No. 13.

### Macroscopic findings

Eighteen cases with available endoscopic data were studied for endoscopic impressions (Table 2, Fig. 2). In two-thirds of the cases, malignant nature was not easily recognizable even by an experienced gastroenterologist (JYA) (Endoscopically assessed Borrmann type 3, 3 of 18 [16.6%], Borrmann type 4, 2 of 18 [11.1%], and Borrmann type 2, 1 of 18 [5.6%]) (Fig. 2). Compared to usual gastric adenocarcinomas, EWDA more frequently showed Borrmann type 4 and 1 lesions in surgically resected specimens (Borrmann type 4, 4 of 18 [22.2%] and Borrmann type 1, 4 of 18 [22.2%]) with less frequent ulcer formation. Also, ulcer proportions of Borrmann type 2 and 3 EWDA were significantly lower than those of control group AGCs (mean value, 28.0% vs. 57.3%,  $p = .0048$ ) (Supplementary Table S1, Supplementary Fig. S2).

### Histologic assessment

Most of the cases were histologically gastric-type (13 of 19 [68.4%]), while the others were intestinal-type EWDA (6 of 19 [31.6%]) (Table 3). Irregular glandular shape was universally present (19 of 19 [100%], pretreatment biopsy; 19 of 19 [100%],

surgically resected specimen), and inharmonious glands were present in the majority (9 of 19 [47.4%], pretreatment biopsy; 11 of 19 [57.9%], surgically resected specimen). About half of the cases showed undulating mucin borders (11 of 19 [57.9%], pretreatment biopsy; 12 of 19 [63.1%], surgically resected specimen) or distended mucins (8 of 19 [42.1%], pretreatment biopsy; 9 of 19 [47.4%], surgically resected specimen). Hyperplastic polyps showed distended mucin in some (6 of 19 [31.6%]) but other descriptive findings of EWDA were not present. Intestinal metaplasias in the adjacent background mucosa tended to be more frequently observed in intestinal-type EWDA than in gastric-type EWDA (gastric-type EWDA, 4 of 13 [30.8%] vs. intestinal-type EDWA, 4 of 6 [66.7%],  $p = .238$ ) (Table 3).

Histologic characteristics worth mentioning in each case were separately recorded (Fig. 1, Supplementary Fig. S1). Case No. 2 exhibited exceptionally large cells with mucin distention, which were approximately 20 times the size of mature lymphocytes. Case No. 3 showed deceptively benign-looking cells with small nuclei, simulating normal foveolar gland epithelium. The same cells were also noted in the patient's omental biopsy indicating metastasis. In case No. 4, the neoplastic glands were cystically

**Table 3.** Histologic and immunohistochemical features of 19 cases of EWDA

Case No.	Histologic type	Hyperplastic polyp (biopsy)	Histologic features in pretreatment biopsies	Histologic features in surgical specimens	Background mucosa in pretreatment biopsies	Background mucosa in surgical specimens
1	Gastric	M	S, U	M, S, U	Atrophy	Atrophy
2	Gastric	-	M, S, U	NA	-	NA
3	Gastric	-	M, S, U	NA	-	NA
4	Gastric	-	I, M, S, U	I, M, S, U	-	-
5	Gastric	M	M, S, U	M, S, U	-	IM
6	Gastric	-	M, S, U	M, S, U	-	-
7	Intestinal	-	S	S	-	-
8	Gastric	M	I, M, S, U	NA	IM	NA
9	Intestinal	-	I, S, U	I, S, U	-	-
10	Gastric	-	I, S	I, S	-	IM
11	Gastric	-	I, S	I, S, U	-	-
12	Intestinal	M	S, U	I, S, U	IM	IM
13	Gastric	-	S, U	I, M, S, U	IM	Atrophy, IM
14	Gastric	-	I, M, S	I, M, S	-	IM
15	Intestinal	-	S	I, S	IM	IM
16	Gastric	-	I, M, S, U	I, M, S, U	-	-
17	Gastric	M	S	S	-	-
18	Intestinal	-	I, S	I, S	IM	IM
19	Intestinal	M	I, S	I, S	IM	IM

EWDA, extremely well-differentiated adenocarcinoma; I, inharmonious disproportionate glands; M, distended mucin; S, irregular glandular shape; U, undulating apical mucin border; NA, not available; IM, intestinal metaplasia.

dilated progressing towards the serosa. Case No. 11 showed mucosal cystic glands invading muscularis propria with gastritis cystica profunda-like morphology.

The epicenters of EWDAs were in the deeper mucosa or submucosa with infrequent ulcer formation. The overlying mucosa was without ulcer but involved by frequent glandular cancerization (Fig. 1I), or focal mucosal openings leading to large, deeply seated glands (Fig. 1D). The latter pattern was reminiscent of lobular endocervical glandular hyperplasia of the uterine cervix. It was also remarkable that desmoplastic reactions were barely observed.

#### Differentiation from non-neoplastic foveolar glands

Regarding differential diagnosis between gastric-type EWDAs and hyperplastic foveolar glands, we focused on three histologic features: (1) irregular glandular shape, (2) irregular spacing of nuclei, and (3) disruption of four lines. Irregular glandular shape was present in all EWDAs in contrast to hyperplastic polyps (Table 3). Irregular spacing of the nuclei was a distinct feature of EWDA, which referred to scattered nuclei not aligned to the basement membrane with disrupted polarity (Fig. 3). Four lines of the foveolar epithelium, formed by the apical mucin cap, base of the mucin cap, cytoplasm and nucleus [6] were disrupted or disappeared in EWDA glands.

#### Molecular features

All 19 cases were variably positive for gastric markers (Fig. 4, Supplementary Table S2). Positive MUC5AC and CDX-2 immunolabeling were closely associated with histological gastric- and intestinal-type EWDAs, respectively. MUC6 and MUC2 expressions were not prominent in both subtypes, unlike the immunohistochemical profile of usual type gastric adenocarcinomas with diffuse expression of either markers. On an immunohistochemical basis, 13 (68.4%) and six (31.6%) cases showed gastric- and intestinal-phenotypes, identical to the histological classifications (Supplementary Table S2). Although p53 and Ki-67 immunolabelings were mildly increased relative to normal foveolar epithelial cells, it was not distinct enough. Instead, their staining patterns were helpful because EWDAs showed diffusely increased staining patterns while benign glands showed locally increased staining in proliferative zones (Fig. 3E, F). C-erbB2 was equivocally expressed in two (case Nos. 2 and 13), but the silver in situ hybridization results were negative.

There also were a few cases with targeted cancer panel sequencing results (case Nos. 2, 3, and 9). A few notable mutations were found: *NRAS* G12D, *STK11* Q220Pfs\*38 (case No. 2), *PTEN* L108R and Y178C (case No. 3), and *KRAS* G12D (case No. 9) (Supplementary Table S3). Even though the functional significance of the *PTEN* L108R and Y178C mutations is not known,

the loss of PTEN protein expression in this tumor (Fig. 4D) suggested at least one of the two *PTEN* mutations be loss of function mutation.

### Evaluation of pretreatment biopsies

One to eight pre-therapeutic endoscopic examinations were performed in 19 patients (median, 2; mean, 2.5). A total of 55

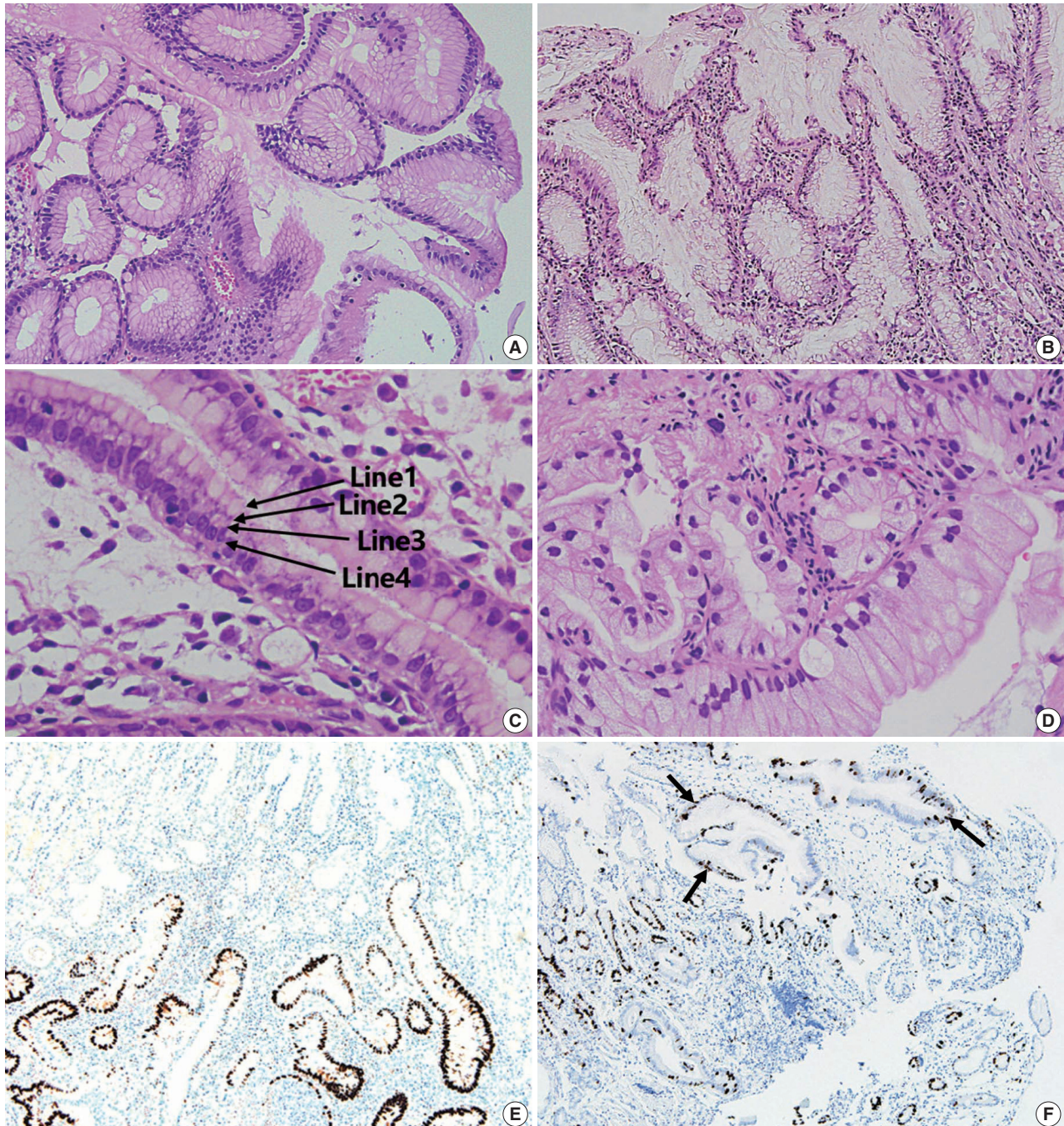


**Fig. 3.** Comparison between extremely well-differentiated adenocarcinoma (EWDA) and its mimickers. (A) Hyperplastic polyp shows an organized gland shape and aligned nuclei. (B) EWDA glands (case 4) show an irregular glandular shape and irregular nuclear spacing. (C) Normal foveolar epithelium displays regular nuclear spacing with maintenance of the “4 lines” (arrows): line 1, the gastric-type mucin vacuole; line 2, the base of the mucin vacuole; line 3, the cytoplasm; and line 4, the nuclei. (D) Case No. 6 shows large tumor cells with ample mucin, hyperchromatic nuclei, and disrupted four lines. (E) p53 expression is markedly increased in the tumor cells in contrast to the background foveolar epithelium of case No. 7 (p53 immunohistochemistry). (F) Ki-67 in normal foveolar epithelium shows increased expression only along the base of the crypts while the tumor glands (arrows) show a diffuse increase in case No. 8 (Ki-67 immunohistochemistry).

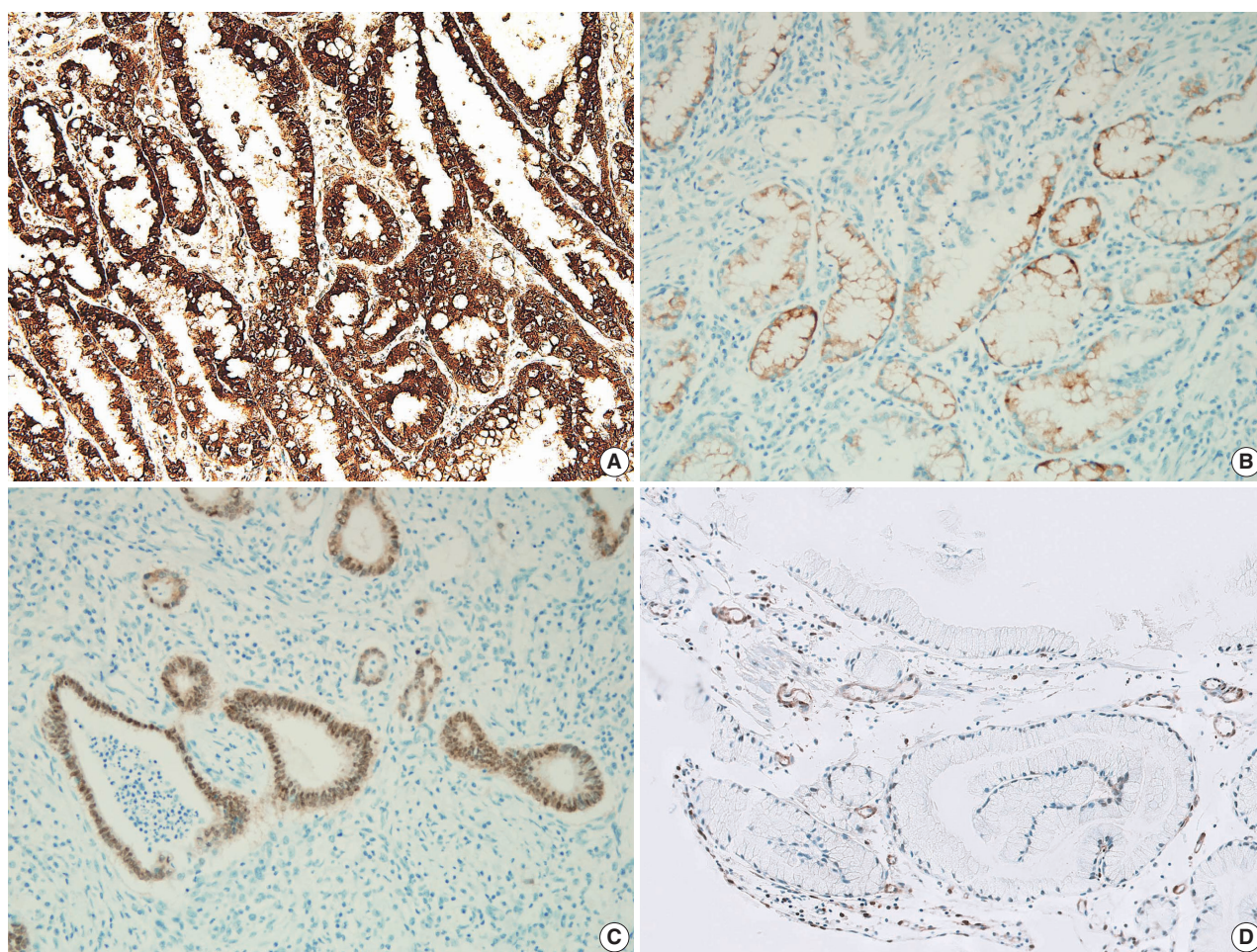


**Fig. 4.** Immunohistochemical pattern of extremely well-differentiated adenocarcinoma (EWDA). (A) Gastric-type EWDA expresses diffuse MUC5AC immunoreactivity in case 5. (B) MUC6 is focally expressed in case No. 5. (C) CDX-2 shows diffuse nuclear expression in an intestinal-type EWDA (case No. 7). (D) PTEN is lost in this PTEN mutant large cancer cells in contrast to the normal expression in endothelial cells in case No. 3.

tissue biopsies from 19 patients were available for review. The original diagnoses were ‘adenocarcinoma’ or ‘suspect for adenocarcinoma’ in 46 biopsies (46 of 55, 84%). Retrospective review of the remaining 11 specimens revealed that 10 of them were initially misdiagnosed (Supplementary Table 4).

## DISCUSSION

EWDA consists of bland-looking malignant cells which is difficult to diagnose and less discussed in the literature. In our study, EWDA were deep-seated tumors in the body of the stomach with less ulcer formation. It was also notable that endoscopically slightly elevated lesions or subepithelial tumor-like lesions were common, which is rarely suspected for malignancy by endoscopists [7,8]. Four histologic features including irregular glandular shape, undulating apical mucin border, and inharmonious glands

and distended mucin were key histologic features of EWDA. In addition, irregular nuclear spacing and disruption of the four lines were helpful in discriminating of gastric-type EWDA from hyperplastic foveolar glands. We believe that our study would help pathologists recognize this deceptively bland subtype of gastric adenocarcinoma.

Less ulcer formation of EWDA could be explained by its undermining growth pattern. The findings were consistent with previous reports which mentioned EWDA preferentially growing beneath the mucosa, forming polypoid masses [1]. Lobular endocervical glandular hyperplasia-like glands in the submucosa, also noted in other studies, were frequently observed accounting for frequent mucosal sparing of EWDA [1,2]. Those findings suggest that some of the EWDA cases might have been originated from a deeper part of the mucosa.

Gastric-type EWDA are especially cryptic because it simu-

lates hyperplastic foveolar glands, and in many circumstances the distinction should be made in small gastric forceps biopsies. Undulating apical mucin border, along with irregular glandular shape, irregular nuclear spacing, and the disruption of four lines of foveolar epithelium, should strongly suggest EWDA especially in ambiguous endoscopic settings. Mucin distension, although present in many EWDA, was sometimes seen in hyperplastic polyps and only marked mucinous distention sizing more than  $\times 20$  that of adjacent lymphocytes would help in differential diagnoses. Inharmoniously large glands in EWDA, as in our cases, also have been described in the literature [1,2], so atypically large or distinct glands should also raise concern for EWDA. Furthermore, even though intestinal metaplasias were rare adjacent to gastric-type EWDA, its pathogenetic significance is yet to be discussed.

One helpful immunohistochemical marker might be Ki-67, because the labeling index was randomly increased in the carcinoma cells in contrast to reactive lesions with only basal cryptal increase, consistent with the findings by Niimi et al. [9]. Another useful marker might be p53 because its expression was increased against the background gastric foveolar epithelium in EWDA [9], although null- or diffuse-type mutation pattern p53 immunolabeling [10] was not identified. Treatment-wise, C-erbB2 expression or actionable genetic alterations were not found in any. Further studies for the therapeutic targets are recommended in the future.

One of the limitations to our study is that the control group of AGC cases were retrieved from a different time period, due to the extreme rarity of EWDA cases. Furthermore, systematic quantitative analyses could not be performed because our study was focused on the morphologic diagnosis of very rare EWDA cases. Also, selection bias towards AGCs occurred because unequivocally metastatic cases were selectively included in the study design. The referral bias as a tertiary medical institution also contributed. Furthermore, NGS results are available only in a small portion of our cases. Patients lost to follow-up also posed problems because prognostic data could not be gathered sufficiently. We suggest that proper epidemiologic data of this rare neoplasm be assessed by a prospective, multi-center study in the future.

In conclusion, EWDA were endoscopically ambiguous elevated tumors with an undermining growth pattern and few ulcers. Mucosal glandular cancerization and submucosal lobular endocervical glandular hyperplasia-like growth pattern were frequently observed histologic patterns. The microscopic features such as irregular glandular shapes, inharmonious glands, glands with ample mucin distension, and undulating apical border were

frequently observed in EWDA. For the timely diagnosis of these deeply seated tumors, generous forceps biopsies are recommended.

### Supplementary Information

The Data Supplement is available with this article at <https://doi.org/10.4132/jptm.2021.10.12>.

### Ethics Statement

Our study was approved by the Institutional Review Board of the Asan Medical Center (#2021-0485) with a waiver of the requirement for informed consent.

### Availability of Data and Material

The datasets generated or analyzed during the study are available from the corresponding author on reasonable request.

### Code Availability

Not applicable.

### ORCID

Jongwon Lee	<a href="https://orcid.org/0000-0003-3057-7874">https://orcid.org/0000-0003-3057-7874</a>
In-Seob Lee	<a href="https://orcid.org/0000-0003-3099-0140">https://orcid.org/0000-0003-3099-0140</a>
Ji Yong Ahn	<a href="https://orcid.org/0000-0002-0030-3744">https://orcid.org/0000-0002-0030-3744</a>
Young Soo Park	<a href="https://orcid.org/0000-0001-5389-4245">https://orcid.org/0000-0001-5389-4245</a>
Jihun Kim	<a href="https://orcid.org/0000-0002-8694-4365">https://orcid.org/0000-0002-8694-4365</a>

### Author Contributions

Conceptualization: JL, JK, YSP, ISL, JYA. Data curation: JK, JL. Methodology: JL, JK, YSP, ISL, JYA. Writing—original draft: JL, JK. Writing—review & editing: JK, JL. Approval of final manuscript: all authors.

### Conflicts of Interest

The authors declare that they have no potential conflicts of interest.

### Funding Statement

No funding to declare.

### References

1. Yao T, Utsunomiya T, Oya M, Nishiyama K, Tsuneyoshi M. Extremely well-differentiated adenocarcinoma of the stomach: clinicopathological and immunohistochemical features. *World J Gastroenterol* 2006; 12: 2510-6.
2. Joo M, Han SH. Gastric-type extremely well-differentiated adenocarcinoma of the stomach: a challenge for preoperative diagnosis. *J Pathol Transl Med* 2016; 50: 71-4.
3. Kim KM, Bilous M, Chu KM, et al. Human epidermal growth factor receptor 2 testing in gastric cancer: recommendations of an Asia-Pacific task force. *Asia Pac J Clin Oncol* 2014; 10: 297-307.
4. Jeong JH, Kim J, Hong YS, et al. *HER2* amplification and cetuximab efficacy in patients with metastatic colorectal cancer harboring wild-type RAS and BRAF. *Clin Colorectal Cancer* 2017; 16: e147-52.
5. Hong YS, Kim J, Pectasides E, et al. Src mutation induces acquired lapatinib resistance in *ERBB2*-amplified human gastroesophageal adenocarcinoma models. *PLoS One* 2014; 9: e109440.
6. Waters KM, Salimian KJ, Voltaggio L, Montgomery EA. Refined criteria for separating low-grade dysplasia and nondysplastic Barrett esophagus reduce equivocal diagnoses and improve prediction

- of patient outcome: a 10-year review. *Am J Surg Pathol* 2018; 42: 1723-9.
7. WHO Classification of Tumours Editorial Board. WHO classification of tumours of the digestive system tumours. Lyon: IARC Press, 2019.
  8. Humphris JL, Jones DB. Subepithelial mass lesions in the upper gastrointestinal tract. *J Gastroenterol Hepatol* 2008; 23: 556-66.
  9. Niimi C, Goto H, Ohmiya N, et al. Usefulness of p53 and Ki-67 immunohistochemical analysis for preoperative diagnosis of extremely well-differentiated gastric adenocarcinoma. *Am J Clin Pathol* 2002; 118: 683-92.
  10. Nakayama T, Ling ZQ, Mukaisho K, Hattori T, Sugihara H. Lineage analysis of early and advanced tubular adenocarcinomas of the stomach: continuous or discontinuous? *BMC Cancer* 2010; 10: 311.

# Fatty acid synthetase expression in triple-negative breast cancer

Jin Hee Park<sup>1</sup>, Hye Seung Han<sup>1</sup>, So Dug Lim<sup>1</sup>, Wook Youn Kim<sup>1</sup>, Kyoung Sik Park<sup>2</sup>,  
Young Bum Yoo<sup>2</sup>, Seung Eun Lee<sup>1</sup>, Wan-Seop Kim<sup>1</sup>

Departments of <sup>1</sup>Pathology and <sup>2</sup>Surgery, Konkuk University Medical Center, Konkuk University School of Medicine, Seoul, Korea

**Background:** Triple-negative breast cancer (TNBC) has a relatively poor prognosis. Research has identified potential metabolic targets, including fatty acid metabolism, in TNBC. The absence of effective target therapies for TNBC led to exploration of the role of fatty acid synthetase (FASN) as a potential target for TNBC therapy. Here, we analyzed the expression of FASN, a representative lipid metabolism-related protein, and investigated the association between FASN expression and Ki-67 and the programmed death ligand 1 (PD-L1) biomarkers in TNBC. **Methods:** Immunohistochemical expression of FASN was analyzed in 166 patients with TNBC. For analytical purposes, patients with 0–1+ FASN staining were grouped as low-grade FASN and patients with 2–3+ FASN staining as high-grade FASN. **Results:** FASN expression was observed in 47.1% of TNBC patients. Low and high expression of FASN was identified in 75.9% and 24.1%, respectively, and no statistically significant difference was found in T category, N category, American Joint Committee on Cancer stage, or recurrence rate between the low and high-FASN expression groups. Ki-67 proliferation level was significantly different between the low and high-FASN expression groups. FASN expression was significantly related to Ki-67 as the level increased. There was no significant difference in PD-L1 positivity between the low- and high-FASN expression groups. **Conclusions:** We identified FASN expression in 166 TNBC patients. The Ki-67 proliferation index was positively correlated with FASN level, indicating higher proliferation activity as FASN increases. However, there was no statistical association with PD-L1 SP142, the currently FDA-approved assay, or FASN expression level.

**Key Words:** Triple-negative breast neoplasms; FASN; Immunohistochemistry; Ki-67; PD-L1 SP142

**Received:** September 29, 2021 **Revised:** October 20, 2021 **Accepted:** October 27, 2021

**Corresponding Author:** Seung Eun Lee, MD, PhD, Department of Pathology, Konkuk University Medical Center, Konkuk University School of Medicine, 120-1 Neungdong-ro, Gwangjin-gu, Seoul 05030, Korea

Tel: +82-2-2030-5644, Fax: +82-2-2030-5629, E-mail: 20150063@kuh.ac.kr

**Corresponding Author:** Wan-Seop Kim, MD, PhD, Department of Pathology, Konkuk University Medical Center, Konkuk University School of Medicine, 120-1 Neungdong-ro, Gwangjin-gu, Seoul 05030, Korea

Tel: +82-2-2030-5642, Fax: +82-2-2030-5629, E-mail: wskim@kuh.ac.kr

Triple-negative breast cancer (TNBC) is defined by a loss of expression of estrogen receptor (ER), progesterone receptor (PR), and human epidermal growth factor receptor 2 (HER-2) [1]. TNBC accounts for about 15% of all breast cancers [2]. TNBC has relatively poor prognosis compared to non-TNBC patients, resulting from a lack of specific treatment methods such as hormone treatment or targeted treatment other than non-specific chemotherapy [3]. TNBC is a heterogeneous group of tumors with different molecular drivers and prognosis, clinical outcomes, and responses to therapy [4]. Various inhibitors, including poly (ADP-ribose) polymerase (PARP), growth factor, Scr, mammalian target of rapamycin (mTOR), and phosphoinositide 3-kinase (PI3K) inhibitors, are intended to increase treatment effectiveness [5]. Based on the high level of programmed death ligand 1 (PD-

L1) expression in TNBC, chemotherapy such as atezolizumab and nab-paclitaxel has been approved by the Food and Drug Administration (FDA) as the first-line treatment in breast cancer patients with locally advanced and metastatic TNBC [6]. Atezolizumab plus nab-paclitaxel-treated patients are linked to improved clinical outcome [7].

The study of metabolic pathways in TNBC is also active, and studies [8] have shown that potential metabolic targets of TNBC include glucose metabolism, fatty acid metabolism, glutamine metabolism, and serine metabolism. Gong et al. [9] identified three metabolic pathway-based TNBC subtypes with distinct molecular features and sensitivities to various metabolic inhibitors, and it was shown that inhibition of lactate dehydrogenase could enhance the anti-programmed death-1 immunotherapy

response in a certain TNBC subtype. Cha et al. [10] identified lipid metabolism–related proteins in breast cancer. Of them, fatty acid synthetase (FASN) is a lipid-producing enzyme that is expressed at low level in normal human tissues but is reported to be highly expressed in breast, colon, prostate, and ovarian cancer [11–14]. The role of FASN as a prognostic factor in breast cancer has been published in previous studies [15,16].

However, few studies have identified the expression of FASN level in TNBC [15,16]. The absence of effective targeted therapy for TNBC and its poor prognosis led to exploration of the role of FASN as a potential target for TNBC therapy [17]. Here, we analyzed the expression of FASN, a representative lipid metabolism–related protein, and the association between FASN level and Ki-67 and PD-L1 expression in patients with aggressive TNBC breast cancer.

## MATERIALS AND METHODS

Among ER- and HER-2–negative breast cancer patients, 166 patients who could be tracked and whose paraffin embedded tissue blocks were in good condition were enrolled in the study. Patient clinical records were used in a retrospective manner to identify clinical information including age, immunohistochemical study, TNM stage, recurrence, chemotherapy, and radiation therapy. We also wanted to quantify the degree of expression and correlate it with clinical information through immunostaining of FASN.

### Patient selection and clinicopathologic evaluation

From January 2012 to December 2018, 166 TNBC patients who underwent primary breast cancer surgical resection at Konkuk University Medical Center (KUMC) Seoul, Korea, were analyzed. Clinicopathological information was obtained by reviewing medical records and hematoxylin and eosin (H&E)–stained sections. The TNBC histopathological data were determined by histological subtype, category T, category N, American Joint Committee on Cancer (AJCC) stage, and Bloom-Richardson histological grade.

### Tissue microarray

All 166 H&E-stained slides were reviewed, and the most representative part of each was selected. Two 3 mm tissue cores derived from representative tumors of formalin-fixed paraffin-embedded tissue blocks were collected. An on-slide control tissue (tonsillar tissue) was used.

### Immunohistochemistry

Immunohistochemistry (IHC) was performed using a Ventana Discovery XT automated slide stainer (Ventana Medical Systems, Tucson, AZ, USA), following antigen retrieval with Cell Conditioning 1 (CC1; citrate buffer pH 6.0, Ventana Medical System) at 37°C for 32 minutes. This was followed by a standard Ventana signal amplification and counterstaining with hematoxylin. Slides were mounted and examined by light microscopy. Appropriate positive and negative controls for IHC were included. We used anti-fatty acid synthase antibodies (Abcam, Cambridge, UK) and SP142 antibodies (Ventana, Mannheim, Germany) in this study.

### Interpretation of IHC results

All IHC markers were determined using light microscopy to assess the proportion and intensity of stained cells. In this study, we classified breast cancer phenotypes according to ER, PR, and HER-2 IHC results and Ki-67 [18]. ER and PR positivity were used to define a cutoff value of 1% positively-stained nuclei [19]. HER-2 staining was analyzed according to the American Society of Clinical Oncology (ASCO)/College of American Pathologists guidelines [20]. HER-2 expression was considered positive when strong (3+) membranous staining was observed, whereas cases with scores of 0 to 1+ were considered negative [10]. The results of immunohistochemical staining for lipid metabolism–related proteins were scored as previously described [21]. Briefly, FASN staining was considered positive when > 10% of the tumor cells were stained, and the intensity was scored from 0 to 3. For analytical purposes, patients with 0–1+ FASN staining were grouped as low-grade FASN and patients with 2–3+ FASN staining as high-grade FASN [15]. SP142 score was assessed as previously described [6].

### Statistical analysis

Data analysis was performed using SPSS ver. 20.0 (IBM Corp., Armonk, NY, USA) for Windows. Chi-square and Fisher's exact tests were used to assess continuous and categorical variables, respectively. Statistical significance was assumed at a p-value < .05. Kaplan-Meier survival curves and log-rank statistics were employed to evaluate the time interval to tumor metastasis and survival duration. A Cox proportional hazards model was used to assess the risk factors of shorter disease-free survival and overall survival.

## RESULTS

### Clinicopathological characteristics of TNBC

A total of 166 TNBC patient results were analyzed in this study, and the clinicopathological characteristics are presented in Table 1. The median age at diagnosis was 51 years (range, 28 to 83

**Table 1.** Clinicopathological characteristics of 166 patients with TNBC

Characteristics	No. of patients
Age (yr)	51 (28–83)
Age (yr)	
≤50	81 (48.8)
>50	85 (51.2)
Histologic type	
IDC, NOS	154 (92.8)
Carcinoma with medullary feature	8 (4.8)
Pleomorphic carcinoma	3 (1.8)
Metaplastic carcinoma	1 (0.6)
T category	
1	66 (39.8)
2	88 (53.0)
3	11 (6.6)
4	1 (0.6)
N category	
0	109 (65.7)
1	40 (24.1)
2	9 (5.4)
3	4 (2.4)
NA	4 (2.4)
Histologic grade	
1	0
2	24 (14.5)
3	142 (85.5)
AJCC stage	
1	33 (19.9)
2	110 (66.3)
3	19 (11.4)
N/A	4 (2.4)
Neoadjuvant CTx	
Yes	10 (6.0)
No	156 (94.0)
CTx	
Yes	154 (92.8)
No	12 (7.2)
RTx	
Yes	140 (84.3)
No	26 (15.7)
Recur	
Yes	26 (15.7)
No	140 (84.3)

Values are presented as median (interquartile range) or number (%). TNBC, triple-negative breast cancer; IDC, invasive ductal carcinoma; NOS, not otherwise specified; NA, not applicable; AJCC, American Joint Committee on Cancer; CTx, chemotherapy; RTx, radiation therapy.

years). The major histologic type of TNBC in KUMC was invasive ductal carcinoma (92.8%), with eight carcinomas with medullary features, three pleomorphic carcinomas, and one metaplastic carcinoma. About 85% of the cases were histologic grade 3, and 66% of the cases were AJCC stage 2. Of these 166 patients, 10 (6.0%) received neoadjuvant chemotherapy, 154 (92.8%) received adjuvant chemotherapy, and 140 (84.3%) received radiation therapy. Among the 166 patients, 26 (15.7%) recurred during follow-up observation. The median time until recurrence was 13.5 months.

### Expression of FASN in TNBC

Two pathologists independently observed and agreed to the final score values, and in some cases, IHC study was performed up to three times. The FASN expression levels in breast cancer patients were classified as grade 0, 1, 2, or 3 according to staining intensity. FASN expression was observed in 47.1% (95/166) of TNBC patients. Intensity grades of 1, 2, or 3 were seen in 33.1% (55/166), 13.3% (22/166), and 10.8% (18/166) of TNBC patients, respectively. Grades 0 and 1 were classified as the low-FASN group and grades 2 and 3 as the high-FASN group (Fig. 1). Low and high expression of FASN was identified in 75.9% (126/166) and 24.1% (40/166) of TNBC patients, respectively. Table 2 shows a comparison between the clinicopathological data of 40 patients with high FASN expression compared with that of 126 patients with low FASN expression. In the high-FASN expression group, more patients were younger than 50 years, while in the low-FASN group, more patients were older than 50 years old. The major cancer type was invasive ductal carcinoma and most were histologic grade 3; therefore, there was no association with high and low FASN expression. No statistically significant differences in T category, N category, AJCC stage, and recurrence rate were found between the high- and low-FASN expression groups.

### Correlation with immunohistochemical study of Ki-67

The Ki-67 proliferation level was statistically different between the FASN low and high expression groups, with median Ki-67 levels of 60% (range, 40% to 80%) and 73% (range, 55% to 87%), respectively, using the Mann-Whitney U test ( $p = .003$ ) (Table 3). The Spearman correlation coefficient was 0.257, indicating weak correlation between Ki-67 proliferation level and FASN expression level ( $p = .001$ ).

### Correlation with PD-L1 SP142 IHC assay

Two pathologists independently observed and agreed to the

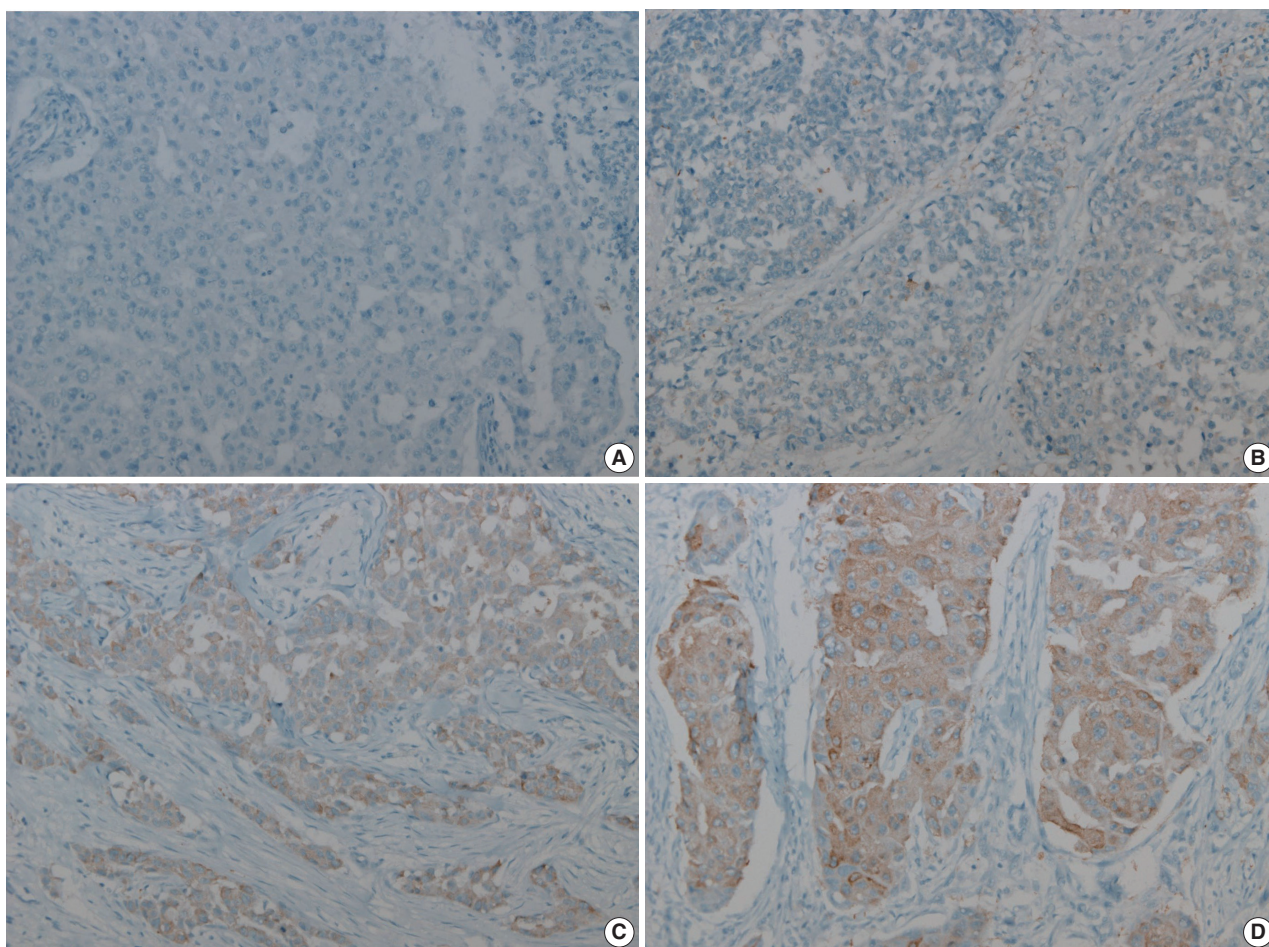


**Fig. 1.** Fatty acid synthetase expression in triple-negative breast cancer: grade 0 (A), grade 1 (B), grade 2 (C), and grade 3 (D).

final score values. PD-L1 expression was assessed using the PD-L1 SP142 assay. Of the 166 cases, 94 available cases were used to perform IHC for PD-L1 SP142. At the 1% cutoff value, 52.6% (50/94) of cases were positive for PD-L1 SP142 in infiltrating immune cells (ICs). We analyzed the correlation between FASN expression level and percentage of PD-L1 SP142 positive infiltrating ICs, but no correlation was identified. There was no statistically significant PD-L1 SP142 positivity between the low- and high-FASN expression groups. A representative case of SP142 expression in the expression of high FASN was confirmed (Fig. 2).

## DISCUSSION

TNBC has no available special treatment other than chemotherapy after surgery, so early detection of recurrence through short-term follow-up observations will help patients with treatment and prognosis [22]. The development of interval breast cancer within the time interval between screening examinations

has more adverse biological features, poorer survival outcomes, and is more highly associated with TNBC [23]. TNBC has high prevalence in young women under 50 and is more common in African Americans [24]. TNBC is known to have relatively poor prognosis compared to non-triple-negative breast cancer, most likely resulting from lack of special treatment methods such as hormone treatment or targeted treatment other than non-specific chemotherapy [25].

The TNBC subtype was classified into four distinct types by Burstein et al. [26] and is being actively studied because of different prognoses and target therapies. Clinical results and treatment responses have changed depending on classification [27]. These inherent differences related to TNBC sub-classification have resulted in a renewed effort to identify driver mutations and more appropriate targeted treatment [28]. For potential therapy, activated progesterone receptor, platinum, tyrosine kinase inhibitor, PI3K/mTOR inhibitor, anti-PD-L1 inhibitors, and/or androgen receptor targeted PI3K inhibitors are thought to be

**Table 2.** Clinicopathological data for 40 patients with high-grade FASN compared with 126 patients with low-grade FASN

	Low (n=126)	High (n=40)	p-value
Age (yr)			.018 <sup>a</sup>
<50	58 (46.0)	27 (67.5)	
>50	68 (54.0)	13 (32.5)	
Histologic type			.319 <sup>b</sup>
IDC, NOS	116 (92.1)	38 (95.0)	
Carcinoma with medullary feature	7 (5.6)	1 (2.5)	
Pleomorphic carcinoma	3 (2.4)	0	
Metaplastic carcinoma	0	1 (2.5)	
T category			.080 <sup>b</sup>
1	44 (66.7)	22 (33.3)	
2	73 (83.0)	15 (17.0)	
3	8 (72.7)	3 (27.3)	
4	1 (100)	0	
N category			.614 <sup>b</sup>
0	79 (72.5)	30 (27.5)	
1	33 (82.5)	7 (17.5)	
2	8 (88.9)	1 (11.1)	
3	2 (50.0)	2 (50.0)	
AJCC stage			.075 <sup>b</sup>
1	18 (54.5)	15 (45.5)	
2	91 (82.7)	19 (17.3)	
3	13 (68.4)	6 (31.6)	
N/A	4 (100)	0	
Histologic grade			.097 <sup>a</sup>
2	15 (11.9)	9 (22.5)	
3	111 (88.1)	31 (77.5)	
Neoadjuvant CTx	10 (7.94)	0	.120 <sup>b</sup>
CTx	119 (94.4)	35 (87.5)	.140 <sup>a</sup>
RTx	105 (83.3)	35 (87.5)	.528 <sup>a</sup>
Recur	23 (18.3)	3 (7.5)	.135 <sup>b</sup>

FASN, fatty acid synthetase; IDC, invasive ductal carcinoma; NOS, not otherwise specified; N/A, not applicable; AJCC, American Joint Committee on Cancer; CTx, chemotherapy; RTx, radiation therapy.

<sup>a</sup>Linear by linear association; <sup>b</sup>Fisher's exact test.

possible [29]. Therefore, these treatments are being attempted in TNBC patients to identify whether they can benefit from a more appropriate and targeted treatment. We performed IHC for FASN, a representative lipid metabolism-related protein, as a candidate for a potential specific target in TNBC.

FASN is a key lipogenic enzyme and is known to be overexpressed in various human cancers [30]. FASN is a lipid-producing enzyme that is expressed at low levels in normal human tissues but is reported to be highly expressed in breast, colon, prostate, ovarian, and endometrial cancers [11-14]. It has been hypothesized that useful indicators of prognosis can be found based on differences in the degree of expression between normal and cancer tissues, and patients with high FASN expression level have been reported to show lower disease-free survival and decreased survival rate [31]. High FASN expression was identified in 45%

**Table 3.** Mann-Whitney U and Spearman's correlation test results with immunohistochemical Ki-67 proliferation index in low- and high-FASN groups

Mann-Whitney U test	Ki-67	p-value
Low FASN, median (range)	60 (40-80)	.003
High FASN, median (range)	72.75 (55.13-87.7)	
Spearman's correlation		
FASN expression level	$\rho=0.257$	.001

FASN, fatty acid synthetase.

of TNBC cases [15] and high-FASN groups have been significantly associated with positive nodal status [15,16]. Therefore, FASN has emerged as a potential target, and FASN inhibitors are being evaluated in clinical trials [32]. First-generation (e.g., orlistat and cerulenin) and next-generation (TVB-3166 and TVB-2640) FASN-targeting drugs have been developed [33]. Adipophilin (ADP) and FASN are two lipid metabolism-related proteins of clinicopathological relevance for IHC expression in salivary duct carcinoma. ADP-positive expression was associated with the presence of prominent nuclear pleomorphism, high Ki-67, and poor prognosis [30].

In this study, we evaluated the association of FASN expression between clinicopathological features, including PD-L1 SP142 expression, and further evaluated its usefulness as a biomarker in TNBC. FASN expression was observed in 47.1% (95/166) of TNBC patients in our study. Staining intensity grades of 1, 2, and 3 were found in 33.1% (55/166), 13.3% (22/166), and 10.8% (18/166) of TNBC patients, respectively. Low (grade 0,1) and high (grade 2,3) expression of FASN was identified in 75.9% (126/166) and 24.1% (40/166) of TNBC, respectively. However, we could not identify an association with lymph node stage or TNM stage [15].

Ki-67 IHC is used as a proliferation marker in breast cancer and is a low-cost measurement method suitable for extensive use in clinical practice [34]. Higher Ki-67 level is associated with increased early recurrence and aggression, resulting in a lower patient survival rate [35]. In a Japanese study, when Ki-67 was greater than 10%, it was related with a high recurrence rate and low survival rate [36]. The Breast Cancer Working Group proposed guidelines for Ki-67 assessment in breast cancer and use of this potentially important marker based on current evidence [37]. Less than 5% of patients do not require chemotherapy, and more than 30% show chemotherapy indication. The ER negative case is referred to as insufficient evaluation for Ki-67 [37]. Another group reported that high Ki-67 expression (cutoff value of 30%) was correlated with early recurrence in luminal B/HER-2 negative breast cancer [38]. TNBC patients in the high Ki-67

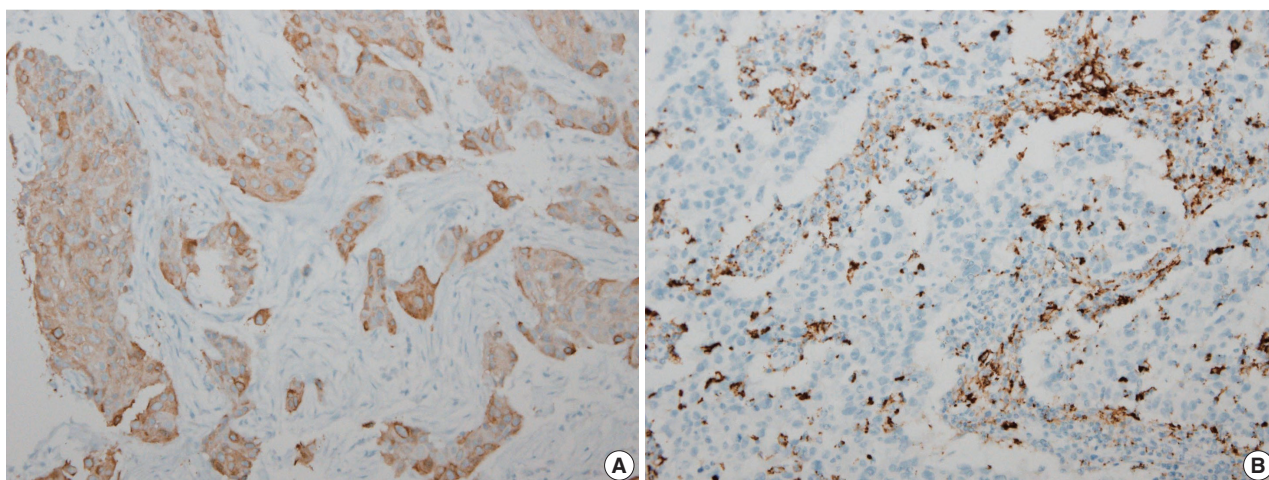


**Fig. 2.** A representative case of SP142 (B) expression in the expression of high fatty acid synthase (FASN) (A) was confirmed.

group seem to benefit more from treatment with carboplatin [39]. The majority of TNBC cases has high Ki-67 expression level ( $\geq 20\%$ ), which is used as a proliferation factor [40]. In our study, 92.8% of cases had Ki-67 expression  $\geq 20\%$ . However, the Ki-67 proliferation level was statistically different between the FASN low and high expression groups. The median Ki-67 value of the low- and high-FASN expression groups was 60% (range, 40% to 80%) and 73% (range, 55% to 87%), respectively.

In 2019, the FDA-approved atezolizumab (TECENTRIQ, Genentech Inc.) treatment in combination with paclitaxel was approved for TNBC patients whose PD-L1 stained tumor-infiltrating ICs were over 1% intensity [41]. PD-L1 is a cell membrane protein expressed in tumor cells and ICs [42]. PD-L1 expression is increased in TNBC and is a positive predictor of immunotherapy [43]. PD-L1 IHC using the VENTANA SP142 assay, the current FDA-approved assay, improved clinical outcome in atezolizumab plus nab-paclitaxel-treated patients [44]. In our study, we investigated the association between PD-L1 and FASN expression level and unfortunately identified no association.

TNBC represents a small proportion of breast cancer subtypes but has the worst outcome [45]. Although this study was based on data from a small number of TNBC cases and short-term follow-up surveys, we included 166 TNBC patients in the study. More research on the expression of FASN on TNBC and its potential inhibitors will help identify new target treatments. Further research is needed on how FASN correlates with other factors in TNBC. In addition, further studies are required with a larger number of TNBC patients to investigate the specific role of FASN in TNBC and the possibility for FASN inhibition as a target treatment for TNBC.

In conclusion, we showed FASN expression in TNBC patients

and Ki-67 proliferation index to be positively correlated with FASN level, indicating higher proliferation activity as FASN increases. However, there was no statistical association with PD-L1 SP142, the currently FDA-approved assay, or FASN expression level.

#### Ethics Statement

The KUMC Institutional Review Board anonymized the archive data prior to the study and waived the requirement for prior consent (KUMC 2021-07-032).

#### Availability of Data and Material

The datasets generated or analyzed during the study are available from the corresponding author on reasonable request.

#### Code Availability

Not applicable.

#### ORCID

Jin Hee Park	<a href="https://orcid.org/0000-0003-1277-7549">https://orcid.org/0000-0003-1277-7549</a>
Hye Seung Han	<a href="https://orcid.org/0000-0002-3591-9995">https://orcid.org/0000-0002-3591-9995</a>
So Dug Lim	<a href="https://orcid.org/0000-0003-2036-0313">https://orcid.org/0000-0003-2036-0313</a>
Wook Youn Kim	<a href="https://orcid.org/0000-0003-4024-8791">https://orcid.org/0000-0003-4024-8791</a>
Kyoung Sik Park	<a href="https://orcid.org/0000-0001-9806-9839">https://orcid.org/0000-0001-9806-9839</a>
Young Bum Yoo	<a href="https://orcid.org/0000-0003-0731-8807">https://orcid.org/0000-0003-0731-8807</a>
Seung Eun Lee	<a href="https://orcid.org/0000-0002-7459-0061">https://orcid.org/0000-0002-7459-0061</a>
Wan-Seop Kim	<a href="https://orcid.org/0000-0001-7704-5942">https://orcid.org/0000-0001-7704-5942</a>

#### Author Contributions

Conceptualization: SEL, WSK. Data curation: KSP, YBY, JHP. Formal analysis: SEL, WYK. Funding acquisition: WSK. Investigation: JHP. Methodology: SEL. Supervision: WSK, HSH. Validation: SEL, SDL. Writing—original draft: JHP, SEL. Writing—review & editing: SEL, WSK, JHP. Approval of final manuscript: all authors.

#### Conflicts of Interest

The authors declare that they have no potential conflicts of interest.

## Funding Statement

This research was supported by the Bio & Medical Technology Development Program of the National Research Foundation (NRF) funded by the Korean government (Ministry of Science and ICT) (No. 2019M3E5D3073475).

## References

- Gluz O, Liedtke C, Gottschalk N, Pusztai L, Nitz U, Harbeck N. Triple-negative breast cancer: current status and future directions. *Ann Oncol* 2009; 20: 1913-27.
- Diana A, Franzese E, Centonze S, et al. Triple-negative breast cancers: systematic review of the literature on molecular and clinical features with a focus on treatment with innovative drugs. *Curr Oncol Rep* 2018; 20: 76.
- Lee KK, Kim JY, Jung JH, Park JY, Park HY. Clinicopathological feature and recurrence pattern of triple negative breast cancer. *J Korean Surg Soc* 2010; 79: 14-9.
- Bianchini G, Balko JM, Mayer IA, Sanders ME, Gianni L. Triple-negative breast cancer: challenges and opportunities of a heterogeneous disease. *Nat Rev Clin Oncol* 2016; 13: 674-90.
- Marotti JD, de Abreu FB, Wells WA, Tsongalis GJ. Triple-negative breast cancer: next-generation sequencing for target identification. *Am J Pathol* 2017; 187: 2133-8.
- Lee SE, Park HY, Lim SD, Han HS, Yoo YB, Kim WS. Concordance of programmed death-ligand 1 expression between SP142 and 22C3/SP263 assays in triple-negative breast cancer. *J Breast Cancer* 2020; 23: 303-13.
- Rugo HS, Loi S, Adams S, et al. PD-L1 immunohistochemistry assay comparison in atezolizumab plus nab-paclitaxel-treated advanced triple-negative breast cancer. *J Natl Cancer Inst* 2021; 113: 1733-43.
- Sun X, Wang M, Wang M, et al. Metabolic reprogramming in triple-negative breast cancer. *Front Oncol* 2020; 10: 428.
- Gong Y, Ji P, Yang YS, et al. Metabolic-pathway-based subtyping of triple-negative breast cancer reveals potential therapeutic targets. *Cell Metab* 2021; 33: 51-64.
- Cha YJ, Kim HM, Koo JS. Expression of lipid metabolism-related proteins differs between invasive lobular carcinoma and invasive ductal carcinoma. *Int J Mol Sci* 2017; 18: 232.
- Sebastiani V, Visca P, Botti C, et al. Fatty acid synthase is a marker of increased risk of recurrence in endometrial carcinoma. *Gynecol Oncol* 2004; 92: 101-5.
- Wang Y, Kuhajda FP, Li JN, et al. Fatty acid synthase (FAS) expression in human breast cancer cell culture supernatants and in breast cancer patients. *Cancer Lett* 2001; 167: 99-104.
- Yang Y, Morin PJ, Han WE, et al. Regulation of fatty acid synthase expression in breast cancer by sterol regulatory element binding protein-1c. *Exp Cell Res* 2003; 282: 132-7.
- Kusakabe T, Nashimoto A, Honma K, Suzuki T. Fatty acid synthase is highly expressed in carcinoma, adenoma and in regenerative epithelium and intestinal metaplasia of the stomach. *Histopathology* 2002; 40: 71-9.
- Giro-Perafita A, Sarrats A, Perez-Bueno F, et al. Fatty acid synthase expression and its association with clinico-histopathological features in triple-negative breast cancer. *Oncotarget* 2017; 8: 74391-405.
- Jiang W, Xing XL, Zhang C, et al. MET and FASN as prognostic biomarkers of triple negative breast cancer: a systematic evidence landscape of clinical study. *Front Oncol* 2021; 11: 604801.
- Flores FH, Vinas G, Oliveras G, et al. Triple negative breast cancer: clinicopathologic characteristics and fatty acid synthase (FASN) expression as a potential target. *Ann Oncol* 2014; 25(Suppl 4): IV60.
- Goldhirsch A, Wood WC, Coates AS, et al. Strategies for subtypes: dealing with the diversity of breast cancer: highlights of the St. Gallen International Expert Consensus on the Primary Therapy of Early Breast Cancer 2011. *Ann Oncol* 2011; 22: 1736-47.
- Hammond ME, Hayes DF, Dowsett M, et al. American Society of Clinical Oncology/College of American Pathologists guideline recommendations for immunohistochemical testing of estrogen and progesterone receptors in breast cancer (unabridged version). *Arch Pathol Lab Med* 2010; 134: e48-72.
- Wolff AC, Hammond ME, Schwartz JN, et al. American Society of Clinical Oncology/College of American Pathologists guideline recommendations for human epidermal growth factor receptor 2 testing in breast cancer. *Arch Pathol Lab Med* 2007; 131: 18-43.
- Sarrio D, Rodriguez-Pinilla SM, Hardisson D, Cano A, Moreno-Bueno G, Palacios J. Epithelial-mesenchymal transition in breast cancer relates to the basal-like phenotype. *Cancer Res* 2008; 68: 989-97.
- Ma D, Jiang YZ, Xiao Y, et al. Integrated molecular profiling of young and elderly patients with triple-negative breast cancer indicates different biological bases and clinical management strategies. *Cancer* 2020; 126: 3209-18.
- Li J, Holm J, Bergh J, et al. Breast cancer genetic risk profile is differentially associated with interval and screen-detected breast cancers. *Ann Oncol* 2015; 26: 517-22.
- Dietze EC, Sistrunk C, Miranda-Carboni G, O'Regan R, Seewaldt VL. Triple-negative breast cancer in African-American women: disparities versus biology. *Nat Rev Cancer* 2015; 15: 248-54.
- Foulkes WD, Smith IE, Reis-Filho JS. Triple-negative breast cancer. *N Engl J Med* 2010; 363: 1938-48.
- Burstein MD, Tsimelzon A, Poage GM, et al. Comprehensive genomic analysis identifies novel subtypes and targets of triple-negative breast cancer. *Clin Cancer Res* 2015; 21: 1688-98.
- Garrido-Castro AC, Lin NU, Polyak K. Insights into molecular classifications of triple-negative breast cancer: improving patient selection for treatment. *Cancer Discov* 2019; 9: 176-98.
- D'Ippolito E, Iorio MV. MicroRNAs and triple negative breast cancer. *Int J Mol Sci* 2013; 14: 22202-20.
- Le Du F, Eckhardt BL, Lim B, et al. Is the future of personalized therapy in triple-negative breast cancer based on molecular subtype? *Oncotarget* 2015; 6: 12890-908.
- Hirai H, Tada Y, Nakaguro M, et al. The clinicopathological significance of the adipophilin and fatty acid synthase expression in salivary duct carcinoma. *Virchows Arch* 2020; 477: 291-9.
- Kim S, Lee Y, Koo JS. Differential expression of lipid metabolism-related proteins in different breast cancer subtypes. *PLoS One* 2015; 10: e0119473.
- Giro-Perafita A, Rabionet M, Planas M, et al. EGCG-derivative G28 shows high efficacy inhibiting the mammosphere-forming capacity of sensitive and resistant TNBC models. *Molecules* 2019; 24: 1027.
- Wang W, Bai L, Li W, Cui J. The lipid metabolic landscape of cancers and new therapeutic perspectives. *Front Oncol* 2020; 10: 605154.
- Mrklic I, Capkun V, Pogorelic Z, Tomic S. Prognostic value of Ki-67 proliferating index in triple negative breast carcinomas. *Pathol Res Pract* 2013; 209: 296-301.
- Ahmed ST, Ahmed AM, Musa DH, Sulayvani FK, Al-Khyatt M, Pity IS. Proliferative index (Ki67) for prediction in breast duct carcinoma.

- cinomas. *Asian Pac J Cancer Prev* 2018; 19: 955-9.
36. Miyashita M, Ishida T, Ishida K, et al. Histopathological subclassification of triple negative breast cancer using prognostic scoring system: five variables as candidates. *Virchows Arch* 2011; 458: 65-72.
  37. Nielsen TO, Leung SC, Rimm DL, et al. Assessment of Ki67 in breast cancer: updated recommendations from the international Ki67 in breast cancer working group. *J Natl Cancer Inst* 2021; 113: 808-19.
  38. Zong Y, Zhu L, Wu J, et al. Progesterone receptor status and Ki-67 index may predict early relapse in luminal B/HER2 negative breast cancer patients: a retrospective study. *PLoS One* 2014; 9: e95629.
  39. Wang W, Wu J, Zhang P, et al. Prognostic and predictive value of Ki-67 in triple-negative breast cancer. *Oncotarget* 2016; 7: 31079-87.
  40. Pan Y, Yuan Y, Liu G, Wei Y. P53 and Ki-67 as prognostic markers in triple-negative breast cancer patients. *PLoS One* 2017; 12: e0172324.
  41. Mavratzas A, Seitz J, Smetanay K, Schneeweiss A, Jager D, Fremd C. Atezolizumab for use in PD-L1-positive unresectable, locally advanced or metastatic triple-negative breast cancer. *Future Oncol* 2020; 16: 4439-53.
  42. Dong H, Strome SE, Salomao DR, et al. Tumor-associated B7-H1 promotes T-cell apoptosis: a potential mechanism of immune evasion. *Nat Med* 2002; 8: 793-800.
  43. Peg V, Lopez-Garcia MA, Comerma L, et al. PD-L1 testing based on the SP142 antibody in metastatic triple-negative breast cancer: summary of an expert round-table discussion. *Future Oncol* 2021; 17: 1209-18.
  44. Li Y, Vennapusa B, Chang CW, et al. Prevalence study of PD-L1 SP142 assay in metastatic triple-negative breast cancer. *Appl Immunohistochem Mol Morphol* 2021; 29: 258-64.
  45. Al-Jussani GN, Dabbagh TZ, Al-Rimawi D, Sughayer MA. Expression of PD-L1 using SP142 CDx in triple negative breast cancer. *Ann Diagn Pathol* 2021; 51: 151703.

## Blocking Toll-like receptor 9 attenuates bleomycin-induced pulmonary injury

Badr Alzahrani<sup>1</sup>, Mohamed M. S. Gaballa<sup>2</sup>, Ahmed A. Tantawy<sup>2</sup>, Maha A. Moussa<sup>3</sup>, Salma A. Shoulah<sup>4</sup>, Said M. Elshafae<sup>2</sup>

<sup>1</sup>Department of Clinical Laboratory Sciences, College of Applied Medical Sciences, Jouf University, Sakaka, Saudi Arabia;

<sup>2</sup>Department of Pathology, Faculty of Veterinary Medicine, Benha University, Tukh;

<sup>3</sup>Department of Statistics, Faculty of Commerce, Benha University, Benha;

<sup>4</sup>Department of Animal Medicine (Infectious Diseases), Faculty of Veterinary Medicine, Benha University, Tukh, Egypt

**Background:** Acute respiratory distress syndrome (ARDS) is one of the most common complications in coronavirus disease 2019 patients suffering from acute lung injury (ALI). In ARDS, marked distortion of pulmonary architecture has been reported. The pulmonary lesions in ARDS include hemodynamic derangements (such as alveolar edema and hemorrhage), vascular and bronchiolar damage, interstitial inflammatory cellular aggregations, and eventually fibrosis. Bleomycin induces ARDS-representative pulmonary damage in mice and rats; therefore, we used bleomycin model mice in our study. Recently, Toll-like receptor 9 (TLR9) was implicated in the development of ARDS and ALI. **Methods:** In this study, we evaluated the efficiency of a TLR9 blocker (ODN2088) on bleomycin-induced pulmonary damage. We measured the apoptosis rate, inflammatory reaction, and fibroplasia in bleomycin- and bleomycin + ODN2088-treated mice. **Results:** Our results showed a significant amelioration in bleomycin-induced damage to pulmonary architecture following ODN2088 treatment. A marked decrease in pulmonary epithelial and endothelial apoptosis rate as measured by cleaved caspase-3 expression, inflammatory reaction as indicated by tumor necrosis factor  $\alpha$  expression, and pulmonary fibrosis as demonstrated by Van Gieson staining and  $\alpha$ -smooth muscle actin immunohistochemistry were observed following ODN2088 treatment. **Conclusions:** All these findings indicate that blocking downstream TLR9 signaling could be beneficial in prevention or mitigation of ARDS through hemodynamic derangements, inflammation, apoptosis, and fibrosis.

**Key Words:** TLR9; ODN2088; Bleomycin; Acute respiratory distress syndrome; Fibrosis

**Received:** November 2, 2021 **Revised:** December 4, 2021 **Accepted:** December 27, 2021

**Corresponding Author:** Said M. Elshafae, PhD, Department of Pathology, Faculty of Veterinary Medicine, Benha University, Moshtohor, Tukh, Qalyubiya 13736, Egypt  
 Tel: +20-1435-363-5372, E-mail: Said.Elshafey@fvvm.bu.edu.eg

In December 2019, several patients in China were infected with a novel coronavirus known as severe acute respiratory syndrome coronavirus 2, the etiological agent underlying acute respiratory disease named coronavirus disease 2019 (COVID-19) [1]. Based on clinical and radiologic data, lung injury is one of the most common complications of COVID-19. In about 20% of COVID-19 patients, acute lung injury (ALI) rapidly progresses into acute respiratory distress syndrome (ARDS) [2]. ARDS development includes acute, subacute, and chronic phases [3]. The acute phase is mainly characterized by alveolar and interstitial edema, endothelial and epithelial damage, and aggregations of inflammatory cells and red blood cells (RBCs) in the alveoli. The predominant changes in the subacute phase are pulmonary edema clearance, type II alveolar pneumocyte hyperplasia, fibroblastic

proliferation, and collagen deposition [3]. The chronic phase of ARDS involves infiltrations of alveolar macrophages in the alveoli and increased fibrosis. The bleomycin-induced lung injury model is a well-characterized model of pulmonary damage, edema, inflammation, and eventual fibrosis that closely resembles the ARDS development pathway [4]. The bleomycin mouse model is an excellent research tool to investigate ARDS due to strong similarities regarding the cells, mediators, and signaling pathways that contribute to pathogenesis.

Bleomycin, generated by the bacterium *Streptomyces verticillus*, is a glycosylated linear non-ribosomal peptide antibiotic. Since bleomycin has potent antitumorigenic properties, it is used as a chemotherapeutic agent against many cancers, including squamous cell carcinomas of the cervix, esophagus, and head and neck;

germ cell tumors; and both Hodgkins and non-Hodgkins lymphoma [5-7]. Bleomycin causes direct cellular damage by disrupting DNA strands, creating free radicals, and inducing oxidative stress [8,9]. Upon damage, the affected cells excrete uric acid and many other factors that initiate aggregation of alveolar macrophages and release of pro-inflammatory cytokines. During the first week after bleomycin administration, marked elevation of pro-inflammatory cytokines (tumor necrosis factor  $\alpha$  [TNF- $\alpha$ ], interleukin [IL]-1, and IL-6) was reported. Upregulation of profibrotic markers (transforming growth factor  $\beta$ 1 [TGF- $\beta$ 1], fibronectin, and collagen) was seen by day 14. By the second to third weeks, patchy fibrotic areas with extracellular matrix (ECM) deposition, mainly in the forms of fibronectin and collagen I, are evident in pulmonary tissue [10].

Toll-like receptors (TLRs) have a vital role in the innate immune system [11-13]. Hyperactivation of TLRs disrupts immune system homeostasis, resulting in extensive pro-inflammatory cytokine production that has a key role in many autoimmune and inflammatory diseases [14]. Among other TLRs, TLR9 was found to promote the release of pro-inflammatory mediators such as TNF- $\alpha$  and IL-1 $\beta$  in ALI and is implicated in several chronic inflammatory pulmonary conditions [15]. Recent studies showed that TLR9 contributes to the development and worsening of ARDS and ALI in COVID-19 patients [16-18]. Furthermore, TLR9 induction was found to activate blood coagulation in humans and mice [19,20]. All these findings suggest that blocking the TLR signaling pathway could be an effective therapeutic strategy for mitigating the clinical presentation of ARDS and ALI in COVID-19 patients.

CpG-oligodeoxynucleotide ODN is an unmethylated, short, single-stranded synthetic DNA molecule that acts as a TLR9 ligand [21]. Activation of TLR9 using the ODN ligand promotes neutrophilic infiltration, pulmonary edema, and systemic inflammation [15,16]. The oligonucleotide ODN2088 (a DNA sequence) inhibits the activity of TLR9 and its downstream signaling effectors by disturbing the co-localization of unmethylated CpG di-nucleotides with TLR9 [22]. A previous study showed that ODN2088 inhibits the liver inflammation and fibrosis induced by CCl<sub>4</sub> [23]. In the present study, a bleomycin-induced lung injury mouse model was used to evaluate the impact of TLR9 inhibition by ODN2088 on the lung damage, inflammation, and fibrosis commonly seen in ARDS in COVID-19 patients.

## MATERIALS AND METHODS

### Chemicals

CpG ODN2088 was purchased from Invitrogen (Carlsbad, CA, USA). ODN 2088 is a TLR9 antagonist with 15 base pairs (5'-tcctggcggggaagt-3'). Bleomycin sulfate (Celon Laboratories Pvt. Ltd., Hyderabad, India) was dissolved in sterile saline solution for injection.

### In vivo experimental design

Swiss Albino mice were purchased from the Facility of Laboratory Animals at the Facility of Veterinary Medicine, Benha University, Egypt. All animal experiments were conducted according to protocols approved by the Benha University Committee of Bioethics in Egypt. Mice were maintained according to the National Institutes of Health standards established in the "Guidelines for the Care and Use of Laboratory Animals." Forty adult 6–8-week-old male Swiss Albino mice (22–30 g) were used in this study. The mice were subdivided equally into four groups. In the first group (control), mice were injected intraperitoneally (IP) with saline (vehicle). In the second group (bleomycin), mice were injected with bleomycin IP (2 mg/mouse) on days 1, 8, and 15. In the third group (ODN2088), the mice were injected IP with CpG ODN2088 (50  $\mu$ g/20 g BW, re-suspended in endotoxin-free water) daily until the day of sacrifice. In the fourth group (bleomycin + ODN2088) (BLEO/ODN2088), the mice received both bleomycin (2 mg/mouse) and ODN2088 (50  $\mu$ g/20 g BW).

### Histopathology

The mice were euthanized after 30 days by cervical dislocation, and pulmonary tissue specimens were collected during necropsy. Lung specimens were fixed in 10% neutral-buffered formalin at room temperature for 72 hours, embedded in paraffin, cut in 4  $\mu$ m sections, and stained with hematoxylin and eosin. Histological images of the slides were collected using a Nikon Eclipse E800 microscope (Melville, NY, USA) equipped with a camera and were analyzed using Fiji ImageJ software (ImageJ 1.51u, National Institutes of Health, Bethesda, MD, USA).

### Van Gieson staining

Pulmonary tissue sections were washed with tap water and incubated in microfuchsin solution (1% acid fuchsin in aqueous saturated picric acid) for 2 minutes. Sections were dehydrated and mounted using DPX mounting agent (Thermo Fisher Scientific, Leicester, UK). Upon staining, collagen fibers appear pink to red, while muscle appears yellowish. The area of positive collagen or

elastic fibers was calculated compared to the total area of the tissue section.

### Immunohistochemistry

The 5- $\mu$ m-thick paraffin-embedded tissue sections were pre-heated and dewaxed in xylene followed by dehydration in ethanol. The tissue sections were incubated with antigen retrieval solution (Dako, Carpinteria, CA, USA) for 40 minutes using a steamer (Black & Decker HS1000, Newark, DE, USA) followed by a cooling step (for 30 minutes at room temperature). The tissue sections were treated with 3% hydrogen peroxide to block endogenous peroxidase activity and washed, and 10% bovine serum albumin was added to block non-specific immunoreactivity. The slides were incubated overnight with either anti-cleaved caspase-3 (1:400, Cat #Asp175, Cell Signaling Technology, Danvers, MA, USA), anti-TNF- $\alpha$  (1:400, NBP1-19532, Novus, Centennial, CO, USA), or anti- $\alpha$ -smooth muscle actin ( $\alpha$ -SMA; 1:50, clone 1A4, Dako) primary antibodies. On the next day, slides were washed three times and incubated with the corresponding biotinylated secondary antibody diluted in phosphate buffered saline (PBS) for 1 hour at 25°C, followed by three PBS washes. The slides were incubated with diaminobenzidine tetrahydrochloride solution for 10 minutes. The slides were washed three times in distilled water and counter stained with hematoxylin. Tissue sections were finally dehydrated using graded alcohols and xylene and then covered with a glass slip [24]. DAB staining (brown color) was recorded as a positive result. Positivity was counted as number of positive cells/number of total cells. ImageJ ver. 1.48 (National Institutes of Health, Bethesda, MD, USA) was used to calculate the percent positivity in all the pulmonary tissues.

### Statistical analysis

All data collected are displayed as mean  $\pm$  standard deviation. Student's unpaired t-test was used to analyze the difference in positivity between bleomycin and BLEO/ODN2088 groups using GraphPad Prism ver. 6.03 (La Jolla, CA, USA). Differences denoted by  $p \leq .05$  were considered statistically significant.

## RESULTS

### ODN2088 restored pulmonary architecture distorted by bleomycin

In control mice, almost all the lung sections had normal pulmonary architecture with clear empty alveoli and thin interalveolar septa (Fig. 1A). The alveoli were lined with flat (type I pneumocytes) and cuboidal cells projecting into the alveolar lumen

(type II pneumocytes). Patent bronchioles lined with simple columnar epithelium were also evident in most sections. Most lungs in ODN2088-treated mice exhibited normal histological appearance with thin interalveolar septa and patent alveoli. In a few lungs, mild alveolar pneumocyte hyperplasia was observed (Fig. 1B). Alveolar emphysema was seen occasionally in some pulmonary areas.

In bleomycin-treated mice, pulmonary architecture was severely distorted in a patchy pattern. Multifocal thickening of interalveolar septa and alveolar collapse were the most pronounced microscopic findings in all the lung sections. Meanwhile, most other alveoli were over-inflated (emphysematous). Alveolar septal thickening was mainly due to moderate to severe mononuclear inflammatory cell infiltration in the interalveolar space (Fig. 1C–E). Moderate type II pneumocyte hyperplasia with reactive atypia and fibroplasia was evident in several pulmonary areas. Focal alveolar histiocytosis characterized by accumulation of foamy macrophages in the alveoli was also prominent in some lung sections. Fine eosinophilic fibrin threads were seen in some alveoli. In many pulmonary sections, hyperplasia of the bronchiolar epithelium was reported. Some hyperplastic bronchioles had cytoplasmic vacuolation and prominent enlarged nuclei in their epithelia, while others suffered from necrosis of their lining epithelia with the presence of desquamated intraluminal cells (Fig. 1F–H). Inflammatory peribronchial cell aggregations and fibrosis were also reported in some foci (Fig. 1H–J). Congestion of peribronchiolar blood vessels and interalveolar capillaries, edema, and hemorrhage were the main vascular changes in bleomycin-treated group. There were extensive perivascular inflammatory cell infiltrates, including lymphocytes and macrophages, affecting some large pulmonary blood vessels along with extravasated RBCs in nearby alveoli (Fig. 1J). Fibrinoid necrosis was also observed in the walls of a few large pulmonary blood vessels in some sections (Fig. 1J). Other vascular alterations included disorganization and hypertrophy of tunica media, fibrous remodeling, and occasional pulmonary vein thrombosis (Fig. 1K). Multifocally, some alveoli were filled with extravasated RBCs, homogenous eosinophilic fluid, and siderophages. In some mice, pleura thickened by edema, fibrin deposition, and occasional infiltration of lymphocytes and macrophages and, rarely, neutrophils were seen (Fig. 1L).

Apparent amelioration of bleomycin-induced lung distortion, marked by distinct restoration of lung architecture, was noticed in the BLEO/ODN2088-treated group compared to the bleomycin-treated group. Most bronchiolar epithelia had mild goblet cell hyperplasia or minimal degenerative/necrotic changes (Fig. 1M). Most alveoli were devoid of fluids, RBCs, fibrin threads,

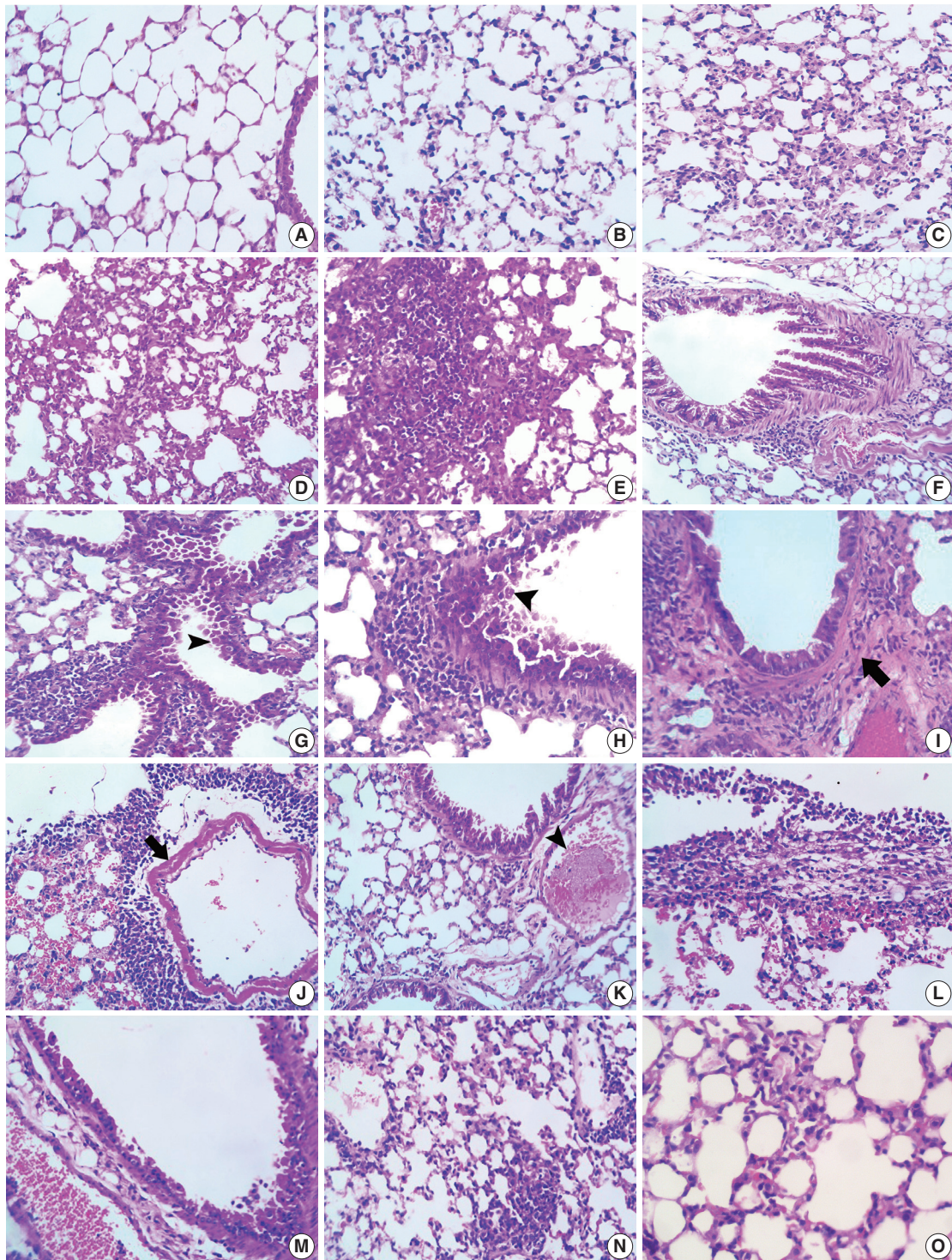


**Fig. 1.** Representative lung photomicrographs in control- (A), ODN2088- (B), bleomycin- (C–L), and bleomycin + ODN2088 (BLEO/ODN2088)-treated mice (M–O). (A) Normal respiratory bronchioli and alveoli in the control group. (B) Mild hyperplasia of alveolar pneumocytes in the lung of an ODN2088-treated mouse. (C–L) Lung sections of mice treated with bleomycin, showing focal to confluent, moderate, to severe aggregation of inflammatory cells in the interalveolar septa (C–E), hyperplastic bronchiolar epithelia (F), peribronchial inflammatory aggregations and necrosis of bronchiolar epithelia (G, H, arrowhead), peribronchial fibroplasia (I, arrow), perivascular (arrow) inflammatory cellular infiltration and intra-alveolar hemorrhage (J), thrombosis in a pulmonary blood vessel (K, arrowhead), and pleural thickening (L). (M–O) Lungs of BLEO/ODN2088-treated mice showing necrosis in a few bronchiolar epithelia (M), small focal inflammatory aggregation in the interstitial space (N), and congested interalveolar blood capillaries (O).

and inflammatory cells. There was no to mild thickening of interlobular septa due to mild mononuclear cell aggregations, congestion of interalveolar blood capillaries, and mild interlobular edema (Fig. 1N, O). Overinflation of alveoli with mild edema was occasionally seen.

#### ODN2088 reduced bleomycin-induced pulmonary fibrosis

Van Gieson staining and  $\alpha$ -SMA immunohistochemistry were used to assess the antifibrotic effects of ODN2088 against pulmonary fibrosis induced by bleomycin. Van Gieson-stained sections demonstrated control and ODN2088-treated mice to have only a thin layer of pink-stained collagen fibers in the tunica adventitia of pulmonary blood vessels and bronchioles. In bleomycin-treated mice, on the other hand, multifocal areas of tightly

packed pink-stained collagen fibers were seen around bronchioles and blood vessels (Fig. 2A, B). Multifocal red-stained collagen fibers were also seen in the interalveolar and interlobular spaces. The pulmonary tissues of the BLEO/ODN2088 group stained with Van Gieson stain were nearly similar to those of the control group (Fig. 2C). Compared to the bleomycin group, the area of Van Gieson-stained collagen fibers was significantly smaller in the BLEO/ODN2088-treated group (Fig. 2D)

#### ODN2088 mitigated bleomycin-induced myofibroblast proliferation in pulmonary tissue

To further confirm the findings of Van Gieson staining, we used  $\alpha$ -SMA as an immunohistochemical marker for myofibroblast proliferation and fibrosis. There was very weak  $\alpha$ -SMA immunos-

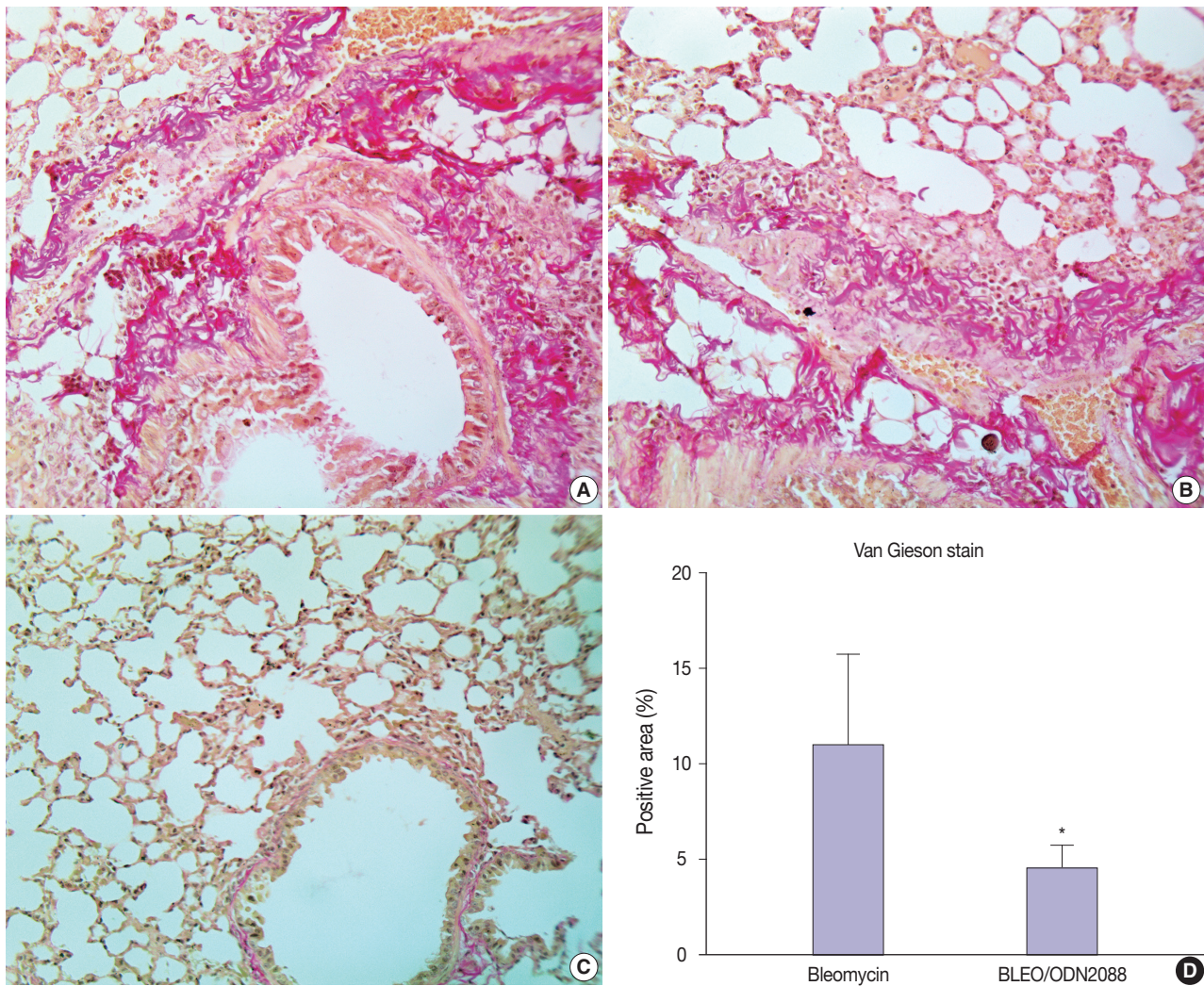


**Fig. 2.** Photomicrographs (A–C) and statistical analysis (D) of Van Gieson staining of pulmonary tissues in bleomycin- (A, B) and bleomycin+ODN2088 (BLEO/ODN2088)-treated mice (C). Data in the bar graph (D) represent mean $\pm$ standard deviation, and significant differences ( $p < .05$ ) are indicated by an asterisk.

taining in the pulmonary tissues of control and ODN2088-treated mice. In bleomycin-treated mice, a marked increase in  $\alpha$ -SMA protein expression (evidenced by brown DAB staining) was seen multifocally in the alveoli, interalveolar septa, and peribronchial connective tissue (Fig. 3A, B). ODN2088 reduced myofibroblast proliferation in the pulmonary tissues of the BLEO/ODN2088-treated group, demonstrated by a marked decline in  $\alpha$ -SMA expression (Fig. 3C, D). Focal areas with mild  $\alpha$ -SMA staining were seen in the interalveolar septa of some lungs in this group.

#### ODN2088 lowered the apoptosis rate in BLEO/ODN2088-treated pulmonary tissues

Staining for cleaved caspase-3 was used to assess the effect of

ODN2088 on apoptosis caused by bleomycin. There was minimal cleaved caspase-3 expression in the control- and ODN2088-treated groups. Extensive damage to pulmonary tissues was seen in bleomycin-treated mice, where there was a marked increase in cleaved caspase-3 expression in many alveolar pneumocytes, bronchiolar epithelial cells, and vascular endothelial cells (Fig. 4A, B). ODN2088 mitigated the pulmonary toxicity of bleomycin in the BLEO/ODN2088 group. The ameliorative effects of ODN2088 were pronounced in bronchiolar epithelium and endothelial cells (Fig. 4C). Compared to the bleomycin group, there were significantly fewer cleaved caspase-3–positive cells in the BLEO/ODN2088-treated group (Fig. 4D).

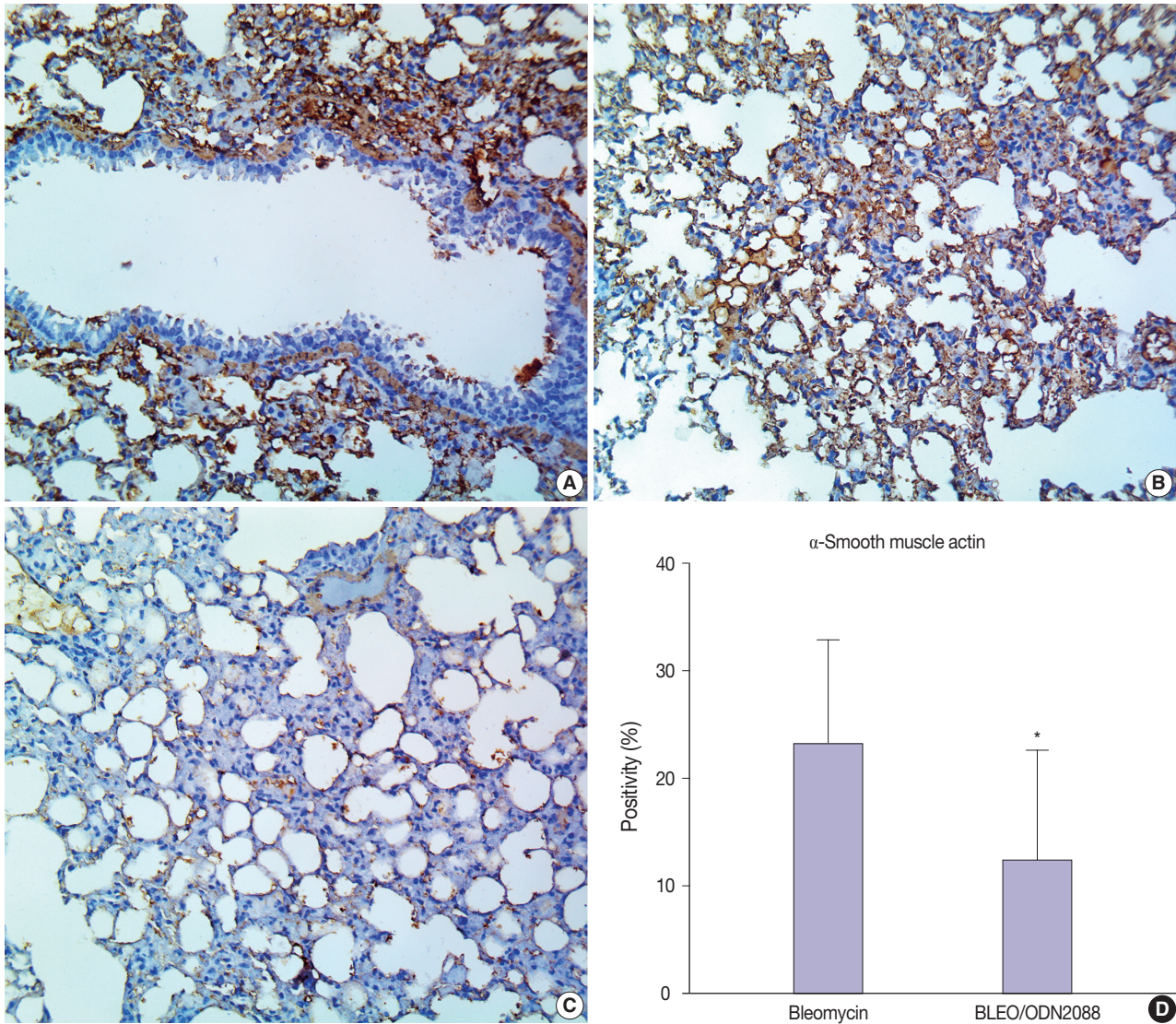


**Fig. 3.** Immunohistochemical photomicrographs (A–C) and statistical analysis (D) of  $\alpha$ -smooth muscle actin ( $\alpha$ -SMA) expression in the pulmonary tissues of bleomycin- (A, B) and bleomycin+ODN2088 (BLEO/ODN2088)-treated mice (C). Data in the bar graph (D) represent mean $\pm$ standard deviation, and significant differences ( $p < .05$ ) are indicated by an asterisk.

### ODN2088 mitigated the bleomycin-induced inflammatory reaction

To assess the potential inhibitory effects of ODN2088 on the bleomycin-induced inflammatory reaction, we evaluated TNF- $\alpha$  expression in pulmonary tissues. Null to mild TNF- $\alpha$  expression was seen in the pulmonary tissues of control and ODN2088-treated mice. In bleomycin-treated mice, extensive TNF- $\alpha$  expression was observed in alveolar macrophages and the inflammatory cellular aggregations in the interalveolar space and peribronchiolar, perivascular, and pleural connective tissue (Fig. 5A, B). ODN2088 markedly reduced TNF- $\alpha$  expression in pulmonary tissues in the BLEO/ODN2088-treated group. There was mild cellular TNF- $\alpha$

expression in the interalveolar septa and peribronchiolar connective tissue (Fig. 5C). In only one mouse, moderate to severe focal TNF- $\alpha$  expression was observed in the inflammatory cells in the interalveolar septa. The number of TNF- $\alpha$  positive cells was much lower in the BLEO/ODN2088-treated group compared to the bleomycin group (Fig. 5D).

## DISCUSSION

Pulmonary damage is one of the most serious complications of diffuse lung diseases, such as idiopathic pulmonary fibrosis, interstitial lung disease, and ARDS [25-29]. Persistent pulmo-

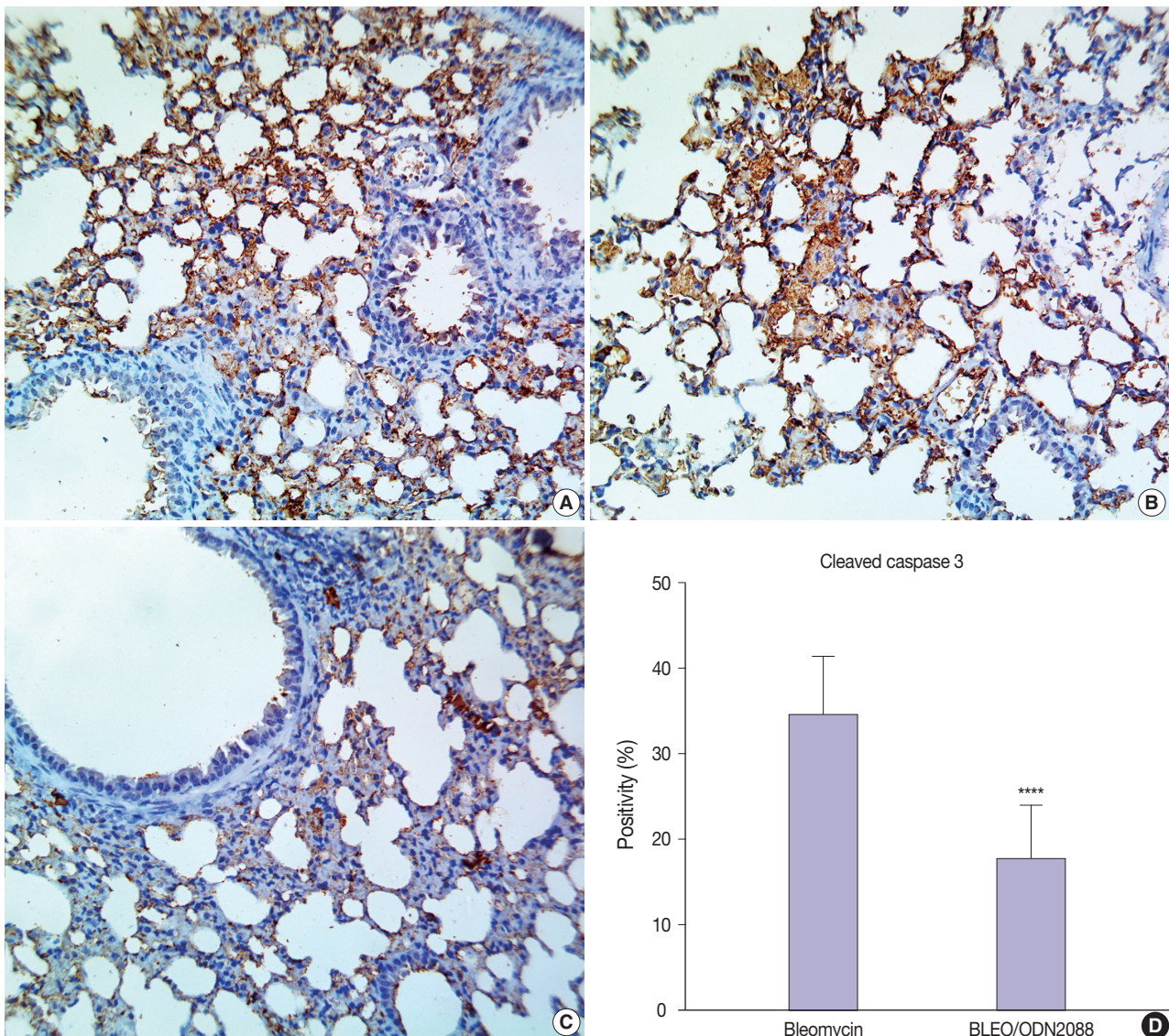


**Fig. 4.** Cleaved caspase-3 (CC3) immunohistochemical photomicrographs (A–C) and statistical analysis of CC3-positive cells (D) in the pulmonary section of bleomycin- and bleomycin+ODN2088 (BLEO/ODN2088)-treated mice. Data in the bar graphs (D) represent mean $\pm$ standard deviation, and significant differences ( $p < .001$ ) are indicated by four asterisks.

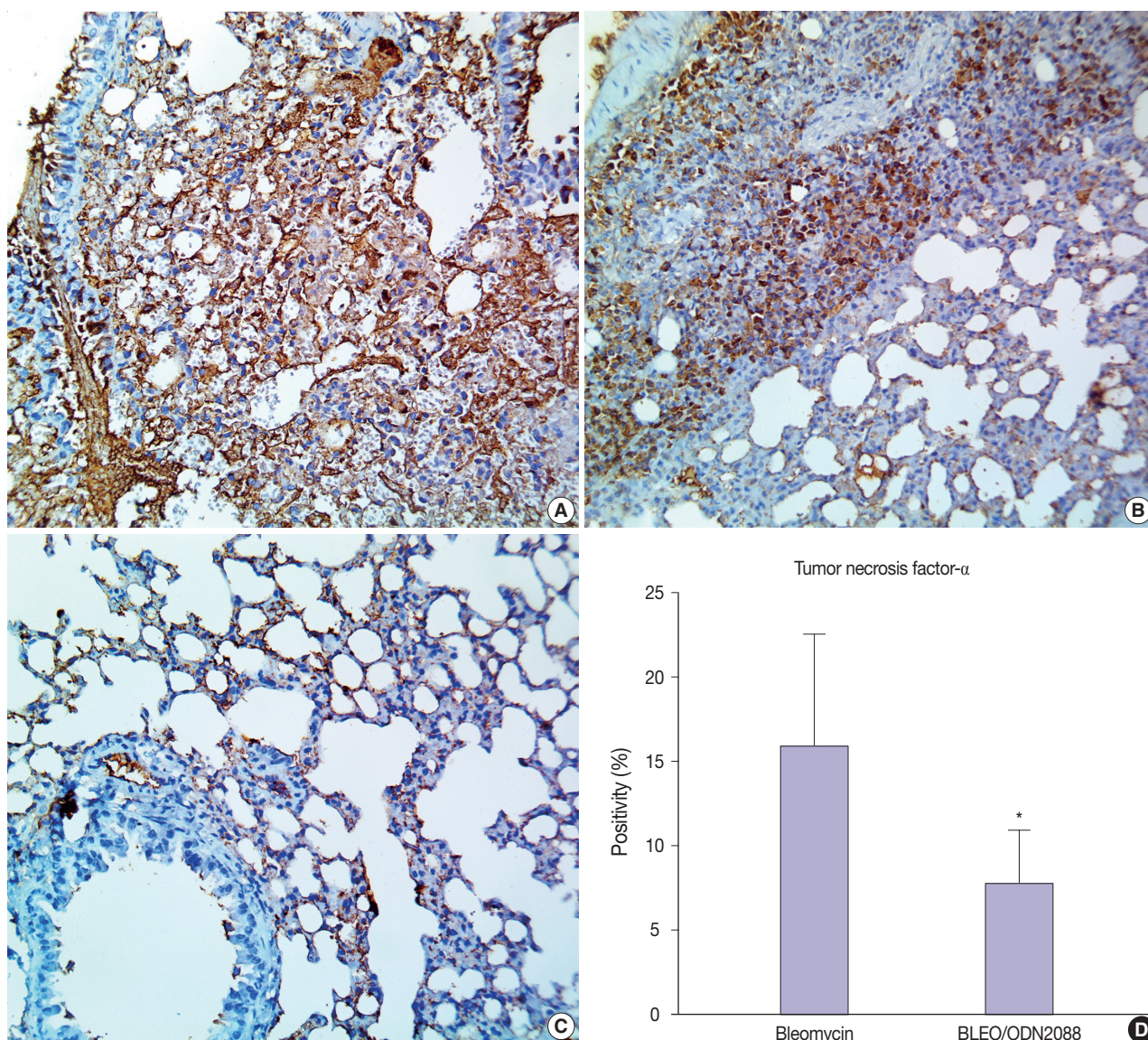


**Fig. 5.** Tumor necrosis factor  $\alpha$  (TNF- $\alpha$ ) immunohistochemical photomicrographs (A–C) and analysis of TNF- $\alpha$  positivity (D) in the lung sections of bleomycin- and bleomycin + ODN2088 (BLEO/ODN2088)-treated mice. Data in the bar graph (D) represent mean  $\pm$  standard deviation, and significant differences ( $p \leq .05$ ) are indicated by an asterisk.

nary damage has been shown to cause inflammation in the lungs, which eventually leads to pulmonary fibrosis [30]. Pulmonary fibrosis causes lung architecture distortion and excessive matrix deposition, which leads to respiratory insufficiency and death [31]. Many efforts are ongoing to alleviate the inflammatory process, lung injury, and pulmonary fibrosis to improve the quality of life in patients suffering from ARDS. There are several animal models that mimic the stages of pulmonary fibrosis in humans. In this research, we used bleomycin to induce lung fibrosis in mice since bleomycin-induced lung injury is a well-studied model of the changes seen in many pulmonary diseases, such as idiopathic

pulmonary fibrosis, interstitial lung disease, and ARDS [26–29, 32]. Prior studies have indicated that ODN2088 is a potent anti-inflammatory agent that halts downstream TLR9 pro-inflammatory pathways [33]. Therefore, the potential efficacy of ODN2088 in preventing bleomycin-induced lung damage, inflammation, and fibrosis was investigated in this study. Our study found that blocking TLR9 with ODN2088 prevented lung fibrosis in bleomycin-treated mice by reducing lung injury and inflammation.

Bleomycin initiates lung injury by generating reactive oxygen species that cause subsequent DNA damage [6]. In addition, bleomycin promotes protein oxidation and lipid peroxidation

and induces an extreme inflammatory response and fibroblastic proliferation in animal models [34]. The fibrosis induced by bleomycin could be attributed to the cytokines secreted from alveolar macrophages following lung injury, such as TGF, IL-1, platelet-derived growth factor, and macrophage inflammatory protein-1 [35]. These cytokines promote the proliferation of myofibroblasts and stimulate the production of abnormal extracellular matrix, leading to fibrosis [36]. Consistent with prior studies on the bleomycin mouse model, the lungs of bleomycin-treated mice in our study showed activation of alveolar macrophages, intense inflammatory response, and fibroblastic and myofibroblastic proliferation, which mimic the stages of lung injury/fibrosis in humans [27,37].

TLRs play an important role in recognizing viruses and triggering the innate immune system [38]. TLR stimulation triggers downstream signaling cascades, resulting in the release of pro-inflammatory cytokines, such as TNF- $\alpha$ , IL-6, IL-1, and interferon type 1. It has been reported that, in severe cases of COVID-19, patients have marked elevation of inflammatory cytokines, such as IL-6, IL-8, IL-10, TNF- $\alpha$ , interferon- $\gamma$ , IL-2, and IL-4 [39,40]. All these findings indicate that targeting TLRs could mitigate the clinical presentation, outcomes, and prognosis of COVID-19. ODN2088 is a murine TLR9 antagonist that has been shown to be potent in preventing hepatic inflammation and fibrosis in a CCl<sub>4</sub>-induced liver fibrosis mouse model [23,33]. In this study, we evaluated ODN2088 as a potential therapeutic agent for prevention of pulmonary injury, inflammation, and fibrosis.

Apoptosis has a vital role in initiating and sustaining fibrosis during the pathophysiology of interstitial lung disease [41]. The pathogenic mechanisms of bleomycin-induced lung fibrosis and idiopathic pulmonary fibrosis (IPF) involve induction of alveolar epithelial cell apoptosis through either the mitochondrial pathway or the caspase cascade linked to the Fas-FasL pathway [42, 43]. Our results showed that ODN2088 greatly decreased the proportion of apoptotic bronchial cells, endothelial cells, and alveolar pneumocytes in bleomycin-treated mice, as represented by low cleaved caspase-3 immunostaining.

Recent studies attributed the lung fibrosis seen in COVID-19 cases to an excessive inflammatory response [44]. TNF- $\alpha$ , an important mediator of inflammation, triggers TGF- $\beta$ 1 and nuclear factor- $\kappa$ B and enhances proliferation and fibroblast differentiation, which ultimately lead to pulmonary fibrosis [45,46]. Previous research showed that a TNF- $\alpha$  antagonist alleviated bleomycin-induced pulmonary fibrosis in mice [47]. In this context, we evaluated ODN2088 as an anti-inflammatory agent against bleomycin-induced pneumonia. In this study, ODN2088 miti-

gated the inflammatory response in injured lungs, as evidenced by low TNF- $\alpha$  expression and a mild inflammatory response in the pulmonary tissues of BLEO/ODN2088-treated mice.

Prior studies emphasized that TLR9 is upregulated in IPF lungs, and CpG-ODN (a TLR agonist) promotes the differentiation of IPF-derived lung fibroblasts into myofibroblasts *in vitro* [48]. In addition, CpG-ODN was found to induce renal interstitial fibrosis in a mouse model of lupus nephritis [49]. Consistent with these previous studies, the present study showed the absence of pulmonary myofibroblasts in ODN2088-treated lung tissues compared to bleomycin-treated ones. Moreover,  $\alpha$ -smooth actin immunostaining and Van Gieson staining were used to confirm the inhibition of myofibroblast differentiation and subsequent fibrosis. The  $\alpha$ -smooth muscle actin expression level and the proportion of Van Gieson-stained collagen fibers were significantly lower in the lungs of BLEO/ODN2088-treated mice compared to those of bleomycin-treated mice. All these findings demonstrate that ODN2088 directly inhibits myofibroblast differentiation and development of pulmonary fibrosis induced by bleomycin.

Furthermore, our *in vivo* study showed a significant ameliorative effect in the lungs of mice given ODN2088 and bleomycin, as evidenced by a decrease in hemodynamic pulmonary lesions caused by bleomycin, such as microvascular damage, pulmonary edema, thrombosis, and hemorrhage. In coronavirus-infected patients, diffuse alveolar damage with serious pulmonary thrombosis and vascular injury has been documented [50], indicating that targeting TLR9 can improve the clinical presentation of ARDS, seen in some COVID-19 patients.

In conclusion, our study demonstrated that ODN2088 was potent in prevention of bleomycin-induced pulmonary injury, inflammation, and fibrosis. ODN2088 markedly diminished alveolar and vascular damages in pulmonary tissues and decreased the production of pro-inflammatory cytokines, inflammatory cellular aggregations, and myofibroblastic proliferation. These findings indicate that blocking TLR9 could be beneficial to treatment of severe acute respiratory syndrome, Middle East respiratory syndrome, and COVID-19 as a novel therapeutic modality to prevent pulmonary injury, fibrosis, and associated hemodynamic abnormalities, especially in the early stages.

#### Ethics Statement

All animal work was approved by the Bioethics Committee of Benha University. All *in vivo* experiments were conducted after the approved by Animal Care and Use Committee of Benha University. Animal welfare and comfort was emphasized during the study. All authors have agreed to publish this manuscript.

### Availability of Data and Material

All data generated or analyzed during the study are included in this published article.

### Code Availability

Not applicable.

### ORCID

Badr Alzahrani <https://orcid.org/0000-0003-4158-640X>  
 Mohamed M. S. Gaballa <https://orcid.org/0000-0003-2949-430X>  
 Ahmed A. Tantawy <https://orcid.org/0000-0002-5017-686X>  
 Maha A. Moussa <https://orcid.org/0000-0002-6987-9012>  
 Salma A. Shoulah <https://orcid.org/0000-0003-2115-1572>  
 Said M. Elshafae <https://orcid.org/0000-0001-6285-5483>

### Author Contributions

Conceptualization: BA, AAT, MMSG, SME. Data curation: AAT, MMSG, SME. Formal analysis: BA, MMSG, AAT, MAM, SAS, SME. Funding acquisition: BA, AAT. Investigation: BA, AAT, MMSG, SME. Methodology: AAT, MMSG, SME. Supervision: AAT, SME. Validation: BA, AAT, MMSG, SME, MAM, SAS. Writing—original draft: BA, MMSG. Writing—review & editing: AAT, SME. Approval of final manuscript: all authors.

### Conflicts of Interest

The authors declare that they have no potential conflicts of interest.

### Funding Statement

No funding to declare.

### References

1. She J, Jiang J, Ye L, Hu L, Bai C, Song Y. 2019 novel coronavirus of pneumonia in Wuhan, China: emerging attack and management strategies. *Clin Transl Med* 2020; 9: 19.
2. Wu Z, McGoogan JM. Characteristics of and important lessons from the coronavirus disease 2019 (COVID-19) outbreak in China: summary of a report of 72314 cases from the Chinese Center for Disease Control and Prevention. *JAMA* 2020; 323: 1239-42.
3. Matthay MA, Zemans RL. The acute respiratory distress syndrome: pathogenesis and treatment. *Annu Rev Pathol* 2011; 6: 147-63.
4. Moore BB, Hogaboam CM. Murine models of pulmonary fibrosis. *Am J Physiol Lung Cell Mol Physiol* 2008; 294: L152-60.
5. Moroni M, Giannetta L, Gelosa G, et al. Second-line chemotherapy with bleomycin, methotrexate, and vinorelbine (BMV) for patients with squamous cell carcinoma of the head, neck and esophagus (SCC-HN&E) pretreated with a cisplatin-containing regimen: a phase II study. *J Chemother* 2003; 15: 394-9.
6. Canellos GP. Lymphoma: present and future challenges. *Semin Hematol* 2004; 41(4 Suppl 7): 26-31.
7. Rimmer Y, Chester J, Joffe J, et al. Accelerated BEP: a phase I trial of dose-dense BEP for intermediate and poor prognosis metastatic germ cell tumour. *Br J Cancer* 2011; 105: 766-72.
8. Gasse P, Riteau N, Charron S, et al. Uric acid is a danger signal activating NALP3 inflammasome in lung injury inflammation and fibrosis. *Am J Respir Crit Care Med* 2009; 179: 903-13.
9. Ruscitti F, Ravanetti F, Essers J, et al. Longitudinal assessment of bleomycin-induced lung fibrosis by Micro-CT correlates with histological evaluation in mice. *Multidiscip Respir Med* 2017; 12: 8.
10. Moore BB, Lawson WE, Oury TD, Sisson TH, Raghavendran K, Hogaboam CM. Animal models of fibrotic lung disease. *Am J Respir Cell Mol Biol* 2013; 49: 167-79.
11. Imai Y, Kuba K, Neely GG, et al. Identification of oxidative stress and Toll-like receptor 4 signaling as a key pathway of acute lung injury. *Cell* 2008; 133: 235-49.
12. Lafferty EI, Qureshi ST, Schnare M. The role of toll-like receptors in acute and chronic lung inflammation. *J Inflamm (Lond)* 2010; 7: 57.
13. Arancibia SA, Beltran CJ, Aguirre IM, et al. Toll-like receptors are key participants in innate immune responses. *Biol Res* 2007; 40: 97-112.
14. Gao W, Xiong Y, Li Q, Yang H. Inhibition of Toll-like receptor signaling as a promising therapy for inflammatory diseases: a journey from molecular to nano therapeutics. *Front Physiol* 2017; 8: 508.
15. Knuefermann P, Baumgarten G, Koch A, et al. CpG oligonucleotide activates Toll-like receptor 9 and causes lung inflammation in vivo. *Respir Res* 2007; 8: 72.
16. Tasaka S, Kamata H, Miyamoto K, et al. Intratracheal synthetic CpG oligodeoxynucleotide causes acute lung injury with systemic inflammatory response. *Respir Res* 2009; 10: 84.
17. Huang L, Chang W, Huang Y, Xu X, Yang Y, Qiu H. Prognostic value of plasma mitochondrial DNA in acute respiratory distress syndrome (ARDS): a single-center observational study. *J Thorac Dis* 2020; 12: 1320-8.
18. Faust HE, Reilly JP, Anderson BJ, et al. Plasma mitochondrial DNA levels are associated with ARDS in trauma and sepsis patients. *Chest* 2020; 157: 67-76.
19. Koupenova M, Mick E, Mikhalev E, Benjamin EJ, Tanriverdi K, Freedman JE. Sex differences in platelet toll-like receptors and their association with cardiovascular risk factors. *Arterioscler Thromb Vasc Biol* 2015; 35: 1030-7.
20. El Kebir D, Damlaj A, Makhezer N, Filep JG. Toll-like receptor 9 signaling regulates tissue factor and tissue factor pathway inhibitor expression in human endothelial cells and coagulation in mice. *Crit Care Med* 2015; 43: e179-89.
21. Hemmi H, Takeuchi O, Kawai T, et al. A Toll-like receptor recognizes bacterial DNA. *Nature* 2000; 408: 740-5.
22. Jurk M, Vollmer J. Therapeutic applications of synthetic CpG oligodeoxynucleotides as TLR9 agonists for immune modulation. *Bio-Drugs* 2007; 21: 387-401.
23. Alzahrani B. Hepatoprotective impact of TLR9 antagonist ODN 2088 against carbon tetrachloride (CCl<sub>4</sub>)-induced hepatic injury. *Am J Biochem Biotechnol* 2020; 16: 9-14.
24. Akishima Y, Akasaka Y, Ishikawa Y, et al. Role of macrophage and smooth muscle cell apoptosis in association with oxidized low-density lipoprotein in the atherosclerotic development. *Mod Pathol* 2005; 18: 365-73.
25. Wang J, Wang BJ, Yang JC, et al. Research advances in the mechanism of pulmonary fibrosis induced by coronavirus disease 2019 and the corresponding therapeutic measures. *Zhonghua Shao Shang Za Zhi* 2020; 36: 691-7.
26. Moeller A, Gilpin SE, Ask K, et al. Circulating fibrocytes are an indicator of poor prognosis in idiopathic pulmonary fibrosis. *Am J Respir Crit Care Med* 2009; 179: 588-94.
27. Liu T, De Los Santos FG, Phan SH. The bleomycin model of pulmonary fibrosis. *Methods Mol Biol* 2017; 1627: 27-42.
28. Amin M, Wu V, Odish M, et al. A case of severe ARDS due to bleomycin-induced lung injury requiring ECMO support. *Chest* 2020; 158(4 Suppl): A1126-7.

29. Daphale A, Acharya S, Shukla S, Alegaonkar S. Bleomycin induced acute respiratory distress syndrome. *J Case Rep* 2017; 7: 55-7.
30. Wilson MS, Wynn TA. Pulmonary fibrosis: pathogenesis, etiology and regulation. *Mucosal Immunol* 2009; 2: 103-21.
31. Noble PW, Barkauskas CE, Jiang D. Pulmonary fibrosis: patterns and perpetrators. *J Clin Invest* 2012; 122: 2756-62.
32. Moeller A, Ask K, Warburton D, Gauldie J, Kolb M. The bleomycin animal model: a useful tool to investigate treatment options for idiopathic pulmonary fibrosis? *Int J Biochem Cell Biol* 2008; 40: 362-82.
33. Alzahrani B, A AMA, Tantawy A. Therapeutic impact of ODN2088 to block TLR9 activity in induced liver fibrosis mice. *Pak J Biol Sci* 2021; 24: 122-31.
34. Chaudhary NI, Schnapp A, Park JE. Pharmacologic differentiation of inflammation and fibrosis in the rat bleomycin model. *Am J Respir Crit Care Med* 2006; 173: 769-76.
35. Chandler DB. Possible mechanisms of bleomycin-induced fibrosis. *Clin Chest Med* 1990; 11: 21-30.
36. Reinert T, da Rocha Baldotto CS, Nunes FA, de Souza Scheliga AA. Bleomycin-induced lung injury. *J Cancer Res* 2013; 2013: 480608.
37. Williamson JD, Sadofsky LR, Hart SP. The pathogenesis of bleomycin-induced lung injury in animals and its applicability to human idiopathic pulmonary fibrosis. *Exp Lung Res* 2015; 41: 57-73.
38. Khanmohammadi S, Rezaei N. Role of Toll-like receptors in the pathogenesis of COVID-19. *J Med Virol* 2021; 93: 2735-9.
39. Lin L, Luo S, Qin R, et al. Long-term infection of SARS-CoV-2 changed the body's immune status. *Clin Immunol* 2020; 218: 108524.
40. He L, Ding Y, Zhang Q, et al. Expression of elevated levels of pro-inflammatory cytokines in SARS-CoV-infected ACE2+ cells in SARS patients: relation to the acute lung injury and pathogenesis of SARS. *J Pathol* 2006; 210: 288-97.
41. Ellson CD, Dunmore R, Hogaboam CM, Sleeman MA, Murray LA. Danger-associated molecular patterns and danger signals in idiopathic pulmonary fibrosis. *Am J Respir Cell Mol Biol* 2014; 51: 163-8.
42. Kuwano K, Kunitake R, Maeyama T, et al. Attenuation of bleomycin-induced pneumopathy in mice by a caspase inhibitor. *Am J Physiol Lung Cell Mol Physiol* 2001; 280: L316-25.
43. Gazdhar A, Fachinger P, van Leer C, et al. Gene transfer of hepatocyte growth factor by electroporation reduces bleomycin-induced lung fibrosis. *Am J Physiol Lung Cell Mol Physiol* 2007; 292: L529-36.
44. Garcia-Revilla J, Deierborg T, Venero JL, Boza-Serrano A. Hyperinflammation and fibrosis in severe COVID-19 patients: galectin-3, a target molecule to consider. *Front Immunol* 2020; 11: 2069.
45. Della Latta V, Cecchetti A, Del Ry S, Morales MA. Bleomycin in the setting of lung fibrosis induction: from biological mechanisms to counteractions. *Pharmacol Res* 2015; 97: 122-30.
46. Zhao Y, Tian B, Sadygov RG, Zhang Y, Brasier AR. Integrative proteomic analysis reveals reprogramming tumor necrosis factor signaling in epithelial mesenchymal transition. *J Proteomics* 2016; 148: 126-38.
47. Altintas N, Erboga M, Aktas C, et al. Protective effect of infliximab, a tumor necrosis factor- $\alpha$  inhibitor, on bleomycin-induced lung fibrosis in rats. *Inflammation* 2016; 39: 65-78.
48. Hinz B. Formation and function of the myofibroblast during tissue repair. *J Invest Dermatol* 2007; 127: 526-37.
49. Anders HJ, Vielhauer V, Eis V, et al. Activation of toll-like receptor-9 induces progression of renal disease in MRL-Fas(lpr) mice. *FASEB J* 2004; 18: 534-6.
50. Angeles Montero-Fernandez M, Pardo-Garcia R. Histopathology features of the lung in COVID-19 patients. *Diagn Histopathol (Oxf)* 2021; 27: 123-7.

# An unusual case of microsatellite instability–high/deficient mismatch repair (MSI-H/dMMR) diffuse large B-cell lymphoma revealed by targeted gene sequencing

Bogyeong Han<sup>1</sup>, Sehui Kim<sup>1</sup>, Jiwon Koh<sup>1</sup>, Jeong Mo Bae<sup>1</sup>, Hongseok Yun<sup>2</sup>, Yoon Kyung Jeon<sup>1,3</sup>

<sup>1</sup>Department of Pathology, Seoul National University Hospital, Seoul National University College of Medicine, Seoul;

<sup>2</sup>Center for Precision Medicine, Seoul National University Hospital, Seoul;

<sup>3</sup>Cancer Research Institute, Seoul National University, Seoul, Korea

Microsatellite instability-high/deficient mismatch repair (MSI-H/dMMR) status has been approved as a tissue-agnostic biomarker for immune checkpoint inhibitor therapy in patients with solid tumors. We report the case of an MSI-H/dMMR diffuse large B-cell lymphoma (DLBCL) identified by targeted gene sequencing (TGS). A 90-year-old female who presented with vaginal bleeding and a large mass in the upper vagina was diagnosed with germinal center-B-cell-like DLBCL, which recurred at the uterine cervix at 9 months after chemotherapy. Based on TGS of 121 lymphoma-related genes and the LymphGen algorithm, the tumor was classified genetically as DLBCL of EZB subtype. Mutations in multiple genes, including frequent frameshift mutations, were detected by TGS and further suggested MSI. The MSI-H/dMMR and loss of MLH1 and PMS2 expression were determined in MSI-fragment analysis, MSI real-time polymerase chain reaction, and immunohistochemical tests. This case demonstrates the potential diagnostic and therapeutic utility of lymphoma panel sequencing for DLBCL with MSI-H/dMMR.

**Key Words:** Diffuse large B-cell lymphoma; Microsatellite instability; Deficient mismatch repair; Targeted gene sequencing

**Received:** April 22, 2021 **Revised:** October 14, 2021 **Accepted:** October 15, 2021

**Corresponding Author:** Yoon Kyung Jeon, MD, PhD, Department of Pathology, Seoul National University Hospital, Seoul National University College of Medicine, 103 Daehak-ro, Jongno-gu, Seoul 03080, Korea  
 Tel: +82-2-740-8323, Fax: +82-2-743-5530, E-mail: ykjeon@snu.ac.kr

Microsatellite instability (MSI) is a condition of genetic hypermutability caused by an impaired DNA mismatch repair system, which arises through a germline or somatic mutation, or a promoter hypermethylation [1]. MSI-high (MSI-H) or mismatch repair deficiency (dMMR) status in solid tumors predicts their response to immune checkpoint blockade [2]. Thus, in 2017, the U.S. Food and Drug Administration (FDA) approved the programmed death-1 (PD-1)–blocking agent pembrolizumab for treatment of unresectable or metastatic MSI-H/dMMR solid tumors, irrespective of cancer type; this was the first cancer site/histology-agnostic biomarker approved by the FDA [3]. However, the prevalence of MSI is highly variable across cancer types; it is very low (< 1%) in non-Hodgkin lymphomas, except immunodeficiency-related lymphomas [4-8]. MSI has been studied widely in colon cancer and endometrial cancer but only rarely in diffuse large B-cell lymphoma (DLBCL) [4,8,9]. The clinical relevance

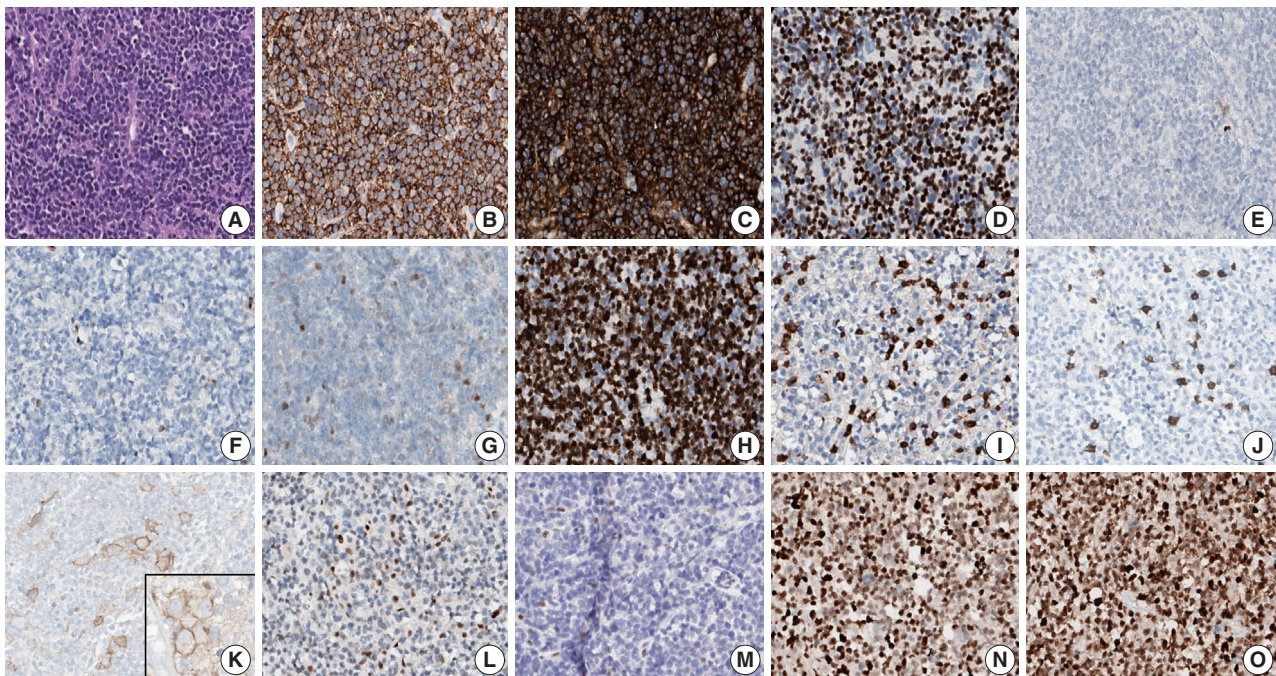
of MSI in patients with DLBCL, in terms of prognostic significance or as a predictor of the response to immune checkpoint blockade, is unknown. Here, we report an unusual case of MSI-H/dMMR DLBCL initially identified by clinical targeted gene sequencing (TGS) and subsequently confirmed by MSI testing.

## CASE REPORT

A 90-year-old female presented with vaginal bleeding. A protruding polypoid mass measuring 5.8 cm was detected in the upper vagina by pelvic magnetic resonance imaging. Positron emission tomography revealed an additional focal hypermetabolic lesion in the presacral area. A tissue biopsy was conducted under the suspicion of cervical cancer. The patient was diagnosed with DLBCL with a germinal center B-cell-like (GCB) phenotype determined by immunohistochemistry (IHC)-based Hans algo-

rhythm, clinical stage of IIA, and Eastern Cooperative Oncology Group performance status of 1. Rituximab and reduced-dose CHOP (cyclophosphamide, doxorubicin, vincristine, and prednisone) resulted in complete remission (CR), but after 9 months, she suffered local relapse at the uterine cervix and underwent tumor excision. Microscopically, the tumor was composed of atypical lymphoid cells with a centroblastic morphology and diffuse arrangement. IHC for CD3, CD20, C-MYC, BCL-2, BCL-6, CD10, MUM1, Ki-67, CD8, and programmed death-ligand 1 (PD-L1) (clone E1L3N) and in situ hybridization for Epstein-Barr virus (EBV) and fluorescence in situ hybridization (FISH) for *MYC* were performed. Tumor cells were positive for CD20, CD10, and BCL-6 but negative for MUM1, BCL-2, C-MYC, and EBV. The Ki-67 labeling index of tumor cells was 80% (Fig. 1A–H). *MYC* translocation was not observed in FISH (data not shown). The tumor was diagnosed again as DLBCL with a GCB phenotype. Scattered CD3<sup>+</sup> or CD8<sup>+</sup> tumor-infiltrating lymphocytes were observed (Fig. 1I, J), and PD-L1 was expressed in tumor-associated macrophages and in about 5% of tumor cells (Fig. 1K). TGS was performed using a customized panel comprising 121 lymphoma-related genes and formalin-

fixed paraffin-embedded sections of the surgical specimen; it revealed 16 mutations across 15 genes including *ARID1A*, *DNMT3A*, *PDCD1*, *SETD2*, *PDGFRA*, *TET2*, *PRDM1*, *CARD11*, *ATM*, *KMT2D*, *B2M*, *CREBBP*, *CIITA*, *GNA13*, and *BTK* (Table 1). The tumor was genetically classified as EZB subtype DLBCL according to the LymphGen algorithm (<https://lmpp.nih.gov/lymphgen/index.php>) [10]. In addition, 34 further mutations (27 missense mutations, 5 frameshift mutations, 1 inframe indel mutation, and 1 stop-gain mutation) in 28 genes were identified as rare germline variants or variants of uncertain significance (data not shown). Although microsatellite markers were not included in this lymphoma panel, the unusually high number of variants, including a large number of frameshift mutations, suggested MSI. A fragmentation assay based on the Bethesda guidelines, immunohistochemistry of four proteins involved in the mismatch repair (MMR) pathway (*MLH1*, *MSH2*, *MSH6* and *PMS2*), and a U-TOP MSI detection test (Seasun Biomaterials Inc., Daejeon, Korea) were conducted. On the fragmentation assay, four (*BAT25*, *BAT26*, *D2S123*, and *D17S2720*) of the five Bethesda microsatellite markers showed features suggestive of MSI (data not shown). A loss of *MLH1* and *PMS2*

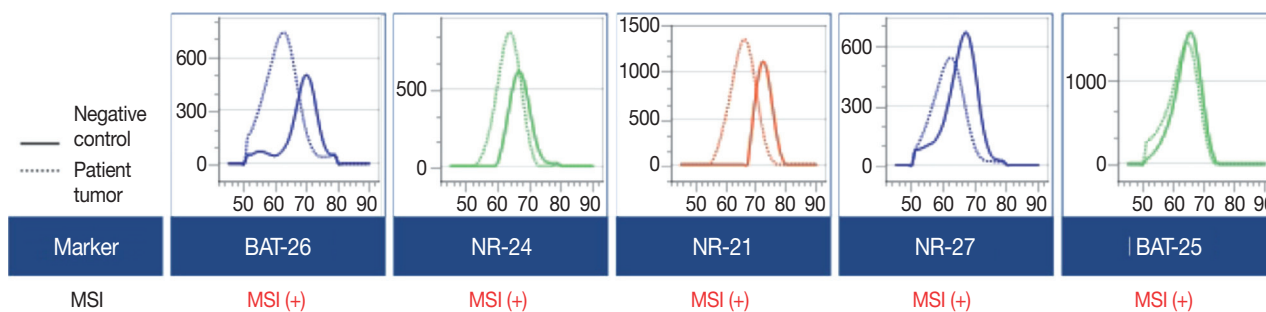


**Fig. 1.** Microscopy and immunohistochemical findings. (A) Atypical lymphoid cells show a centroblastic morphology and diffuse growth pattern. Atypical lymphoid cells are positive for CD20 (B), CD10 (C), and BCL6 (D) and are negative for MUM1 (E), BCL2 (F), and C-MYC (G). The Ki-67 labeling index was 80% (H). Scattered small CD3<sup>+</sup> cells (I) and CD8<sup>+</sup> cells (J) are observed. Programmed death-ligand 1 is expressed mainly in tumor-associated macrophages and occasionally in tumor cells (insert, about 5% of tumor cells in the whole slide) (K). Immunohistochemistry reveals mismatch repair proteins and loss of expression of *MLH1* (L) and *PMS2* (M) but intact expression of *MSH6* (N) and *MSH2* (O).

**Table 1.** Variants found in DLBCL by targeted sequencing based on 121 lymphoma-related genes (excluding rare germline variants or variants of uncertain significance)

Gene	Chr	Position	Reference sequence	Exon	cDNA change	AA change	VAF (%)
<i>ARID1A</i>	chr1	27105930	NM_006015.4	20	c.5548dupG	p.Asp1850fs	34.32
<i>DNMT3A</i>	chr2	25457242	NM_022552.4	23	c.2645G>A	p.Arg882His	44.45
<i>PDCD1</i>	chr2	242795103	NM_005018.2	2	c.105delC	p.Thr36fs	36.23
<i>SETD2</i>	chr3	47125614	NM_014159.6	12	c.5656G>A	p.Glu1886Lys	41.73
<i>PDGFRA</i>	chr4	55151558	NM_006206.4	17	c.2347delT	p.Ser783fs	42.52
<i>TET2</i>	chr4	106193857	NM_001127208.2	10	c.4319G>A	p.Arg1440Gln	44.39
<i>PRDM1</i>	chr6	106555015	NM_001198.3	7	c.2132C>A	p.Ala711Asp	43.55
<i>CARD11</i>	chr7	2983911	NM_032415.5	5	c.619C>T	p.Arg207Cys	42.73
<i>ATM</i>	chr11	108216612	NM_000051.3	58	c.8561G>A	p.Arg2854His	40.91
<i>KMT2D</i>	chr12	49420238	NM_003482.3	48	c.15511C>T	p.Arg5171Trp	43.12
<i>KMT2D</i>	chr12	49431873	NM_003482.3	34	c.9265dupG	p.Val3089fs	36.08
<i>B2M</i>	chr15	45003779	NM_004048.2	1	c.35T>C	p.Leu12Pro	44.60
<i>CREBBP</i>	chr16	3786070	NM_004380.2	28	c.4694delA	p.Lys1565fs	42.97
<i>CIITA</i>	chr16	11001304	NM_001286402.1	11	c.1965dupC	p.Gly656fs	82.74
<i>GNA13</i>	chr17	63052509	NM_006572.5	1	c.203T>G	p.Met68Arg	43.85
<i>BTK</i>	chrX	100613407	NM_000061.2	12	c.993A>G	p.Ile331Met	45.38

Chr, chromosome; AA, amino acid; VAF, variant allelic frequency.

**Fig. 2.** Microsatellite instability (MSI) test results. MSI was detected in all five quasi-monomorphic markers using the U-TOP MSI detection test, revealing the MSI-high (MSI-H) status of the tumor. Genomic DNA from HeLa cells was used as a negative control.

protein expression was detected by immunohistochemistry (Fig. 1L–O), and the U-TOP MSI detection test, which uses five quasi-monomorphic mononucleotide markers that do not require samples of normal tissue from the patient for comparison [11], showed MSI in all five markers, confirming the MSI-H/dMMR status of the tumor (Fig. 2). The patient was treated by radiotherapy of the involved site and has been in metabolic CR for the past 7 months.

## DISCUSSION

MSI-H or dMMR status is the first tissue-agnostic biomarker approved by the FDA for cancer therapy and, more specifically, for pembrolizumab therapy [3]. Patients with MSI-H/dMMR tumors have shown a favorable clinical response to PD-1 blockade, regardless of cancer type [2]. This illustrates the need for MSI-H tumor detection. MSI-PCR of the Bethesda panel to as-

sess three dinucleotide repeats (D2S123, D5S346, D17S250) and two mononucleotide repeats (BAT26, BAT25) is the gold standard for detecting MSI. According to the revised Bethesda guidelines, pentaplex PCR with five quasi-monomorphic mononucleotide repeats can detect MSI with high sensitivity and specificity and might not need matched normal tissue [1]. Together with immunohistochemistry for MMR proteins, it allows determination of MMR status [1]. MSI testing performed in endometrial, colorectal, and gastric cancers has revealed high variability in the frequency of MSI-H among cancers [4,12]. However, the frequency of MSI-H non-Hodgkin lymphoma generally is low (0%–2%), which has hampered standardized MSI testing as a routine diagnostic method [4,12]. Recently, next-generation sequencing (NGS)-based TGS using a panel of tumor markers has been introduced for molecular pathologic diagnosis. In solid tumors, NGS-based MSI tests have shown high sensitivity and specificity in the absence of control normal tissue [4–7].

Although unified criteria for detection of MSI by NGS are lacking, many laboratories are using MMR-related genes and MSI markers, as well as bioinformatics algorithms, for tumor diagnosis [4-7].

The FDA has approved PD-1 blockade therapy based on its efficacy in patients with hematologic malignancies, including Hodgkin lymphoma and primary mediastinal large B-cell lymphoma [13,14]. A recent study demonstrated the potential benefit of PD-1 blockade in combination with R-CHOP in patients with treatment-naïve DLBCL overexpressing PD-L1 [15]. However, both the MSI landscape and efficacy of PD-1 blockade for MSI-H lymphoma remain unclear. A previous study reported DLBCL with defects in DNA repair genes, including tumor suppressor genes, MMR-related genes (e.g., *MSH2* and *MSH6*), and non-homologous end-joining pathway-related genes, and it suggested an association of genomic instability phenotype with tumorigenesis of DLBCL [16]. However, recent analyses of NGS data showed that MSI-H in non-Hodgkin lymphoma, including DLBCL, is either extremely rare (<1%) or not a feature of these tumors [4-7]. In contrast to those reports, a study using a commercial MSI kit, based on eight mononucleotide repeat markers and two pentanucleotide repeat markers, identified MSI-H and microsatellite instability–low (MSI-L) in 3% (3/92) and 10% (9/92) of DLBCLs, respectively [9]. According to the authors, patients with MSI-H DLBCL tended to have a better prognosis than those with microsatellite stable DLBCL, although the difference was not significant [9]. They also reported that MSI-L DLBCL was associated with a poor response to chemotherapy [9]. These results suggest that MSI status could be a useful biomarker for DLBCL.

Reports on the prognostic and therapeutic impacts of molecular genetic classification of DLBCL indicate the potential utility of TGS in individually tailored treatment for DLBCL [10,17]. The LymphGen algorithm classified DLBCLs into five genetic subtypes: MCD (including *MYD88* L265P and *CD79B* mutations), BN2 (including *BCL6* translocations and *NOTCH2* mutations), N1 (including *NOTCH1* mutations), EZB (including *EZH2* mutations and *BCL2* translocations), and A53 (aneuploid with TP53 inactivation) [10]. Our inclusion of 121 lymphoma-related genes allowed successful genetic determination of the tumor as EZB, which is the most common genetic subtype of GCB-DLBCL [10]. TGS also revealed frequent frameshift mutations and C:G → A:T transversions, as previously reported in MMR-mutated DLBCLs [16]. Although MMR gene mutations could not be identified directly using our lymphoma panel, the unique mutational pattern of our patient's tumor was sug-

gestive of an MSI-H/dMMR DLBCL. The MSI status of the tumor was confirmed by two kinds of MSI tests for microsatellite markers (i.e., MSI-fragmentation assay and MSI-pentaplex real-time PCR using U-TOP MSI detection test), as well as by immunohistochemistry for four MMR proteins.

However, because our patient did not receive PD-1 blockade therapy, the efficacy for treating this type of tumor could not be determined. Nonetheless, this case shows that MSI-H/dMMR can be present in DLBCL, albeit rarely, and the utility of TGS for detection of MSI-H/dMMR in hematolymphoid malignancies.

### Ethics Statement

This study was approved by the Institutional Review Board (IRB) of Seoul National University Hospital (No. 2012-160-1184) and written informed consent from the patient was waived by IRB decision.

### Availability of Data and Material

The datasets generated or analyzed during the study are available from the corresponding author on reasonable request.

### Code Availability

Not applicable.

### ORCID

Bogyong Han <https://orcid.org/0000-0003-0391-7415>  
 Sehui Kim <https://orcid.org/0000-0002-6640-3051>  
 Jiwon Koh <https://orcid.org/0000-0002-7687-6477>  
 Jeong Mo Bae <https://orcid.org/0000-0003-0462-3072>  
 Hongseok Yun <https://orcid.org/0000-0003-2776-5954>  
 Yoon Kyung Jeon <https://orcid.org/0000-0001-8466-9681>

### Author Contributions

Conceptualization: YKJ, JMB. Data curation: BH, SK. Formal analysis: JK, JMB, HY. Investigation: BH, JMB, HY. Visualization: BH, SK. Writing—original draft: BH, SK. Writing—review & editing: JK, YKJ. Approval of final manuscript: all authors.

### Conflicts of Interest

The authors declare that they have no potential conflicts of interest.

### Funding Statement

This study was funded by Basic Science Research Program (grant No.: NRF-2016R1D1A1B01015964) through the National Research Foundation (NRF) funded by the Ministry of Education, Science and Technology (MEST).

### References

1. Umar A, Boland CR, Terdiman JP, et al. Revised Bethesda Guidelines for hereditary nonpolyposis colorectal cancer (Lynch syndrome) and microsatellite instability. *J Natl Cancer Inst* 2004; 96: 261-8.
2. Le DT, Durham JN, Smith KN, et al. Mismatch repair deficiency predicts response of solid tumors to PD-1 blockade. *Science* 2017; 357: 409-13.
3. Marcus L, Lemery SJ, Keegan P, Pazdur R. FDA approval summary: pembrolizumab for the treatment of microsatellite instability-high

- solid tumors. *Clin Cancer Res* 2019; 25: 3753-8.
4. Bonneville R, Krook MA, Kautto EA, et al. Landscape of microsatellite instability across 39 cancer types. *JCO Precis Oncol* 2017; 2017: PO.17.00073.
  5. Middha S, Zhang L, Nafa K, et al. Reliable pan-cancer microsatellite instability assessment by using targeted next-generation sequencing data. *JCO Precis Oncol* 2017; 2017: PO.17.00084.
  6. Albayrak A, Garrido-Castro AC, Giannakis M, et al. Clinical pan-cancer assessment of mismatch repair deficiency using tumor-only, targeted next-generation sequencing. *JCO Precis Oncol* 2020; 4: 1084-97.
  7. Trabucco SE, Gowen K, Maund SL, et al. A novel next-generation sequencing approach to detecting microsatellite instability and pan-tumor characterization of 1000 microsatellite instability-high cases in 67,000 patient samples. *J Mol Diagn* 2019; 21: 1053-66.
  8. Duval A, Raphael M, Brennetot C, et al. The mutator pathway is a feature of immunodeficiency-related lymphomas. *Proc Natl Acad Sci U S A* 2004; 101: 5002-7.
  9. Tian T, Li J, Xue T, Yu B, Li X, Zhou X. Microsatellite instability and its associations with the clinicopathologic characteristics of diffuse large B-cell lymphoma. *Cancer Med* 2020; 9: 2330-42.
  10. Wright GW, Huang DW, Phelan JD, et al. A probabilistic classification tool for genetic subtypes of diffuse large B cell lymphoma with therapeutic implications. *Cancer Cell* 2020; 37: 551-68.
  11. Suraweera N, Duval A, Reperant M, et al. Evaluation of tumor microsatellite instability using five quasimonomorphic mononucleotide repeats and pentaplex PCR. *Gastroenterology* 2002; 123: 1804-11.
  12. Hause RJ, Pritchard CC, Shendure J, Salipante SJ. Classification and characterization of microsatellite instability across 18 cancer types. *Nat Med* 2016; 22: 1342-50.
  13. Armand P, Rodig S, Melnichenko V, et al. Pembrolizumab in relapsed or refractory primary mediastinal large B-cell lymphoma. *J Clin Oncol* 2019; 37: 3291-9.
  14. Kuruvilla J, Ramchandren R, Santoro A, et al. Pembrolizumab versus brentuximab vedotin in relapsed or refractory classical Hodgkin lymphoma (KEYNOTE-204): an interim analysis of a multicentre, randomised, open-label, phase 3 study. *Lancet Oncol* 2021; 22: 512-24.
  15. Smith SD, Till BG, Shadman MS, et al. Pembrolizumab with R-CHOP in previously untreated diffuse large B-cell lymphoma: potential for biomarker driven therapy. *Br J Haematol* 2020; 189: 1119-26.
  16. de Miranda NF, Peng R, Georgiou K, et al. DNA repair genes are selectively mutated in diffuse large B cell lymphomas. *J Exp Med* 2013; 210: 1729-42.
  17. Dubois S, Vially PJ, Mareschal S, et al. Next-generation sequencing in diffuse large B-cell lymphoma highlights molecular divergence and therapeutic opportunities: a LYSA study. *Clin Cancer Res* 2016; 22: 2919-28.

# Colorectal adenocarcinoma with enteroblastic differentiation: diagnostic challenges of a rare case encountered in clinical practice

Evi Abada<sup>1</sup>, Ifeoma C. Anaya<sup>2</sup>, Othuke Abada<sup>3</sup>, Anthony Lebbos<sup>4</sup>, Rafic Beydoun<sup>1</sup>

<sup>1</sup>Department of Pathology, Wayne State University School of Medicine/Detroit Medical Center, Detroit, MI; <sup>2</sup>Larkin Community Hospital, South Miami, FL; <sup>3</sup>Ascension St. John Hospital, Detroit, MI; <sup>4</sup>Michigan State University, East Lansing, MI, USA

Colorectal adenocarcinoma with enteroblastic differentiation (CAED) is a rare subtype of colonic adenocarcinoma characterized by increased  $\alpha$ -fetoprotein (AFP) production and the expression of at least one enteroblastic marker including AFP, glypican 3 (GPC3), or Spalt like transcription factor 4 (SALL4). We report a case of a 26-year-old female who presented with low back pain and constipation which persisted despite supportive measures. Imaging revealed multiple liver lesions and enlarged retroperitoneal nodes. Tumor markers including AFP were markedly elevated. On biopsy, samples from the liver revealed infiltrating glands lined by columnar-type epithelium with mostly eosinophilic granular to focally clear cytoplasm. By immunohistochemistry, the tumor showed immunoreactivity with AFP, hepatocyte antigen, GPC3, SALL4, CDX2, SATB2, and cytokeratin 20. A colonoscopy performed subsequently revealed a mass in the sigmoid colon and biopsy of this mass revealed a similar histology as that seen in the liver. A diagnosis of CAED was made, following the results of gene expression profiling by the tumor with next-generation sequencing which identified pathogenic variants in *MUTYH*, *TP53*, and *KDM6A* genes and therefore supported its colonic origin. Cases such as this underscores the use of ancillary diagnostic techniques in arriving at the correct diagnosis in lesions with overlapping clinicopathologic characteristics.

**Key Words:** Colorectal neoplasms; Colorectal adenocarcinoma with enteroblastic differentiation; Alpha fetoprotein

**Received:** August 21, 2021 **Revised:** October 26, 2021 **Accepted:** October 27, 2021

**Corresponding Author:** Evi Abada, MD, MS, Department of Pathology, Wayne State University School of Medicine/Detroit Medical Center, 3990 John R. Road, Detroit, MI 48201, USA

Tel: +1-313-577-1102, Fax: +1-313-577-0057, E-mail: [gs5839@wayne.edu](mailto:gs5839@wayne.edu)

Colorectal adenocarcinoma with enteroblastic differentiation (CAED) is a rare subtype of colorectal adenocarcinoma with expression of enteroblastic markers including glypican 3 (GPC3), Spalt like transcription factor 4 (SALL4), and  $\alpha$ -fetoprotein (AFP) [1]. The incidence of CAED compared with other types of colorectal carcinoma (CRC) have been reported to be 0.72% [1]. Many cases consist of cells which have a clear cytoplasm, but some cases present with eosinophilic cytoplasm, while others may be poorly differentiated. The unifying characteristic for these different phenotypes is the expression of at least one enteroblastic marker by the tumor.

In contrast to the conventional type, gastrointestinal adenocarcinoma with enteroblastic differentiation tends to be aggressive with frequent lymphovascular infiltration, metastasis to the liver, and lymphatics. This corresponds with a poor prognosis [2,3]. Most AFP-producing tumors are reported to arise from organs of the foregut endoderm such as the stomach, bile duct, and

pancreas [4]. However, AFP-producing colorectal adenocarcinoma is extremely rare, possibly because the colorectum originates from the hindgut endoderm [4,5].

AFP is an oncofetal glycoprotein produced by the fetal liver, yolk sac, and a small amount from the fetal gastrointestinal epithelium [6]. Serum levels are elevated after birth but decrease significantly by the second year of life [4]. Thus, an increase in serum AFP is abnormal in adults as it is produced by certain tumors, making it a useful tumor marker for the diagnosis and monitoring of treatment [7].

In addition to AFP, the oncofetal proteins GPC3 and SALL4, expressed in germ cell tumors, are immunohistochemically associated with AFP-producing gastric cancers and their related counterparts. Other markers include cytokeratin (CK) 7, CK 20, and caudal-type homeobox 2 (CDX2) which aid in differentiating between tumors of the breast, gynecological tract, liver, and lung origin [8].

Here we present a case of chemo-refractory CAED in a young female who initially presented with multiple liver lesions, and a mass in the sigmoid colon, with diagnostic considerations of a primary hepatocellular carcinoma (HCC), germ cell tumor, and CAED, and the use of ancillary diagnostic techniques in arriving at the correct diagnosis.

## CASE REPORT

This is a case of a 26-year-old female who presented clinically with a history of low backache and constipation, which persisted despite supportive measures. Imaging studies revealed multiple liver lesions, with enlarged retroperitoneal lymph nodes. Tumor markers at presentation included an AFP of 39,493 ng/mL, car-

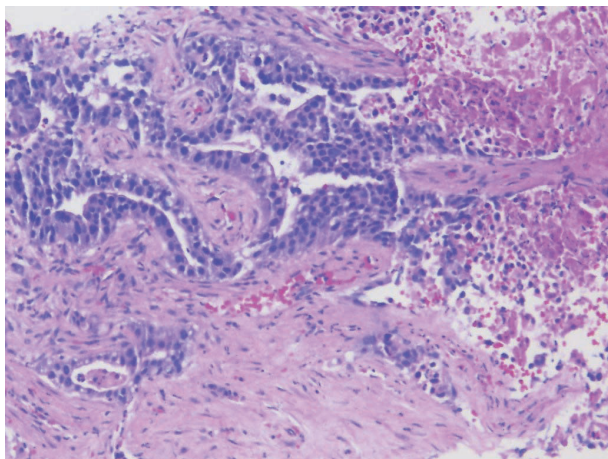


**Fig. 1.** Liver mass biopsy showing infiltrative malignant glands and a focus of necrosis is also seen.

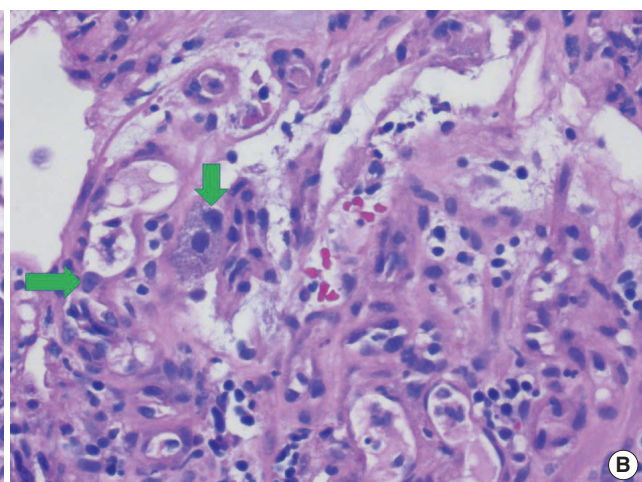
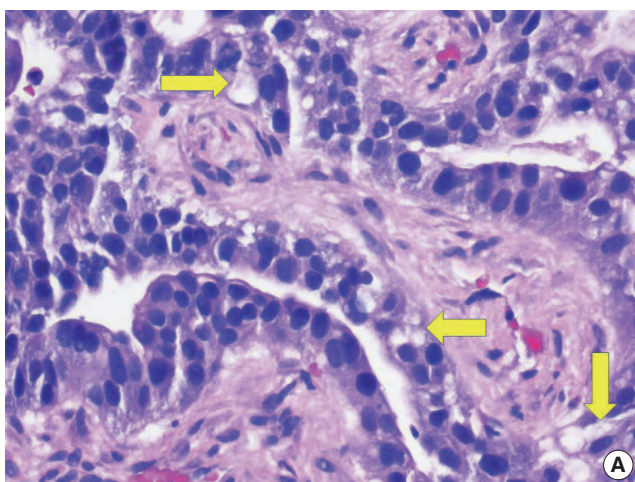


**Fig. 2.** (A) Higher magnification of hepatic mass showing cells with moderate amounts of mostly granular eosinophilic to focally clear cytoplasm (arrows). (B) Higher magnification of hepatic mass showing tumor cells with moderate amounts of mostly granular eosinophilic cytoplasm and inconspicuous nucleoli (arrows).

cinoembryonic antigen of 3,040 ng/mL, cancer antigen (CA) 19-9 of 621 U/mL, and CA 125 of 42 U/mL.

A biopsy of her liver nodules was performed and histopathologic review of tissue sections revealed segmental necrosis with infiltrating adenocarcinoma (Fig. 1). The tumor cells had moderate amounts of mostly granular eosinophilic to focally clear cytoplasm (Fig. 2A) and nuclei with densely homogenous chromatin and occasional inconspicuous nucleoli (Fig. 2B). Immunohistochemistry (IHC) revealed that the tumor cells were immunoreactive for AFP (Fig. 3A), Sal-like protein 4 (Fig. 3B), CK20 (Fig. 3C), and showed strong diffuse immunoreactivity with CDX2 (Fig. 3D). Hepatocyte specific antigen was also positive on IHC. However, CK7, PAX8, and S100 were all negative. A colonoscopy performed subsequently, revealed a mass in the sigmoid colon and biopsy of this mass revealed a similar histology as that seen in the liver (Fig. 4A–C). IHC expression in the colonic tumor showed similar expression as that in the liver. Considering the fact that CDX2 positivity would be unlikely in a primary HCC, a diagnosis of CAED was favored based on a combination of serum tumor markers, tumor morphology, and IHC expression in the tumor cells. Additional testing performed on the tumor cells include human epidermal growth factor receptor 2, which was interpreted as equivocal (2+) on IHC and negative by fluorescence in situ hybridization. *KRAS* mutations were identified in the tumor cells, but programmed death-ligand 1 (PD-L1) was negative. IHC stains for mismatch repair (MMR) proteins MLH1, MSH2, MSH6, and PMS2 showed no loss of expression (no evidence of MMR deficiency). She was commenced on targeted therapy including FOLFOX (leucovorin calcium [folinic

acid], fluorouracil, and oxaliplatin) and bevacizumab. However, with suboptimal improvement in her clinical disease, a second opinion was sought.

She underwent additional imaging studies which revealed new satellite lesions in the liver and previously undiscernible lesions

in bilateral ovaries, which was highly suspicious for advancing metastatic disease. With the discovery of new lesions in the ovary, her previous biopsies from the liver nodules and colonic mass were re-reviewed and a diagnosis of poorly differentiated carcinoma, most suggestive of yolk sac tumor was rendered in the original

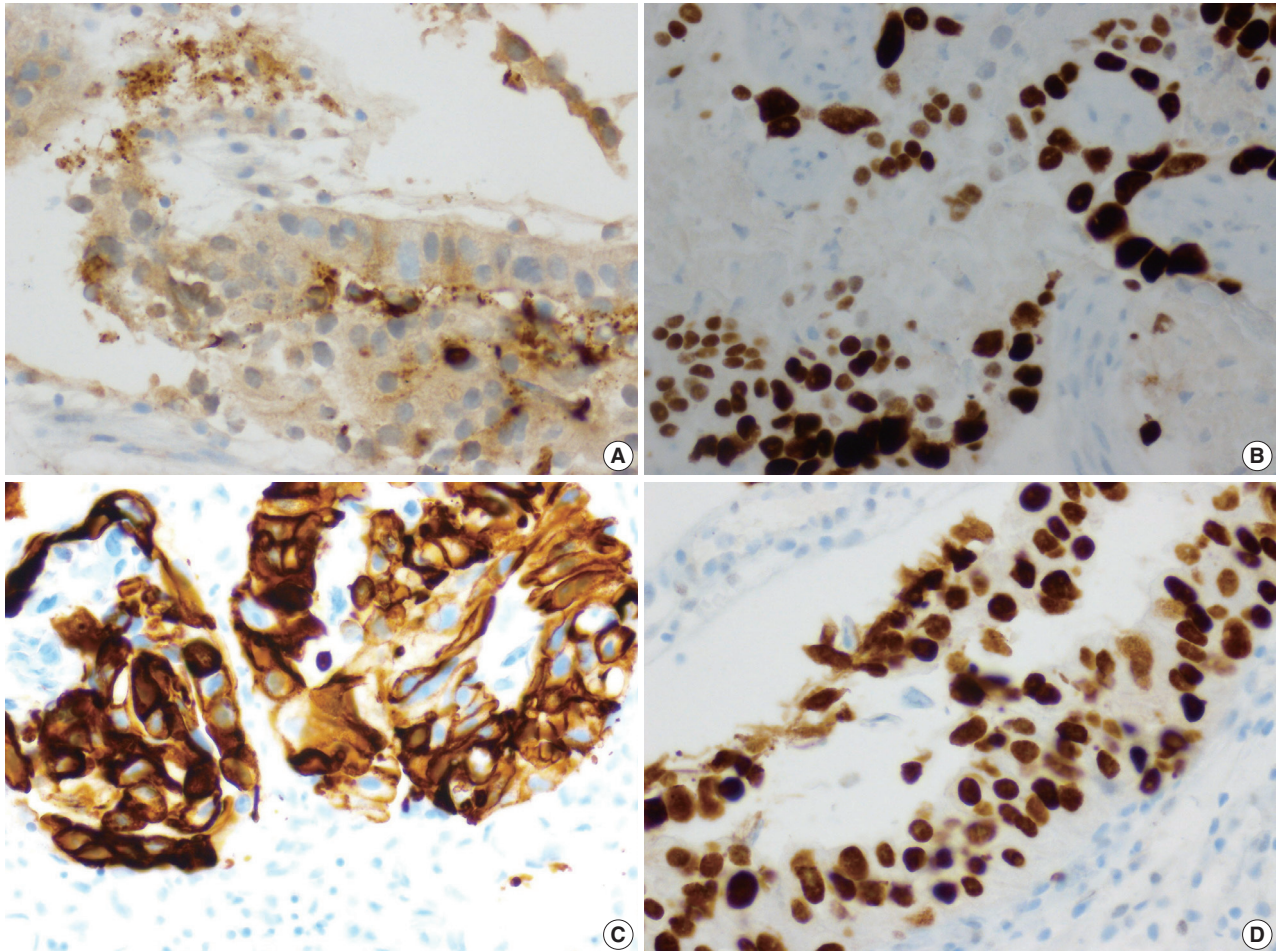


**Fig. 3.** Immunohistochemical stains show that the tumor cells are immunoreactive for  $\alpha$ -fetoprotein (A), Sal-like protein 4 (B), cytokeratin 20 (C), and CDX2 (D).

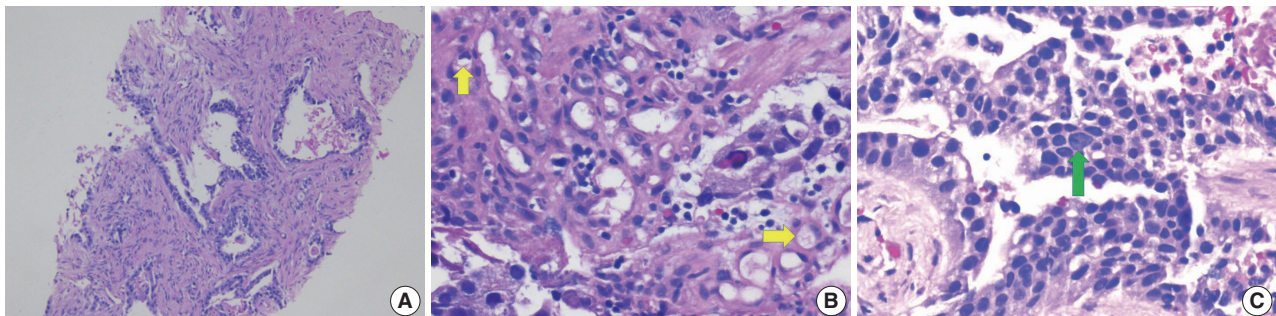


**Fig. 4.** (A) Biopsy of sigmoid colon mass showing infiltrative malignant glands. (B) Higher magnification of colonic mass showing cells with moderate amounts of mostly granular eosinophilic to focally clear cytoplasm (arrows). (C) Higher magnification of colonic mass showing tumor cells with moderate amounts of mostly granular eosinophilic cytoplasm and a cell with inconspicuous nucleolus (arrow).

liver and colonic tumor specimens. Other differentials that were considered included a mixed germ cell tumor or teratoma. She was commenced on chemotherapy for germ cell tumors (cisplatin, etoposide, and bleomycin) but showed disease progression on imaging studies. This prompted a decision to send the specimens from the liver and colon for tumor gene expression profiling by next-generation sequencing (NGS). NGS identified several pathogenic variants including *MUTYH* (exon 13, p.G396D), *TP53* (exon 5, p.R175H), and *KDM6A* (exon 16, p.S532fs). Additionally, estrogen receptor and progesterone receptor by IHC were both negative. Based on the constellation of clinical findings and test results, a diagnosis of CAED was upheld and she is being evaluated for autologous transplant for chemo-refractory CAED.

## DISCUSSION

The incidence of AFP-producing gastric carcinoma has been documented to be within the range of 1.3%–15% worldwide with the incidence of the colorectal variant being significantly lower compared to the gastric [9]. This was first reported by Nakajima et al. in 1985 [10]. Prior reports suggest that CAED is more common in males and tends to be located in the left colon [1,2].

Furuya et al. in their case report in 2011 reported the first case of primary AFP-producing clear cell adenocarcinoma of the colon in an 81-year-old man, which is considered extremely rare when compared to that of gastric origin [11]. They made a distinction between a primary colonic tumor and metastasis from the gynecological tract or other organs by whole-body computed tomography (CT) and immunostaining. CT results revealed tumor deposits in the colon and lung only with CK7 negative and CD20 positive immunoreactivity [11].

Histologically, the tumor cells display a spectrum of morphologic patterns. One report describes tumor cells that displayed typical adenocarcinoma morphologies composed of cuboidal or columnar cells with clear cytoplasm resembling the primitive gut [12]. The enteroblastic component was seen occurring concurrently with typical well or moderately differentiated tubular adenocarcinomas [12]. Another report describes the tumor's morphology as characterized by a solid-type poorly differentiated carcinoma, mainly composed of eosinophilic cells with focal glandular differentiation on hematoxylin and eosin stains [13].

Our patient is a young, 26-year-old female, an interesting demographic in contrast to most documented cases of CAED. Her primary tumor was located on the left side (sigmoid colon) with multiple liver, nodal, and bilateral ovarian involvements war-

ranting the diagnostic consideration of mixed germ cell tumor especially with unresponsiveness to conventional chemotherapy. However, with tumor progression on imaging following the administration of chemotherapy for germ cell tumor and the IHC profile, a diagnosis of chemo-refractory CAED was ultimately favored, based on the constellation of clinicopathologic findings and results of gene expression of the tumor cells by NGS. Of note is that the *MUTYH* gene encodes a DNA glycosylase involved in oxidative DNA damage repair and mutations in the gene predispose to colon and stomach cancers. A germline mutation in *TP53* predisposes to multiple cancers, including colorectal cancer.

Clear cell changes were proposed by Eloy et al. [14] to be a result of degenerative changes with an accumulation of cytoplasmic lipid-like material and not necessarily the accumulation of cytoplasmic glycogen and mucin. Therefore, mucin and glycogen may go undetected in some cases of CAED [14]. In our case, we observed mostly eosinophilic granular cytoplasm, with only a focal clear cell component (Fig. 2).

AFP production in gastric carcinoma was suggested by Matsunou et al. [15] to be due to a form of retro-differentiation towards fetal intestine as clear cell carcinoma with morphology similar to the developing gut epithelium, or fetal hepatocytes, i.e., hepatoid carcinoma. AFP-producing colorectal cancers are generally observed to be poorly to moderately differentiated, a histological characterization that makes it different from AFP-producing gastric cancers which are commonly poorly differentiated. However, both rapidly progresses and metastasizes frequently to the liver with a poor prognosis [4]. Poor differentiation, deep submucosal invasion, lymphatic invasion, vascular invasion, or a positive resection margin are risk factors for lymph node metastasis in submucosal colorectal cancers [16].

Due to limited data on CAED, only very few studies and case reports have documented the results of ancillary studies including genomic [1,13] and microsatellite instability (MSI) characteristics [1]. One study reports an MSI-high rate in CAED of 12.2% [1], which is almost similar to that reported in conventional CRC [17]. The tumor in this case showed intact expression of MMR proteins (MLH-1, PMS-2, MSH-2, MSH-6) by IHC in CAED. NGS analyses from one study revealed that the most frequently mutated gene in CAED is *TP53*, at a rate of 52.4% [1] which is almost similar to the *TP53* mutation rate in conventional CRC [18,19]. The *KRAS* mutation from the same study was reported at 27.6%, similar to the rate in conventional CRC [20]. We detected a *KRAS* mutation in our CAED case; however, PD-L1 was negative. Other mutated genes that have been reported in CAED

include *APC* (44.8%), *BRAF* (20.7%), *NRAS* (17.2%), and *PIK3CA* (17.2%) [1]. We recognize the limitation of this case as diagnosis relied on biopsy specimens from the colonic and liver tumors. However, given the advanced stage at disease presentation, neoadjuvant treatment modalities were pursued for possible disease control before surgery.

There are no specific treatment guidelines yet for patients with AFP-producing colorectal cancers. Therefore, treatment regimens are employed according to multiple guidelines and personal experience. Most will undergo the conventional treatments for colorectal cancers which include surgery and chemotherapy with many dying within a year of initiating therapy [21]. Our patient is being evaluated for autologous stem cell transplant following disease progression on standard chemotherapy for conventional CRC and germ cell tumor.

In summary, CAED is a rare subtype of CRC with poor prognosis and poses diagnostic difficulties on account of its clinical and histopathologic similarities to primary HCC and germ cell tumors. Ancillary diagnostic modalities including gene expression profiling in the tumor cells by DNA sequencing techniques, may be necessary to correctly diagnose this entity, especially in challenging cases as was encountered in this case. Therefore, pathologists need to be aware of this rare tumor, as a missed diagnosis could significantly impact the clinical care and outcome of patients.

### Ethics Statement

As this is a case study without identifiers, our institution does not require approval from the institutional review board or its equivalent.

### Availability of Data and Material

Data sharing not applicable to this article as no datasets were generated or analyzed during the study.

### Code Availability

Not applicable.

### ORCID

Evi Abada <https://orcid.org/0000-0001-5061-2687>  
Ifeoma C. Anaya <https://orcid.org/0000-0001-9941-6660>  
Anthony Lebbos <https://orcid.org/0000-0003-4048-4217>

### Author Contributions

Conceptualization: EA, RB. Data curation: EA, RB. Methodology: all authors. Project administration: EA. Resources: all authors. Supervision: all authors. Visualization: all authors. Writing—original draft: all authors. Writing—review & editing: all authors. Approval of final manuscript: all authors.

### Conflicts of Interest

The authors declare that they have no potential conflicts of interest.

### Funding Statement

No funding to declare.

### References

1. Yamashiro Y, Saito T, Hayashi T, et al. Molecular and clinicopathological features of colorectal adenocarcinoma with enteroblastic differentiation. *Histopathology* 2020; 77: 492-502.
2. Murakami T, Yao T, Mitomi H, et al. Clinicopathologic and immunohistochemical characteristics of gastric adenocarcinoma with enteroblastic differentiation: a study of 29 cases. *Gastric Cancer* 2016; 19: 498-507.
3. Liu X, Sheng W, Wang Y. An analysis of clinicopathological features and prognosis by comparing hepatoid adenocarcinoma of the stomach with AFP-producing gastric cancer. *J Surg Oncol* 2012; 106: 299-303.
4. Anzai H, Kazama S, Kiyomatsu T, et al. Alpha-fetoprotein-producing early rectal carcinoma: a rare case report and review. *World J Surg Oncol* 2015; 13: 180.
5. Ren F, Weng W, Zhang Q, et al. Clinicopathological features and prognosis of AFP-producing colorectal cancer: a single-center analysis of 20 cases. *Cancer Manag Res* 2019; 11: 4557-67.
6. Bergstrand CG, Czar B. Demonstration of a new protein fraction in serum from the human fetus. *Scand J Clin Lab Invest* 1956; 8: 174.
7. O'Connor GT, Tatarinov YS, Abelev GI, Uriel J. A collaborative study for the evaluation of a serologic test for primary liver cancer. *Cancer* 1970; 25: 1091-8.
8. Bae JM, Lee TH, Cho NY, Kim TY, Kang GH. Loss of CDX2 expression is associated with poor prognosis in colorectal cancer patients. *World J Gastroenterol* 2015; 21: 1457-67.
9. McIntire KR, Waldmann TA, Moertel CG, Go VL. Serum alpha-fetoprotein in patients with neoplasms of the gastrointestinal tract. *Cancer Res* 1975; 35: 991-6.
10. Nakajima T, Okazaki N, Morinaga S, Tsumuraya M, Shimosato Y, Saiki S. A case of alpha-fetoprotein-producing rectal carcinoma. *Jpn J Clin Oncol* 1985; 15: 679-85.
11. Furuya Y, Wakahara T, Akimoto H, et al. Clear cell adenocarcinoma with enteroblastic differentiation of the ascending colon. *J Clin Oncol* 2011; 29: e647-9.
12. Murakami T, Yao T, Yatagai N, et al. Colorectal adenocarcinoma with enteroblastic differentiation: a clinicopathological study of five cases. *Histopathology* 2020; 76: 325-32.
13. Ogiwara S, Furihata M, Fukami K, Yamashita A, Yao T, Osada T. Hepatoid adenocarcinoma with enteroblastic differentiation in the sigmoid colon: lessons from a rare case. *Am J Gastroenterol* 2019; 114: 684-5.
14. Eloy C, Lopes JM, Faria G, et al. Clear cell change in colonic polyps. *Int J Surg Pathol* 2009; 17: 438-43.
15. Matsunou H, Konishi F, Jalal RE, Yamamichi N, Mukawa A. Alpha-fetoprotein-producing gastric carcinoma with enteroblastic differentiation. *Cancer* 1994; 73: 534-40.
16. Yasuda K, Inomata M, Shiromizu A, Shiraishi N, Higashi H, Kitano S. Risk factors for occult lymph node metastasis of colorectal cancer invading the submucosa and indications for endoscopic mucosal resection. *Dis Colon Rectum* 2007; 50: 1370-6.
17. Nojadedh JN, Behrouz Sharif S, Sakhinia E. Microsatellite instability in colorectal cancer. *EXCLI J* 2018; 17: 159-68.
18. Iacopetta B. *TP53* mutation in colorectal cancer. *Hum Mutat* 2003; 21: 271-6.

19. Li XL, Zhou J, Chen ZR, Chng WJ. P53 mutations in colorectal cancer: molecular pathogenesis and pharmacological reactivation. *World J Gastroenterol* 2015; 21: 84-93.
20. Natsume S, Yamaguchi T, Takao M, et al. Clinicopathological and molecular differences between right-sided and left-sided colorectal cancer in Japanese patients. *Jpn J Clin Oncol* 2018; 48: 609-18.
21. Nakamura Y, Matsuda K, Yokoyama S, et al. Alpha-fetoprotein-producing rectal cancer successfully responded to preoperative chemoradiotherapy: case report. *Surg Case Rep* 2018; 4: 111.

## Recurrent malignant solitary fibrous tumor of the scalp: a case report and literature review

Ahmed Rabie<sup>1</sup>, Abdulkarim Hasan<sup>2</sup>, Yasein Mohammed<sup>2</sup>, Ayman Abdelmaksoud<sup>3</sup>, Ali A. Rabaan<sup>4</sup>

<sup>1</sup>Department of Pathology, Faculty of Medicine, Al-Azhar University, Damietta Branch, Damietta;

<sup>2</sup>Department of Pathology, Faculty of Medicine, Al-Azhar University, Cairo;

<sup>3</sup>Mansoura Dermatology, Venereology and Leprosy Hospital, Mansoura, Egypt;

<sup>4</sup>Molecular Diagnostic Laboratory, Johns Hopkins Aramco Healthcare Dhahran, Dhahran, Saudi Arabia

Solitary fibrous tumor (SFT) is a rare type of mesenchymal neoplasm that first was discovered in the pleura but can also affect the peritoneum, lungs, mediastinum, and skin. Cutaneous malignant SFT is an extremely rare tumor that resembles dermatofibrosarcoma protuberance (DFSP) histologically and immunohistochemically. Herein, we describe a case of malignant SFT that presented as a recurrent mass on the scalp. The first lesion was totally excised one year before recurrence and was diagnosed as a DFSP based on the histopathology and cluster of differentiation 34 immunostaining positivity. Re-examination of the previously examined specimen was considered. Activator of transcription 6 positivity was also detected in the tissue, confirming the diagnosis of a recurrent malignant SFT rather than DFSP. There was no evidence of recurrence, locoregional, or distant metastases at six months after lesion removal with a safety margin.

**Key Words:** Solitary fibrous tumor; Skin cancer; Immunohistochemistry; STAT6

**Received:** August 4, 2021 **Revised:** October 26, 2021 **Accepted:** October 29, 2021

**Corresponding Author:** Abdulkarim Hasan, MD, Department of Pathology, Faculty of Medicine, Al-Azhar University, Cairo 11884, Egypt  
 Tel: +20-224012932, Fax: +20-224012932, E-mail: doctorabdulkarim7@gmail.com

Solitary fibrous tumor (SFT) is a type of fibroblastic mesenchymal tumor that originates in the pleura. Extra-pleural sites have been described, including the head and neck, peritoneum, retroperitoneum, genitourinary system, and pelvis. SFTs have been reported rarely in the skin [1-3]. The majority of SFTs is benign in nature, with a few cases of metastasizing tumors exhibiting a variety of clinical symptoms [2,4]. Malignant SFT is the most aggressive form, with a higher rate of local recurrence and distant metastasis [5]. It is an extremely rare lesion, particularly in the skin, and frequently presents a histopathological challenge, as many skin malignancies exhibit spindle cell proliferation with frequent histological overlap, resulting in a broad histologic differential diagnosis [3,6,7]. Immunohistochemistry is a valuable technique for malignant SFT diagnosis since it often reacts to CD34, signal transducer, and activator of transcription 6 (STAT6) markers but not to cytokeratins (CK), smooth muscle actin (SMA), CD31, S100, or CD68 [7,8]. Immunohistochemistry is required for accurate diagnosis of challenging and rare malignant

lesions [9]. The present study describes a case of a recurrent malignant SFT on the scalp.

### CASE REPORT

A 51-year-old male patient who was seemingly healthy presented with a recurrent subcutaneous occipital mass one year after excision. The mass was diagnosed as dermatofibrosarcoma protuberance (DFSP) based on histomorphology and CD34-positive immunostaining, with a size of 5×4 cm and free margins of at least 0.2 cm. The clinical examination of the new lesion revealed an 8×7 cm subcutaneous mass with overlying skin ulceration, raising the possibility of recurrent DFSP or a neoplastic epithelial lesion consistent with squamous cell carcinoma. The radiological assessment showed no associated lytic or sclerotic bony lesions. For histopathological examination, the lesion was removed surgically with a safety margin. Gross investigation revealed ulcerated skin overlying a well-defined, lobulated, white, and focally

necrotic mass (Fig. 1). A spindle cell tumor organized in irregular short bundles with staghorn blood vessels was revealed under microscopic analysis. Tumor cells had large, rounded vesicular nuclei and conspicuous micronuclei, with a small to moderate proportion of eosinophilic cytoplasm. Tumor cell nuclei exhibited a moderate degree of pleomorphism and frequent mitosis, approximately seven mitoses per 10 high-power fields (HPFs), with occasional atypical forms and foci of necrosis (Fig. 2). The tumor had invaded the overlying skin. A storiform pattern was not present. There were no dedifferentiated or anaplastic spots. All surgical margins were devoid of tumor cells, with the nearest free margin measuring 0.5 cm (side and deep margins).

In the first immunohistochemical panel study, CD34 was significantly positive in most tumor cells, but SMA, desmin, S100, pan-CK, and epithelial membrane antigen showed negative re-

sults. B-cell lymphoma 2 (BCL2) marker exhibited weak focal staining. Based on the histomorphological and immunohistochemical results, histopathological differential diagnosis was performed, including malignant solitary fibrous tumor, fibrosarcoma on top of dermatofibrosarcoma, and malignant peripheral nerve sheath tumor. Further immunohistochemical investigation of SOX10, STAT6, and Ki67 was considered, where the Ki67 labeling index was 30%, and STAT6 exhibited a strong diffuse nuclear positivity (Fig. 3), whereas SOX10 was not expressed. Re-cut and re-examined tissue blocks and slides from previous surgery confirmed the same histomorphology, including the lack of storiform pattern. STAT6 immunohistochemical staining of the primary lesion showed diffuse nuclear positivity.

Consequently, the final diagnosis was recurrent malignant SFT (TNM stage T3). Metastatic risk assessment revealed an interme-

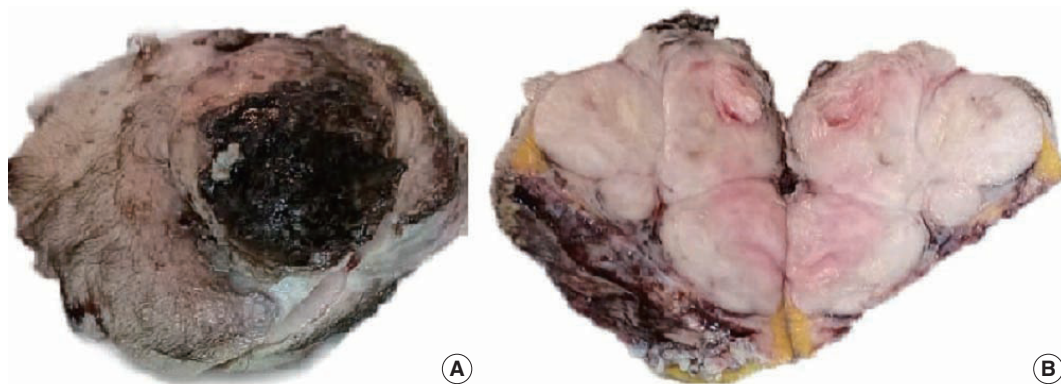


**Fig. 1.** A gross picture showing ulcerated skin (A) and fairly defined lobulated whitish mass with central focal necrosis (B).

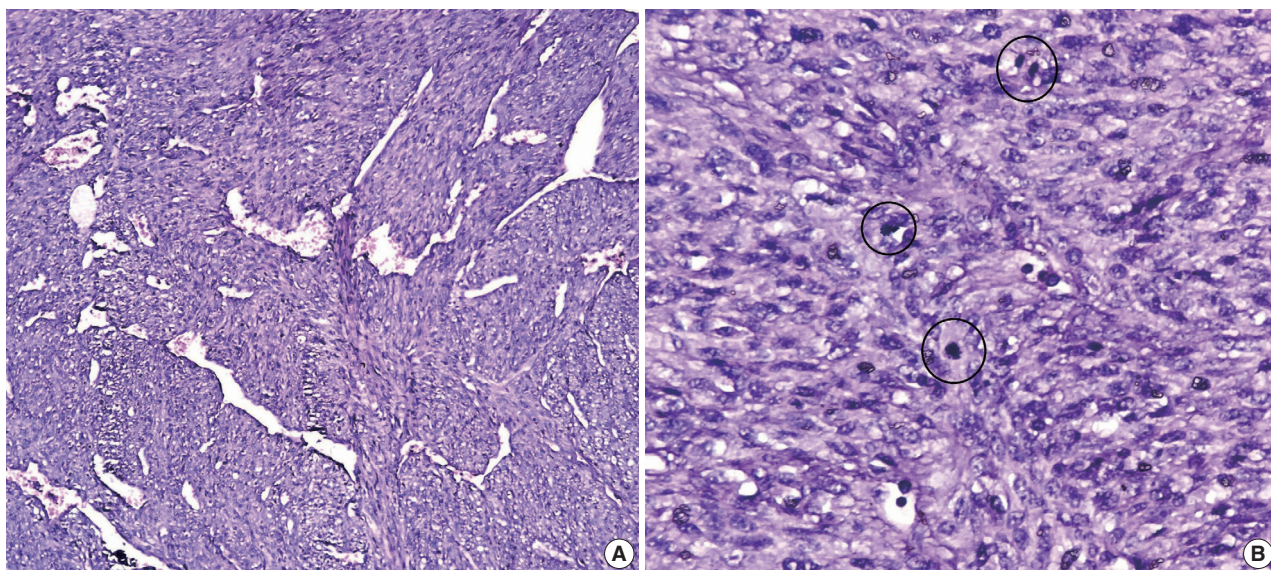


**Fig. 2.** A histopathology picture showing a cellular spindle cell tumor arranged in irregular short bundles with staghorn blood vessels (A) and mitotic figures (circles) (B).

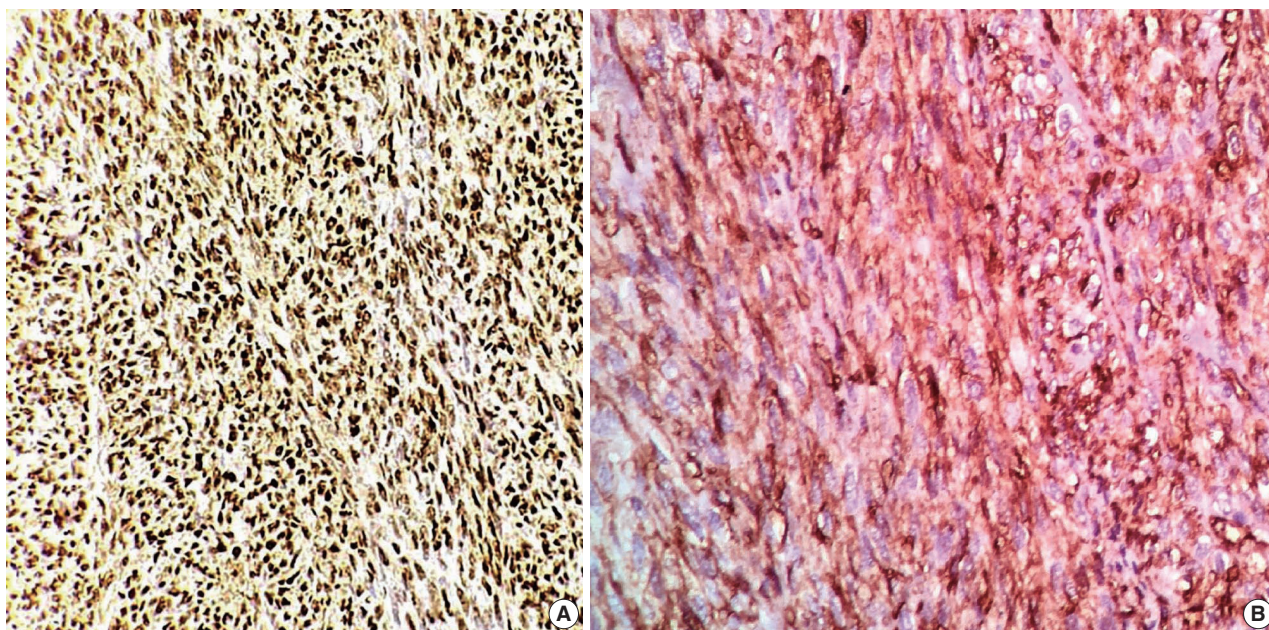


**Fig. 3.** Immunohistochemical staining. (A) The STAT6 result is positive (diffuse nuclear staining). (B) The CD34 finding is positive (cytoplasmic staining).

diate-risk solitary fibrous tumor. The patient was referred to the oncology department for further evaluation and showed no signs of metastasis at first presentation. Six months later, regular follow-up indicated no evidence of recurrence or distant metastasis.

## DISCUSSION

SFT first was described in 1931 by Klemperer and Rabin as “localized fibrous mesothelioma” [10]. SFT and hemangiopericytoma previously were considered to be distinct entities; however, beginning with the 2013 World Health Organization classification of soft tissue tumors, SFT and hemangiopericytoma are now considered the same neoplasm—except in the central nervous system, where meningeal hemangiopericytoma remains a distinct entity [4]. SFT is frequently found in adults aged 20 to 70 years but has been recorded in children on rare occasions [11]. Although SFTs were initially classified as pleural tumors, they can be found in various tissues, such as the liver, lungs, kidneys, thyroid, neurological system, soft tissue, and skin [9,12]. Cutaneous SFT is an extremely rare neoplasm, presenting as a painless, superficial, and well-circumscribed mass that can be confused clinically with lipoma or epidermal cyst [3]. A summary of previously reported cases of scalp SFT and the current one is illustrated in Table 1 [13–24]. Confirming a diagnosis of unusual skin and soft tissue mass lesions, including SFT, is challenging and requires careful sampling of the tumor mass followed by

careful pathological examination [25,26]. Although fine-needle aspiration cytology is used frequently to diagnose skin and soft tissue masses [27], no definitive cytological findings of SFT have been identified. SFT requires suitable clinical and radiological correlation and immunochemical tests for preoperative diagnosis [28,29]. SFT is classified histologically as storiform, hemangiopericytic, herring-bone, diffuse sclerosing, or neural-type palisading. SFT spindle cells proliferate in a “patternless” manner and form dense collagen bundles embedded in the stroma with elaborate vasculature [3]. Malignant SFTs are differentiated from benign SFTs by their high degree of cellularity, size greater than 5 cm, number of mitoses per HPF, presence of immature or pleomorphic tumor cells, and necrosis foci.

A correlation between number of mitoses per HPF and prognosis was observed. At least four mitoses per 10 HPFs are associated with metastasis and recurrence [4,30]. There are differential diagnoses for malignant SFT, such as benign SFT, DFSP, nerve sheath tumors, synovial sarcoma, liposarcoma, and leiomyomyosarcomas [31]. Clinico pathological correlation of SFT might not be sufficient to reach a definitive diagnosis. SFTs previously were diagnosed by immunohistochemical expression of various markers, including CD34, CD99, and BCL2; however, these markers carry a poor specificity [7,32]. CD34 is expressed highly in SFTs but also in other tumors that are included in the differential diagnosis of SFTs—namely, DFSP. CD34 is absent in around 5% to 10% of SFTs, mostly in dedifferentiated and ma-

**Table 1.** A review of existing literature, including case reports and series of scalp SFTs

Reference	Site	Age (yr)	Sex	Tumor behavior	Tumor size (cm)	+ve stains	-ve stains
Present case	Scalp (occipital)	51	M	Malignant	8 × 7	CD34, STAT6, Ki67 (30%)	SOX10, actin, desmin, S100, pan-CK, EMA
Vasile et al. (2020) [13]	Scalp (meningeal-derived)	68	M	Malignant	6 × 4	STAT6, BCL2, CD99, vimentin	CK, CK5/2, keratin 34 beta E-12, EMA, P40, S-100, MART-1, desmin, progesterone receptor
Mori et al. (2018) [14]	Scalp (mid-occipital)	37	F	Benign	2.5 × 2	CD34, STAT6	S-100, Melan-A, Sox10
Feasel et al. (2018) [15]	Scalp	81	F	Benign	4	CD34, STAT6	S-100, cytokeratins
		55	F		1.8		
		64	F		2		
		31	F		3		
		31	F		NA		
Kim et al. (2017) [16]	Scalp (left side)	20	F	Benign (myxoid)	4 × 1.5	CD34	BCL2, SMA, S-100, desmin
Shirley et al. (2016) [17]	Scalp (posterior)	37	F	Malignant	6 × 4.5	FLI-1, BCL2, CD99, CD34	CD57, EMA, HMB-45, S100, CD31
Omori et al. (2014) [18]	Scalp (posterior)	64	M	Benign	4.5 × 2	CD34, BCL2	EMA, SMA, desmin, S-100
Rizk et al. (2013) [19]	Scalp (parietal region)	2	M	Benign	NA	CD34	SMA, desmin, h-caldesmon, S-100
Tourabi et al. (2008) [20]	Scalp (left occipital)	-	-	Benign	NA	NA	NA
Erdag et al. (2007) [21]	Scalp	58	M	Benign	NA	CD34, CD99	Keratin, EMA, desmin, S-100
Ramdlal and Madaree (2001) [22]	Scalp	2.5	F	Benign (aggressive)	15.5	CD34	Desmin, S-100
Cowper et al. (1999) [23]	Scalp	38	M	Benign	4	CD34, vimentin	Cytokeratin, EMA, SMA, desmin, factor XIIIa, S-100
Okamura et al. (1997) [24]	Scalp (subcutaneous)	37	F	Benign	NA	CD34	Markers for smooth muscle, neural, and epithelial differentiation

SFT, solitary fibrous tumor; STAT6, signal transducer, and activator of transcription 6; CK, cytokeratin; EMA, epithelial membrane antigen; BCL-2, B-cell lymphoma 2; NA, not available; SMA, smooth muscle actin.

lignant instances [33]. Cancers of the nervous system, melanocytic cells, fat, and smooth muscle can be recognized by their positivity for tumor-specific markers such as S100, desmin, and SMA, which are non-reactive with SFT tumor cells [8]. Our case was misdiagnosed previously as DFSP based on histomorphology and CD34 positivity. However, the absence of a storiform pattern in the tissue and the presence of the STAT6 marker validated our findings on both initial and recent/recurrent specimens. Detection of the *NAB2::STAT6* fusion gene in SFTs is a reliable distinction from other spindle cell tumors. *NAB2* is a transcriptional repressor of the early growth response transcription factor, and its fusion with *STAT6* can convert the repressor into a transcriptional activator, driving neoplastic progression [34]. This finding led to identification of STAT6 immunohistochemical study as a highly sensitive and specific marker for SFTs, whereas DFSP is STAT6-negative [35]. Surgical resection with safety margins is the preferred treatment for both malignant SFTs and DFSP, but chemo- and radiotherapy can be challenging. Adjuvant chemotherapy and radiotherapy are not used widely due to the rarity of SFTs. However, chemotherapy can be beneficial in malignant situations where the tumor appears to be radiation-responsive,

implying a more significant chance of reduction in local recurrence [36,37].

While SFT of the scalp is uncommon, malignant SFT is even more uncommon and should be distinguished carefully from other spindle cell tumors of the skin, especially DFSP. To the best of our knowledge, this case is the third report of malignant SFT on the scalp and the first reported case of recurrent SFT at this anatomical site. CD34 immunostaining is insufficient to specify a malignant SFT of the skin. Thus, STAT6 markers should be included in the immunohistochemical panel for differential diagnosis of challenging cases of superficial spindle cell neoplasms.

#### Ethics Statement

Ethical committee approval from the Faculty of Medicine, Al-Azhar University board is provided (ID: IRB 00012367-21-03-008). Informed consent was obtained from the patient.

#### Availability of Data and Material

All data generated or analyzed during the study are included in this published article (and its supplementary information files).

#### Code Availability

Not applicable.

**ORCID**

Ahmed Rabie <https://orcid.org/0000-0002-4033-8554>  
 Abdulkarim Hasan <https://orcid.org/0000-0003-0391-306X>  
 Yasein Mohammed <https://orcid.org/0000-0002-1290-5910>  
 Ayman Abdelmaksoud <https://orcid.org/0000-0003-4848-959X>  
 Ali A. Rabaan <https://orcid.org/0000-0002-6774-9847>

**Author Contributions**

Conceptualization: AR, AH, YM, AA, AAR. Data curation: AR, AH, YM. Formal analysis: AR, AH, AA, AAR. Investigation: AR, AH, YM, AA, AAR. Project administration: AH. Resources: AR, AH, AA, AAR. Software: AR, AH, AA. Supervision: AR, AAR. Validation: AR, AH, YM, AA, AAR. Visualization: AR, AH, YM. Writing—original draft: AH, AA. Writing—review & editing: AR, AH, YM, AA, AAR. Approval of final manuscript: all authors.

**Conflicts of Interest**

The authors declare that they have no potential conflicts of interest.

**Funding Statement**

No funding to declare.

**References**

- Hasegawa T, Matsuno Y, Shimoda T, Hasegawa F, Sano T, Hirohashi S. Extrathoracic solitary fibrous tumors: their histological variability and potentially aggressive behavior. *Hum Pathol* 1999; 30: 1464-73.
- Zhou Y, Chu X, Yi Y, Tong L, Dai Y. Malignant solitary fibrous tumor in retroperitoneum: a case report and literature review. *Medicine (Baltimore)* 2017; 96: e6373.
- Shin K, Kim TW, Lee HJ, et al. A case of malignant solitary fibrous tumor of the skin. *Ann Dermatol* 2019; 31: 226-8.
- Fletcher CD, Bridge JA, Lee JC. Extrapleural solitary fibrous tumour. In: Fletcher CD, Bridge JA, Hogendoorn PC, Meertens F, eds. *WHO classification of tumours of soft tissue and bone*. 4th ed. Lyon: IARC Press, 2013; 80-2.
- Lococo F, Cesario A, Cardillo G, et al. Malignant solitary fibrous tumors of the pleura: retrospective review of a multicenter series. *J Thorac Oncol* 2012; 7: 1698-706.
- Creytens D, Ferdinande L, Van Dorpe J. Histopathologically malignant solitary fibrous tumor of the skin: a report of an unusual case. *J Cutan Pathol* 2016; 43: 629-31.
- Ronchi A, La Mantia E, Gigantino V, et al. A rare case of malignant solitary fibrous tumor in prostate with review of the literature. *Diagn Pathol* 2017; 12: 50.
- Geramizadeh B, Marzban M, Churg A. Role of immunohistochemistry in the diagnosis of solitary fibrous tumor, a review. *Iran J Pathol* 2016; 11: 195-203.
- Kwon JH, Song JS, Jung HW, Lee JS, Cho KJ. Malignant solitary fibrous tumor with heterologous rhabdomyosarcomatous differentiation: a case report. *J Pathol Transl Med* 2017; 51: 171-5.
- Klemperer P, Coleman BR. Primary neoplasms of the pleura: a report of five cases. *Am J Ind Med* 1992; 22: 1-31.
- Guo W, Xiao HL, Jiang YG, et al. Retrospective analysis for thirty-nine patients with solitary fibrous tumor of pleura and review of the literature. *World J Surg Oncol* 2011; 9: 134.
- Geramizadeh B, Banani A, Moradi A, Hosseini SM, Foroutan H. Intrapulmonary solitary fibrous tumor with bronchial involvement: a rare case report in a child. *J Pediatr Surg* 2010; 45: 249-51.
- Vasile G, Mancuso C, White R, et al. Rare meningeal-derived malignant hemangiopericytoma/solitary fibrous tumor grade II-III presenting as a subcutaneous mass on the scalp. *JAAD Case Rep* 2020; 6: 861-3.
- Mori S, Lezcano C, Miraflor AP, Busam KJ, Lee EH. Solitary fibrous tumor presenting on the scalp: a potential diagnostic pitfall. *J Cutan Pathol* 2018; 45: 557-60.
- Feasel P, Al-Ibraheemi A, Fritchie K, et al. Superficial solitary fibrous tumor: a series of 26 cases. *Am J Surg Pathol* 2018; 42: 778-85.
- Kim JH, Kim DC, Lee R, et al. Myxoid solitary fibrous tumor on the scalp. *Arch Craniofac Surg* 2017; 18: 269-72.
- Shirley BM, Kang DR, Sakamoto AH. Malignant solitary fibrous tumor of the scalp. *J Maxillofac Oral Surg* 2016; 15: 245-8.
- Omori Y, Saeki H, Ito K, et al. Solitary fibrous tumour of the scalp. *Clin Exp Dermatol* 2014; 39: 539-41.
- Rizk T, Awada A, Sebaaly A, Hourani R. Solitary fibrous tumor of the scalp in a child. *J Neurosurg Pediatr* 2013; 11: 79-81.
- Tourabi K, Moussaoui A, Khaless A, et al. Solitary fibrous tumor of the scalp: a case report. *Ann Chir Plast Esthet* 2008; 53: 526-30.
- Erdag G, Qureshi HS, Patterson JW, Wick MR. Solitary fibrous tumors of the skin: a clinicopathologic study of 10 cases and review of the literature. *J Cutan Pathol* 2007; 34: 844-50.
- Ramdial PK, Madaree A. Aggressive CD34-positive fibrous scalp lesion of childhood: extrapulmonary solitary fibrous tumor. *Pediatr Dev Pathol* 2001; 4: 267-75.
- Cowper SE, Kilpatrick T, Proper S, Morgan MB. Solitary fibrous tumor of the skin. *Am J Dermatopathol* 1999; 21: 213-9.
- Okamura JM, Barr RJ, Battifora H. Solitary fibrous tumor of the skin. *Am J Dermatopathol* 1997; 19: 515-8.
- Hasan A, Nafie K, Monazea K, Othman A, Salem A, Ismail A. A rare case of recurrent eccrine poroma underlying gluteal abscess. *Int J Surg Case Rep* 2020; 75: 29-31.
- Wallace SJ, Teixeira R, Miller NF, Raj M, Sheikh H, Sharma R. Extrapleural superficial solitary fibrous tumor on the posterior shoulder: a case report and review of the literature. *Eplasty* 2018; 18: e31.
- Hasan A, Deyab A, Monazea K, et al. Clinico-pathological assessment of surgically removed abdominal wall endometriomas following cesarean section. *Ann Med Surg (Lond)* 2021; 62: 219-24.
- Gupta N, Barwad A, Katamuthu K, et al. Solitary fibrous tumour: a diagnostic challenge for the cytopathologist. *Cytopathology* 2012; 23: 250-5.
- Galed-Placed I, Lopez-Solache L, Reguera-Arias A. Solitary fibrous tumor of the tongue: cytopathologic fine needle aspiration findings. *J Cytol* 2019; 36: 186-7.
- Demicco EG, Wagner MJ, Maki RG, et al. Risk assessment in solitary fibrous tumors: validation and refinement of a risk stratification model. *Mod Pathol* 2017; 30: 1433-42.
- Bishop JA, Rekhman N, Chun J, Wakely PE Jr, Ali SZ. Malignant solitary fibrous tumor: cytopathologic findings and differential diagnosis. *Cancer Cytopathol* 2010; 118: 83-9.
- Paner GP, Aron M, Hansel DE, Amin MB. Non-epithelial neoplasms of the prostate. *Histopathology* 2012; 60: 166-86.
- Masuda Y, Kurisaki-Arakawa A, Hara K, et al. A case of dedifferentiated solitary fibrous tumor of the thoracic cavity. *Int J Clin Exp Pathol* 2014; 7: 386-93.
- Robinson DR, Wu YM, Kalyana-Sundaram S, et al. Identification of recurrent NAB2-STAT6 gene fusions in solitary fibrous tumor by

- integrative sequencing. *Nat Genet* 2013; 45: 180-5.
35. Doyle LA, Vivero M, Fletcher CD, Mertens F, Hornick JL. Nuclear expression of STAT6 distinguishes solitary fibrous tumor from histologic mimics. *Mod Pathol* 2014; 27: 390-5.
36. Cardillo G, Lococo F, Carleo F, Martelli M. Solitary fibrous tumors of the pleura. *Curr Opin Pulm Med* 2012; 18: 339-46.
37. Martin-Broto J, Stacchiotti S, Lopez-Pousa A, et al. Pazopanib for treatment of advanced malignant and dedifferentiated solitary fibrous tumour: a multicentre, single-arm, phase 2 trial. *Lancet Oncol* 2019; 20: 134-44.

## And the story goes on: non-conventional dysplasia of the colorectum

Lavisha S. Punjabi, Yi Neng Lai, Anjula Thomas

Department of Anatomical Pathology, Sengkang General Hospital, Singapore

The adenoma-carcinoma sequence of carcinogenesis in the colorectum, featuring the progressive accumulation of alterations of *APC*, *KRAS*, *p53*, and other genes, was elucidated in the 1990s and has since become a textbook example of the step-wise model of carcinogenesis. In recent decades, our understanding of colorectal dysplasia has expanded through the study of the clinical, morphologic, molecular aspects of serrated dysplasia and non-conventional dysplasia in inflammatory bowel disease (IBD). Hence, we read with interest Choi's timely review of the seven morphologic subtypes of non-conventional dysplasia in IBD [1].

The assessment of dysplasia in the context of IBD is a widely accepted and long-held area of diagnostic difficulty, associated with fair to moderate interobserver agreement even among subspecialty pathologists [2]. The question that naturally arises from the discovery of these unusual morphologic subtypes of dysplasia, that was to some extent based on retrospective study and generous resection specimens, is its applicability and impact on routine reporting of limited endoscopic biopsies. It is plausible that awareness of these morphologic subtypes could facilitate more accurate histologic recognition of dysplasia.

Alternatively, the devil's advocate may posit that the subtlety of some of these morphologic subtypes may make the diagnosis of dysplasia in superficial biopsies inconclusive and ambiguous. Of note, hypermucinous dysplasia shows progressively less cytologic atypia towards the surface and is thus a more subtle form of dysplasia than we are accustomed to recognizing. Contrary to its low-grade appearance however, this subtype harbors a higher

rate of *KRAS* alterations and aneuploidy [3,4], rendering it a high-risk lesion that should not be missed. From the clinical point of view, it would therefore be important to recognize non-conventional dysplasia, particularly the high-risk subtypes, and recommend short-term follow-up for these lesions, despite the concern about the ambiguous diagnosis for dysplasia. Conversely, from the healthcare systems point of view, a higher overall "indefinite for dysplasia" call rate may result in increased healthcare costs, particularly if the number needed to treat is high. Evidently, prospective evaluation of the impact on and of reporting, including inter-observer and intra-observer reproducibility among both subspecialty and general pathologists, is required, albeit conceivably limited by relatively small case numbers.

As with many areas in pathology, new knowledge often undergoes a process of "splitting," investigation and then meaningful "lumping." A prime example of this process, although out of the field of gastrointestinal pathology, is the study of subtypes of non-mucinous adenocarcinoma of the lung, that began with meticulous morphologic descriptions, such as lepidic, acinar, complex glandular, papillary, micropapillary and solid. Subsequent data on the prognostic implications of each of these subtypes facilitated meaningful grouping within a three-tier grading system formulated by the International Association for the Study of Lung Cancer, incorporated in the latest iteration of the World Health Organization classification of thoracic tumors. Similarly, further study of the behavior of the morphologic subtypes of non-conventional dysplasia in the colorectum may eventually allow formulation of broader categories in the future. In addition, one may contend that serrated lesions in IBD and sporadic serrated lesions could be united, given the similarity in clinical, pathologic, and molecular features.

As a matter of topical interest and therapeutic relevance, findings of a recent study by Kim et al. [5] concluded that *NTRK*-rearranged colorectal carcinomas progress exclusively via the serrat-

**Received:** October 13, 2021 **Revised:** December 27, 2021

**Accepted:** December 28, 2021

**Corresponding Author:** Lavisha S. Punjabi, MBBS

Department of Anatomical Pathology, Sengkang General Hospital, 110 Sengkang E Way, Singapore 544886

Tel: +65-6930-5000, E-mail: lavisha.s.punjabi@gmail.com

ed pathway of neoplasia, thus expanding the molecular landscape of serrated colorectal lesions. To the best of our knowledge, oncogenic gene fusions including *NTRK* fusions have yet to be studied in serrated lesions in IBD, and would indeed form an interesting research question.

In conclusion, while we have made strides in expanding the concepts of colorectal dysplasia, the present-day story of colorectal carcinogenesis in IBD is an unfinished one, with many curious questions, practical and scientific, yet to be solved.

#### Ethics Statement

Not applicable.

#### Availability of Data and Material

Data sharing not applicable to this article as no datasets were generated or analyzed during the study.

#### Code Availability

Not applicable.

#### ORCID

Lavisha S. Punjabi <https://orcid.org/0000-0003-0479-1690>

#### Author Contributions

Conceptualization: LSP. Writing—original draft: LSP. Writing—review & editing: YNL, AT. Approval of final manuscript: all authors.

#### Conflicts of Interest

The authors declare that they have no potential conflicts of interest.

#### Funding Statement

No funding to declare.

#### References

1. Choi WT. Non-conventional dysplastic subtypes in inflammatory bowel disease: a review of their diagnostic characteristics and potential clinical implications. *J Pathol Transl Med* 2021; 55: 83-93.
2. Laine L, Kaltenbach T, Barkun A, et al. SCENIC international consensus statement on surveillance and management of dysplasia in inflammatory bowel disease. *Gastrointest Endosc* 2015; 81: 489-501.
3. Lee H, Rabinovitch PS, Mattis AN, Lauwers GY, Choi WT. Non-conventional dysplasia in inflammatory bowel disease is more frequently associated with advanced neoplasia and aneuploidy than conventional dysplasia. *Histopathology* 2021; 78: 814-30.
4. Andersen SN, Lovig T, Clausen OP, Bakka A, Fausa O, Rognum TO. Villous, hypermucinous mucosa in long standing ulcerative colitis shows high frequency of K-ras mutations. *Gut* 1999; 45: 686-92.
5. Kim JH, Hong JH, Choi YL, et al. *NTRK* oncogenic fusions are exclusively associated with the serrated neoplasia pathway in the colorectum and begin to occur in sessile serrated lesions. *J Pathol* 2021; 255: 399-411.

## Renal cell carcinoma concomitant with multiple myeloma

Anubhav Narwal<sup>1</sup>, Prashant Ramteke<sup>1</sup>, Lalit Kumar<sup>2</sup>, Saumyaranjan Mallick<sup>1</sup>

Departments of <sup>1</sup>Pathology and <sup>2</sup>Medical Oncology, All India Institute of Medical Sciences, New Delhi, India

The concomitant presentation of multiple myeloma (MM) and renal cell carcinoma (RCC) in same patient is rare. The risk of developing a secondary neoplasia in primary malignancies is much higher (~31%) compared to the general population. The most common hematological malignancy associated with RCC is non-Hodgkin lymphoma. An association between MM and RCC has been reported previously, but literature on the topic is sparse. Secondary malignancies concomitant with MM are thought to be mostly due to the use of chemotherapeutic agents (alkylating agents) in addition to genetic and environmental factors. As treatment of RCC does not include alkylating agent, their role in post RCC, MM can be debated and indicates shared risk factor beyond chemotherapy as aetiology. The fact is supported by SEER (Epidemiology and End Results registry) data of bidirectional occurrence RCC followed by MM and vice versa. These shared risk factors include age, lifestyle, environmental factors and genetic mutations [1-3]. Although many hypotheses have been proposed to establish an association between MM and RCC, none have been proven. Here we report an association of incidentally-detected clear cell RCC in a known case of MM.

Our patient was a 63-year-old male with a baseline diagnosis of MM IgA kappa (International Staging System II/Durie-Salmon Staging System III A) in 2011. He received four cycles of RD regimen (lenalidomide-dexamethasone) and exhibited a complete response. He underwent autologous stem cell transplant in 2011 followed by thalidomide maintenance. After treatment, the patient had his first relapse in November 2015, for which he received four cycles VRD (bortezomib-lenalidomide-dexameth-

asone), to which he exhibited a partial response and was kept on RD maintenance.

In January 2020, the patient was re-evaluated and was found to have 68% plasma cells on bone marrow. M-band was 5.5 g/dL; serum-free light-chain (SFLC) kappa 898 and lambda of 14.6 with SFLC ration 61.5. Bone marrow fluorescent in-situ hybridization analysis demonstrated a deletion in the 16q23 chromosome. Whole-body positron emission tomography computed tomography scan showed multiple lytic lesions in the left parietal, sphenoid, basiocciput, clivus, bilateral mandible, humeri, sternum, ribs, femur, and sacrum along with a lower pole left renal mass. The patient was started on dexamethasone pulse therapy followed by bortezomib, pomalidomide and dexamethasone, meanwhile the renal mass was evaluated. Renal mass biopsy showed features of clear cell RCC. The patient has completed three cycles of the chemotherapy and is under follow-up monitoring (Fig. 1).

Ojha et al. [1] found that the relative risk of RCC is higher (89%) among post MM cases than MM in post RCC (51%) compared to the general population. The index patient is a 63-year-old male with MM and concomitant RCC as a second primary malignancy after a time gap of 120 months [1].

The recently proposed bidirectional association between MM and RCC, may be related to certain genetic risk factors. The roles of c-met receptor (family of *MET* gene) and its ligand hepatocyte growth factor are well-established in MM and RCC. Hence, *MET* may be a candidate gene for understanding the bidirectional association between MM and RCC [1,4]. Both synchronous and metachronous occurrence of MM and RCC have been described in literature, with time intervals between the two varying from 1 to 300 months for metachronous cases. There is a male predominance with median age of 50 years. The most common histological type was clear cell-type with occasional cases of chromophobe- and transitional-type RCC. RCC was treated by partial or complete nephrectomy in these cases. MM exhibited

Received: October 26, 2021 Revised: January 6, 2022

Accepted: January 21, 2022

Corresponding Author: Saumyaranjan Mallick, MD

Department of Pathology, All India Institutes of Medical Sciences (AIIMS), New Delhi 110029, India

Tel: +91-9013957818, Fax: +91-11-26588663, E-mail: drsmallick.aiims@gmail.com

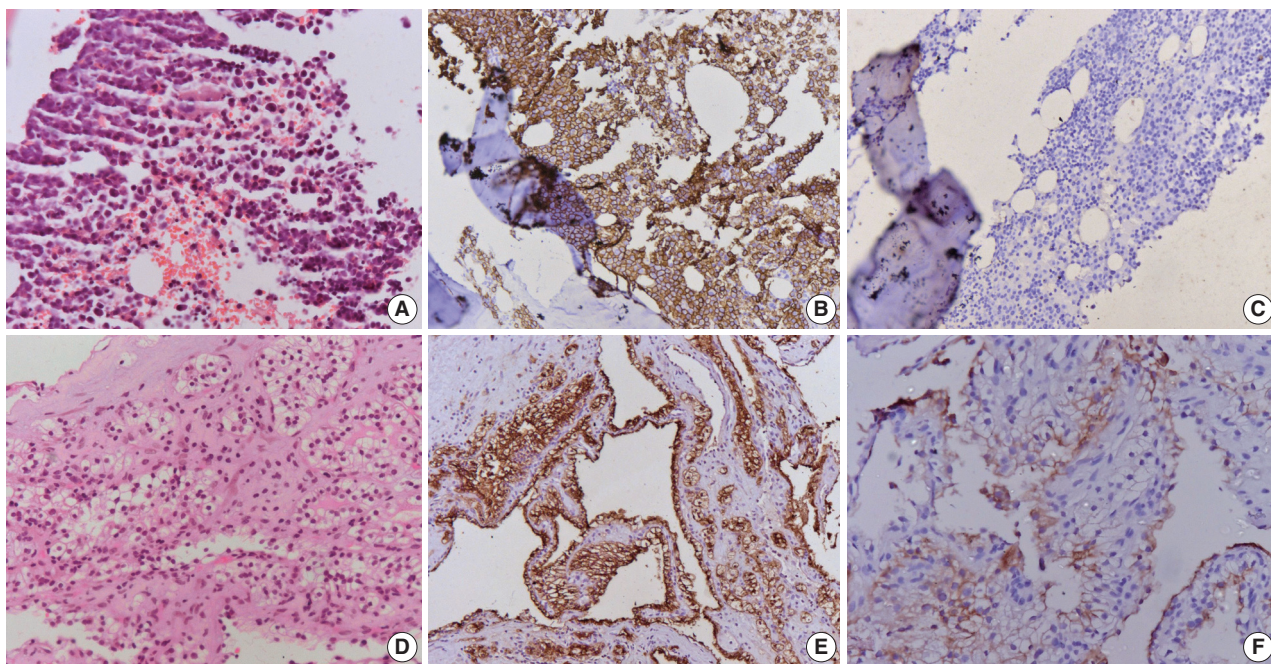


**Fig. 1.** (A) Microphotograph of lytic lesion biopsy shows sheets of mature plasma cells with mild atypia. (B) Cells are immunopositive for CD138, (C) while negative for cytokeratin. (D) Biopsy of the renal mass shows cells arranged in sheets with clear cytoplasm and small nuclei. The cells are immunopositive for cytokeratin (E) and CD10 (F).

morphology ranging from classical to anaplastic variant [5,6].

However, considering the previous literature and the present case, myeloma should be suspected in RCC patients with new lytic bone lesions, and any renal masses should be carefully investigated in MM patients.

#### Ethics Statement

Not applicable.

#### Availability of Data and Material

Availability of Data and Material: Data sharing not applicable to this article as no datasets were generated or analyzed during the study.

#### Code Availability

Not applicable.

#### ORCID

Anubhav Narwal <https://orcid.org/0000-0003-0708-9346>  
 Prashant Ramteke <https://orcid.org/0000-0003-4163-2170>  
 Lalit Kumar <https://orcid.org/0000-0002-9210-2500>  
 Saumyanjan Mallick <https://orcid.org/0000-0003-4366-5873>

#### Author Contributions

Conceptualization: SM. Data curation: AN. Formal analysis: AN. Investigation: LK. Methodology: PR. Writing—original draft: AN, PR. Writing—review & editing: SM. Approval of final manuscript: all authors.

#### Conflicts of Interest

The authors declare that they have no potential conflicts of interest.

#### Funding Statement

No funding to declare.

#### References

- Ojha RP, Evans EL, Felini MJ, et al. The association between renal cell carcinoma and multiple myeloma: insights from population-based data. *BJU Int* 2011;108:825-30.
- Shields LB, Kalebastay AR. Concurrent renal cell carcinoma and hematologic malignancies: Nine case reports. *World J Clin Oncol* 2020;11:644-54.
- Li N, Liu X, Song Y, et al. The synchronous presence of multiple myelomas and other primary malignant tumors: case series with literature review. *Cancer Manag Res* 2020;12:2829-38.
- Sakai A, Kawano M, Kuramoto A. Interleukin-6 produced by renal-cell carcinoma cells and progression of multiple myeloma. *N Engl J Med* 1991;324:1893-4.
- Choueiri TK, Baz RC, McFadden CM, et al. An association between renal cell carcinoma and multiple myeloma: a case series and clinical implications. *BJU Int* 2008;101:712-5.
- Padhi S, Sahoo PK, Banerjee D, et al. Renal cell carcinoma and plasma cell myeloma: unique association and clinical implications. *Urol Ann* 2014;6:252-6.



PathologyOutlines.com

## What's new in molecular genetic pathology 2022: immune checkpoint inhibitor biomarkers and select solid tumors

Patricia C. Tsang, MD<sup>1</sup> and Guoli Chen, MD<sup>2</sup>

<sup>1</sup>MedStar Washington Hospital Center, Pathology & Laboratory Medicine, Washington, DC, USA

<sup>2</sup>Geisinger Medical Laboratories, Geisinger Health, Danville, Pennsylvania, USA

Received: January 12, 2022

Accepted: January 25, 2022

Corresponding Author: Patricia C. Tsang, MD  
 MedStar Washington Hospital Center, Pathology & Laboratory Medicine, Washington, DC, USA  
 E-mail: patctsang@hotmail.com

### ORCID

Patricia C. Tsang

<https://orcid.org/0000-0003-0523-9793>

Guoli Chen

<https://orcid.org/0000-0002-4426-6156>

This article has been published jointly, with consent, in both Journal of Pathology and Translational Medicine and PathologyOutlines.com.

### Abstract

Predictive biomarker testing plays a critical role in targeted immuno-oncology, including the use of immune checkpoint inhibitors (ICI) for various solid tumors. Molecular advancements in cancers of the breast, kidney and brain have continued to propel tumor classification and precision therapy.

### GENE FUSION NOMENCLATURE

The HUGO Gene Nomenclature Committee has released a new recommendation to denote gene fusion with a double colon, e.g., *BCR::ABL* [1].

### IMMUNE CHECKPOINT INHIBITOR BIOMARKERS

- Programmed cell death ligand 1 (PDL1) immunohistochemistry (IHC) uses various scoring systems and cutoffs for particular antibody clones to quantify PDL1 expression as a predictive biomarker for specific FDA approved ICI. For example:

- The PDL1 pharmDX 22C3 immunostain is a companion diagnostic for non small cell lung carcinoma (NSCLC) patients eligible for pembrolizumab immunotherapy.
- The tumor proportion score (TPS) is calculated by dividing the total number of PDL1 positive tumor cells by the total number of tumor cells ( $\geq 1\%$  positive cutoff).
- The combined positive score (CPS) is based on dividing the number of PDL1 positive cells (tumor cells, lymphocytes, macrophages) by the number of tumor cells to predict pembrolizumab efficacy in metastatic gastric and gastroesophageal junctional carcinoma, bladder cancer and cervical cancer (Fig. 1). It has the same cutoff of  $\geq 1\%$ , using the 22C3 antibody clone.

- The PDL1 SP142 clone is an FDA approved complementary diagnostic to predict response of metastatic NSCLC to atezolizumab. The evaluation is based on either the proportion of tumor area occupied by PDL1 expressing tumor infiltrating immune cells of any intensity or the percentage of PDL1 expressing tumor cells of any intensity.
- Deficient mismatch repair (dMMR) / high microsatellite instability (MSI-H) is predictive of ICI efficacy in colorectal cancers and other solid tumors. While it is commonly tested by IHC, assays based on PCR or next generation sequencing (NGS) are available.
- High tumor mutational burden (TMB) may also serve as a predictor of immunotherapy response. TMB reflects the number of somatic mutations per megabase of tumor genomic sequence. It can be determined by whole exome sequencing (WES) or targeted sequencing of gene panels (usually  $\geq 200$  genes). Cutoff values have not yet been unified and may vary in respect to different assay platforms and ICI drug targets. Recently, Foundation Medicine's FoundationOne<sup>®</sup> CDx, which includes MSI and TMB assessment, was approved as a companion diagnostic for pembrolizumab with a cutoff of  $\geq 10$  mutations per megabase, regardless of solid tumor type.

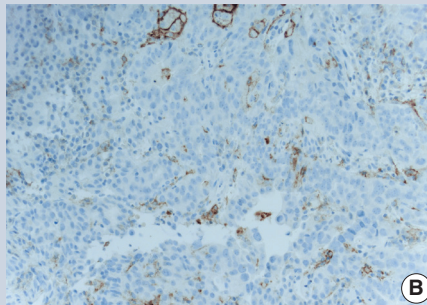
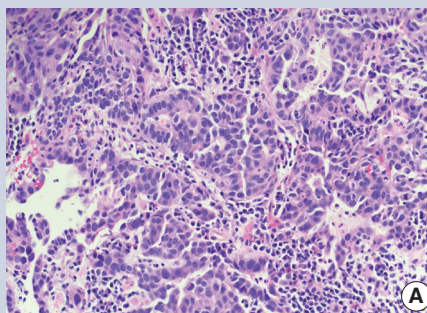


**Fig. 1.** Esophagogastric adenocarcinoma. (A) H&E stain, 40 x. (B) PD-L1 22C3 immunostain demonstrating a combined positive score of close to 20% (positive:  $> 1\%$ ), indicating response to pembrolizumab.

### BREAST CARCINOMA

- NGS can simultaneously detect alterations of multiple genes involved in breast cancers. Clinically actionable genomic changes include *ERBB2* (*HER2*) amplification (prevalence  $\sim 15\%$ ), *BRCA1/BRCA2* mutations (5%–10%), *PIK3CA* mutations (30%–40%) and *ETV6::NTRK3* fusion in secretory breast carcinoma ( $< 0.2\%$  of breast cancers).
- *BRCA1* and *BRCA2* inactivating mutations carry a lifetime cumulative risk of 60% and

Sponsored by an unrestricted grant from Geisinger Medical Laboratories: Dedicated to Laboratory Excellence

55% to develop breast cancer, respectively. Poly-ADP-ribose polymerase (PARP) inhibitors are FDA approved targeted therapy for *BRCA1/BRCA2* associated breast cancer.

- API3K (phosphoinositide 3-kinase) inhibitor, alpelisib, is FDA approved for advanced breast cancers that are *PIK3CA* altered, HER2 (-) and hormone receptor (+).
- Seen in ~30% of breast cancers, *TP53* mutation is associated with an increased likelihood of pathologic complete remission following chemotherapy, while wild type *TP53* appears to induce cell cycle arrest instead of cell death, resulting in residual disease following chemotherapy [2].
- Multigenomic prognostic profiling is being used to predict the risk of breast cancer recurrence. Commercial platforms include:
  - Oncotype DX® (Genomic Health Inc.): 21 gene reverse transcription PCR assay for predicting the likelihood of recurrence and chemotherapy benefit in hormone receptor (+) patients on endocrine therapy.
  - MammaPrint (Agendia, Inc.): 70 gene expression profile by microarray for predicting the risk of distant metastasis. Patients with high clinical risk but low genomic risk based on MammaPrint might not require chemotherapy.
  - EndoPredict® (Myriad Genetics): 11 gene RNA expression profile for predicting the risk of recurrence in hormone receptor (+) / HER2 (-) patients who are node (+) or (-) on endocrine therapy.
  - Prosigna® (Veracyte): 50 gene reverse transcription PCR assay for assessing the risk of recurrence in 10 years for hormone receptor (+) early stage breast cancer and identifying the subset of patients who may not benefit from chemotherapy.

## RENAL CELL CARCINOMA (RCC)

- In addition to recurrent *VHL* alterations and 3p deletion, clear cell RCC frequently carries other genetic alterations. *BAP1* or *SETD2* mutated RCCs behave aggressively, while *PBRM1* mutations predict a poor prognosis in localized RCC but a favorable outcome in advanced disease.
- Chromosome 7 or 17 polysomy and trisomy are the most common chromosomal changes in type 1 papillary RCC. Type 2 tumors are heterogeneous and may harbor *CDKN2A* silencing, *SETD2* mutations and other alterations.
- Some hybrid oncocytic chromophobe tumors (HOCT) are associated with Birt-Hogg-Dubé syndrome (BHD) or renal oncocytosis, while others are sporadic. BHD can be confirmed by germline mutations in the *FLCN* tumor suppressor gene.
- Renal cell neoplasms with *TFE3*, *TFEB* and *MITF* rearrangements are now grouped together as MiT family translocation RCC.

- Loss of SMARCB1 expression by IHC supports a diagnosis of medullary carcinoma.
- Negative or abnormal IHC staining for fumarate hydratase (FH), positive IHC staining for 2-succino-cysteine (2SC) or *FH* gene mutation supports FH deficient RCC / hereditary leiomyomatosis and RCC (HLRCC). Succinate dehydrogenase (SDH) deficient RCCs are associated with germline mutations of the *SDH* subunits (usually *SDHB*), as demonstrable by negative SDHB IHC staining. Genetic counseling is recommended for FH-deficient or SDH deficient RCC.
- Molecular profiling has helped to define new and emerging RCC variants, e.g., eosinophilic solid and cystic RCC associated with tuberous sclerosis (*TSC1* or *TSC2* gene alterations), RCC with *TSC/MTOR* mutations, *TCEB1* mutated RCC, RCC with *TFEB/6p21/VEGFA* amplification and *ALK* rearranged RCC [3].

## BRAIN TUMORS

- Primary glioblastoma (GBM) may harbor 10q loss of heterozygosity (LOH) (70%), *EGFR* amplification (36%), *CDKN2A* deletion (31%)

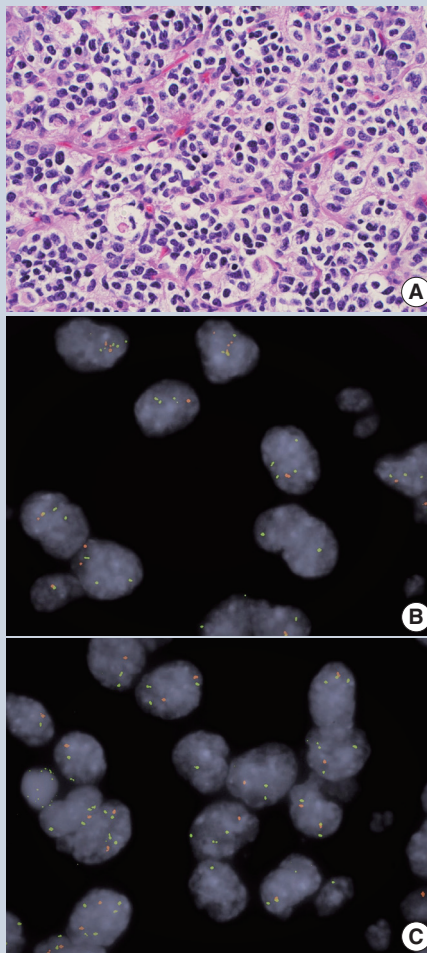


**Fig. 2.** (A) Oligodendroglioma showing perinuclear clearing and delicate capillary network (H&E stain, 20 x). Co-deletion of 1p (B) and 19q (C) by dual color FISH. Target (orange) to control (green) signal ratio of  $\leq 0.8$  indicates loss of the target allele.

and *PTEN* mutations (25%), all of which denote aggressive disease.

- *MGMT* promoter hypermethylation (30%–40% of primary GBM) predicts improved response to alkylating agents and a lower risk of tumor recurrence.
- Associated with improved survival, *IDH1* or *IDH2* mutations are common in grades II and III astrocytoma, oligodendroglioma and secondary GBM, and uncommon in primary GBM. When present, they help to distinguish low-grade astrocytoma (~70%) from gliosis.
- Co-deletion of 1p / 19q (detectable by FISH / PCR / microarray) is characteristic of oligodendroglioma (Fig. 2), predicting response to conventional therapy. Equivocal FISH can be subsequently assessed by LOH analysis via PCR. *ATRX* loss of function mutations, which correlate well with negative IHC, favor diffuse astrocytoma over oligodendroglioma.
- Diffuse midline glioma is characterized by a K27M substitution in the histone H3 genes, *H3F3A* or *HIST1H3B/HIST1H3C*, resulting in hypomethylation and H3 protein inactivation. These tumors may also harbor mutations in *TP53* (42%) or *ACVR1* (24%) [4].
- *BRAF* fusion, most commonly with *KIAA1549*, is observed in 59%–90% of pilocytic astrocytomas.

## Reference

1. Bruford EA, Antonescu CR, Carroll AJ, et al. HUGO Gene Nomenclature Committee (HGNC) recommendations for the designation of gene fusions. *Leukemia* 2021; 35: 3040-3.
2. Shahbandi A, Nguyen HD, Jackson JG. TP53 mutations and outcomes in breast cancer: reading beyond the headlines. *Trends Cancer* 2020; 6: 98-110.
3. Henske EP, Cornejo KM, Wu CL. Renal Cell Carcinoma in tuberous sclerosis complex. *Genes (Basel)* 2021; 12: 1585.
4. Price G, Bouras A, Hambardzumyan D, Hadjipanayis CG. Current knowledge on the immune microenvironment and emerging immunotherapies in diffuse midline glioma. *EBioMedicine* 2021; 69: 103453.

## Meet the Authors

Dr. Tsang joined the Pathology Outlines editorial board in 2019 and has been serving as Deputy Editor in Chief for Clinical Pathology for PathologyOutlines since 2020. She works as Chair of Pathology & Laboratory Medical Director at MedStar Washington Hospital Center in Washington, D.C. She has been practicing molecular pathology for more than a decade.

Dr. Chen is currently an Associate and Attending Pathologist at Geisinger Medical Center, where he participates in the clinical, academic and teaching services in surgical pathology and molecular diagnostics. He has been actively publishing and lecturing on topics related to molecular pathology of solid tumors.

